THÈSE

En vue de l'obtention du

DOCTORAT DE L'UNIVERSITÉ DE TOULOUSE

Délivré par : *l'Université Toulouse 3 Paul Sabatier (UT3 Paul Sabatier)*

Présentée et soutenue le *4 Octobre 2016* **par :**

CHRISTIAN VASSALLO

USING HUMAN-INSPIRED MODELS FOR GUIDING ROBOT LOCOMOTION

JURY

M. PHILIPPE FRAISSE	Prof. à l' Univ. de Montpellier 2	Rapporteur
M. FRANCESCO NORI	Tenure Track Researcher IIT	Rapporteur
M. PHILIPPE SOUÈRES	Directeur de Recherche CNRS	Membre du Jury
M. OLIVIER STASSE	Directeur de Recherche CNRS	Membre du Jury
M. JULIEN PETTRÉ	Chargé de Recherche INRIA	Membre du Jury

École doctorale et spécialité :
EDSYS : Robotique 4200046
Unité de Recherche :
Laboratoire d'Analyse et d'Architecture des Systèmes
Directeur(s) de Thèse :
M. Philippe SOUÈRES et *M. Olivier STASSE*
Rapporteurs :
M. Philippe FRAISSE et *M. Francesco NORI*

A miei genitori Paolo e Giulia,
che mi hanno insegnato ad amare.

A mio fratello Enrico,
che mi ha mostrato come diventare.

To Andrea, Nemo and Andreas,
because I wouldn't have done this without them.

A Shila,
il mio più bel dolce ricordo.

Acknowledgement

First of all, I would like to thank Philippe Fraisse and Francesco Nori for reviewing this thesis. I really appreciate your availability and commitment.
I would like to thank the European Commission for founding the project KoroiBot of which this thesis is part. It allowed to have really interesting collaborations with different partners and know new people.

These three years have been the most important and difficult ones of my life. It has been really challenging to leave my country, my family, my friends and start a new life in a foreign place, knowing nobody. I want to thank Francesco Morsillo, who helped me in the first days introducing me to my first "Toulouse family". Luckily, I have found an amazing work team and I want to thank all the members of Gepetto that in these years were always available and funny. In particular, I want to thank Maximilian Naveau because he helped me a lot with French bureaucracy and supported me in bad working time.

I gratefully acknowledge my supervisor Philippe Souères. He never stopped to believe in me, even when I was really far from results. He helped me many times, also for my personal problems, and he really showed me one of the best examples of people that I would like to become. Thank you very much Philippe.

I also want to thank Olivier Stasse. He encouraged me so much at the beginning of my thesis, and sometimes I was feeling below his expectations. However, at the end he was happy about my work and I realized that he was just trying to get the best out of me. Thank you Olivier.

I want to express my sincerest gratitude to Julien Pettré, Anne-Hélène Olivier and Armel Crétual. It has been a pleasure to work with them. Our work has been really intensive but I have always been greatly motivated by their experience and easygoing approach. In particular, I really appreciated the way they made me feel comfortable when I was in Rennes. It has been really precious and an experience of life. Thank you so much.

A special thank is for my bros Andrea, Andreas, Olivier, Nemo, Nemanja and François. They have been amazing colleagues and friends. They are examples of great people. I shared with them the best memories here in Toulouse and, also, the worst ones. They always have been there for me. They always offered me their shoulders to cry on. Always. I cannot forget this, I will never do. Thank you bros.

Un ringraziamento speciale va alla mia famiglia che, seppur distante, mi è sempre rimasta vicino dall'inizio alla fine. A mia Zia Ro e a mio Zio Chicco, che mi hanno sempre rifornito di cibo e amore ogni volta che tornavo dall' Italia. Quante volte son tornato tardi da lavoro e un'ottima cena era già pronta grazie a voi. A mia cugina Patrizia, che per ore e ore ha sempre ascoltato i miei problemi al telefono dandomi preziosi consigli. Come potrei dimenticare? Grazie.

A mia madre Giulia e a mio padre Paolo, che non hanno mai smesso di credere in me. È grazie a loro, più di tutti, se sono riuscito a terminare i miei studi. Mi hanno aiutato a crescere, a credere in me, a non mollare e a non perdere la retta via. A mio fratello Enrico, alla piccola Gaia e a Silvia, che mi hanno tenuto compagnia per tutti questi anni da dietro uno schermo, riuscendo a farmi sorridere anche quando non ne avevo proprio voglia.

Thank to everybody that in these years shared with me amazing memories. Thank you Michele, Giulio, Matilde, Giovanni, Roberta, Laura, Mylène, Hager, Justin, Justine and Léa. You have been really important experiences of my life. All of you.

I love to say "My bad time is not still over" and that's true. But thanks to all these people, I would say that "my bad time" have been so amazing :)

Contents

Introduction **1**

1 How humans avoid moving obstacle crossing their way? **17**

1.1 Introduction . . . 19
1.2 Minimal Predicted Distance . . . 21
1.3 Materials and Methods . . . 22
  Participants . . . 22
  Apparatus . . . 23
  Participant Task . . . 23
  Recorded Data . . . 23
  Experimental plan . . . 24
  Robot Behavior . . . 24
1.4 Obstacle Control . . . 26
1.5 Analysis . . . 28
  Signed Minimal Predicted Distance . . . 28
  Kinematic data . . . 28
  Statistics . . . 30
1.6 Results . . . 30
1.7 Discussion . . . 35
1.8 Conclusion . . . 36

2 Human and Robot interaction:
cooperative strategies for collision avoidance **39**

2.1 Introduction . . . 41
2.2 Materials and Methods . . . 43
  2.2.1 Participants . . . 43
  2.2.2 Apparatus . . . 43
  2.2.3 Participant Task . . . 44
  2.2.4 Recorded Data . . . 44
  2.2.5 Experimental plan . . . 45
2.3 Robot Behavior . . . 45
  2.3.1 Passive Behavior . . . 46
  2.3.2 Cooperative Behavior . . . 46
2.4 Analysis . . . 47

2.4.1 Kinematic data 47
2.4.2 Statistics 49
2.5 Results 49
2.5.1 Passive Robot 49
2.5.2 Cooperative Robot 53
2.5.3 Crossing Distance 57
2.6 Discussion 57
2.7 Conclusion 58

3 Learning Movement Primitives for the Humanoid Robot HRP2 59
3.1 Introduction 61
3.1.1 Modeling of whole-body movements in computer graphics 61
3.1.2 Biological motor control of multi-step sequences 62
3.1.3 Related approaches in humanoid robotics 62
3.2 System architecture 64
3.2.1 Human data 64
3.2.2 Stack Of Tasks (SoT) 69
3.2.3 Walking Pattern Generator (WPG) with Dynamic Filter 72
3.2.4 Robotics Implementation 73
3.2.5 Overall architecture 74
3.3 Results 75
3.3.1 Real Experiments 75
3.4 Conclusions 77

4 The geometry of confocal curves for passing through a door 79
4.1 Introduction 81
4.2 Problem Statement 84
4.3 Some Basic Geometry Around The Door 85
4.3.1 Elliptic Coordinates 88
4.3.2 Kinematic Model of the vehicle in Elliptic Coordinates 89
4.4 Feedback Control Law in Elliptic Coordinates 90
4.5 The Bundle of circles 92
4.5.1 Bipolar Coordinates 94
4.5.2 Kinematic model of the vehicle in bipolar coordinates 95
4.5.3 A simple strategy to steer the vehicle through the door exploiting the geometric properties of the bundle of circles 95

4.6 Feedback Control Law in Bipolar Coordinates 96
4.7 Simulations 98
4.8 Experiments 103
    4.8.1 Technical Details 103
    4.8.2 Experimental Results 107
4.9 Analysis of FOV limits 108
    4.9.1 Control strategy in case of FOV limits 111
4.10 Conclusions 112

Conclusion and Perspectives **113**

A Mobile Robot *Robulab10* **123**
A.1 Robulab10 Motion Control 125
    A.1.1 The robotic platform 125
    A.1.2 Robot Remote Control 126

Bibliography **129**

List of Figures

1 Project components of KoroiBot and Interdisciplinary foundations. 4

2 The seven humanoid robot platforms of the KoroiBot consortium dreaming of human walking capabilities. 5

3 Challenges of the KoroiBot project. In red the challenges addressed by the LAAS-CNRS. 5

4 Pert chart of the KoroiBot work packages and their interrelationships Our studies concerned WP1 and WP2. 6

5 An overview of two different scenarios tested in this study. In the left picture, two TurtleBots dressed with some papers to make them look bigger. The participant had to walk straight and avoid them. In the right picture, we improved the experimental setup introducing some occluding walls and considering the wheeled robot Robulab that is faster and looks heavier. Each experimental setup, required at least one week of work to be realized and calibrated. 8

6 An overview of the experimental setup of the study presented in Chap. 2. . 10

7 An illustrated overview of the work presented in Chap. 3. In the left, an avatar is reproducing some movements recorded from a human. In the center, an avatar of the humanoid robot HRP-2 is performing the same movements but in a realistic simulation. In the right, a snapshot of real experiments done with the robot HRP-2 at LAAS-CNRS. 12

8 An overview of the experimental setup of the work shown in Chap. 4. The wheeled robot is the same as the one used for the works presented in Chap. 1– 2. The entire work was done at LAAS-CNRS. 13

9 Illustration of four different tasks. From top-left to bottom-right: walking on a soft mattress, walking on a beam, stepping stones, walking stairs up. The kinematic data and the related normal forces are depicted in the smaller images. 14

10 (Left) The robot is moving according to the position of the red pylon engine in order to maintain the same distance (1 meter). (Right) Situation of the experiment: the robot has to go in the vicinity of the pylon engine, depicted in blue, avoiding the red moving toolbox. The robot has to re-plan its path in real-time. In both cases, the robot is tracking the objects using the motion capture system. 15

1.1 Illustration of the mpd evolution during the reaction phase between two humans crossing each other [Olivier 2012]. We defined t_{see} as the instant of time in which the participant starts to see the other one, and t_{cross} as the crossing time. From the picture, we observe that the mpd at t_{see} is around 0.32m, that means the participants will not collide but they are going to pass near to each other. Once the Reaction phase starts, the mpd is increasing because one of the participants (or perhaps both of them) is reacting to increase the future distance at t_{cross}. In the end of the reaction phase, the mpd is around 0.7m. 22

1.2 a) One of the participants equipped with the full body marker set. b) the mobile robot Robulab10. 23

1.3 Experimental apparatus and task. In this trial the robot was moving from RSP1 to RSP2. Participant decided to pass behind the robot. 24

1.4 Representation of the tracking problem. 27

1.5 Example of the analysis of one trial in which a switch of mpd sign occurred. a) robot and pedestrian trajectories during the trial: triangles and star points are their position at t_{rob} and t_{cross} respectively. b) velocity profile of the walker and the obstacle. c) mpd components. d) mpd evolution during reaction phase (between t_{rob} and t_{cross}). 29

1.6 Example of the analysis of one of PosPos trials. 29

1.7 smpd plots for all the 243 trials, after resampling over the interaction time $[t_{rob}, t_{cross}]$. 30

1.8 Three examples of participant-robot trajectories, for PosPos (a), PosNeg (b) and NegNeg (c) category of trial. The part of the trajectory corresponding to the interaction $[t_{rob}, t_{cross}]$ is bold. Time equivalent participant-robot positions are linked by dotted line. 31

1.9 (a) Mean evolution of smpd for each category of trial ± 1 SD. (b) Time derivative of the mean smpd. 32

1.10 a) Comparison between initial and final values of smpd at t_{rob} and t_{cross} for all trials of each non-empty category (PosPos, PosNeg, NegNeg). A significant difference in values means that adaptations were made to the trajectory by the participant (**p<0.01, ***p<0.001). b) Comparison between initial and final values of smpd at t_{rob} and t_{cross} for all the trials of each subgroup of the PosPos category. c) Total variation for smpd over the interaction. d) Minimum distance observed between the robot and the participant at t_{cross}, with trial grouped by passing order of the participant. . 33

2.1 Experimental apparatus and task. The covered area was extended with respect to the previous work. 44

2.2 Experimental setup when robot is cooperative. The pedestrian moves from PSP to the gate through the MEZ. At 0.67m before crossing the gate, the actor is able to see the robot (t_{see}). In the following trial, the robot decelerates and passes behind the actor, going through VP1. The red robot and the red actor illustrate the hypothetical crossing configuration. 47

2.3 (a) smpd>0: The robot starts from RPS1, decelerates and turns right. (b) smpd<0: the robot starts from RPS1, accelerates and turns left. (b) smpd<0: the robot starts from RPS2, accelerates and turns right. 48

2.4 smpd plots for all the 278 trials, after resampling over the interaction time $[t_{rob}, t_{cross}]$. 50

2.5 Examples of participant and robot trajectories for each category of trial. The bold trajectory represents the interaction time $[t_{rob}, t_{cross}]$. 51

2.6 Mean evolution of smpd ±1 Standard Deviation for the three categories where the robot is passive. 52

2.7 smpd plots for all the 278 trials, after resampling over the interaction time $[t_{see}, t_{cross}]$. 54

2.8 Mean evolution of smpd ±1 the Standard Deviation (SD) for the three categories where the robot is cooperative. The category NegPos was not considered. 55

2.9 Examples of participant and robot trajectories for each category of trial. The bold trajectory represents the interaction time $[t_{see}, t_{cross}]$. 56

3.1 General overview of the system architecture. 64

3.2 Illustration of important intermediate postures of the human behavior: step with initiation of reaching, standing while opening of drawer, and reaching for the object. 65

3.3 Predictive planning of real human trajectories. Distances from the pelvis to the front panel of the drawer (green, yellow and red), and the distance between the front panel and the object (blue) for the ten trials (reproduced from [Mukovskiy 2015a]). (b) The result of the re-targeting process: human avatar and HRP-2 robot during drawer opening task. 66

3.4 Extracted source signals. 67

3.5 Architecture for the online synthesis of body movements using dynamic primitives, [Giese 2009a]. This figure represents the module "Kinematic Pattern Synthesis" (see page 74) 68

3.6 Scheme of the feedback loop used to control the humanoid robot HRP-2. $[v^{ref}, \omega^{ref}]$ are respectively the linear and angular velocity and $q^{upperbody}$ the upper body joint trajectories computed from the kinematic pattern synthesis. $q, \dot{q}, \ddot{q}$ are respectively the generalized position and velocity vectors computed using the Stack of Tasks (SoT). 74

3.7 (a) Off-line synthesized trajectories generated with the OpenHRP simulator. (b) The humanoid robot HRP-2 in LAAS-CNRS during the experiments. 75

3.8 Forces on the vertical axis (z) measured during the experiment. 77

4.1 Objective: to steer a vehicle through a door using only visual measures. The door is represented by two landmarks, F^L and F^R and the vehicle, represented as a directed point, has an on-board camera and is subject to nonholonomic constraints. 86

4.2 Elliptic coordinate system. Ellipses and hyperbolae intersect perpendicularly. 87

4.3 For any point $O_c = (x, z)$ there always exists a circle C_α passing through O_c and the projections in the motion plane of landmarks F^L and F^R. The angle at the circumference α is constant along C_α. Notice that, the tangent and perpendicular line in O_c to the hyperbola through O_c, intersect the X_W axis in points A and B, respectively. The segment $\overline{AB}$ is the diameter of circle C_α. 92

4.4 The bipolar coordinate system consists of two orthogonal bundles of circles. Starting from the same point O_c, circle $C_\alpha^\perp$ crosses segment $\overline{F^L F^R}$ in a point which is closer to the middle of the door than the one reachable by following the hyperbola through O_c. 93

4.5 Function $F(\tau, \hat{\alpha})$ for different values of $\hat{\alpha}$ and τ and $K = 1$. The minimum is at the origin, i.e. at the middle of the door. 96

4.6 Vector field obtained as the gradient of $F(\tau, \hat{\alpha})$ with $K = 1$. 97

4.7 Trajectories of the vehicle starting from the same initial configuration $q = (200, -50, 7\pi/6)$, for different values of a in the control law: $a = 40$ cm (the actual value), $a = 80$ cm (twice the actual value) and $a = 20$ cm (half of the actual value). 100

4.8 Simulations with the feedback control law in elliptic coordinates: trajectories of the vehicle without and with white Gaussian noise, representing continuous and dashed lines, respectively. The vehicle leaves a room in (a), (b) and enters a room from a corridor (c), by passing through a door. 101

4.9 Simulations with the feedback control law in bipolar coordinates: trajectories of the vehicle with and without white Gaussian noise, representing continuous and dashed lines, respectively. The vehicle leaves a room in (a), (b) and enters a room from a corridor (c), by passing through a door. 102
4.11 Experimental setup. 103
4.10 PT7137 camera 103
4.12 Experimental results obtained applying the control law in elliptic coordinates. The control parameters are $w = 0.0012$, $K = 0.7$ and $\lambda = 310$, an the average linear velocity $v = 0.3$ m/s. 108
4.13 Experimental results obtained applying the control law in bipolar coordinates. The control parameters are $K = 2$, $K_1 = 4$ and $K_\nu = 0.15$. Average linear velocity of 0.4 m/s. 109
4.14 Analysis of the FOV limits. 110

4.15 Some examples of trajectories with the same final orientation, generated by the control laws in elliptic and bipolar coordinates and by Humans. In (a), (b) and (c) the final orientation is 120 deg. (a) By elliptic coordinates. (b) By bipolar coordinates. (c) By humans (from, [Arechavaleta 2008] courtesy of the authors). 121

A.1 (a) The basic version of Robulab10 and (b) the one with the Pan–Tilt camera PT7137 mounted on the top used for the experiments. 125

List of Tables

1.1 Organization of the trials. 25

2.1 Organization of the trials 45
2.2 Statistical analysis results of the smpd data during t_{rob} and t_{cross} in the case that the robot is passive. The Wilcoxon signed-rank test was performed using Statistica v.8 51
2.3 Statistical analysis results of the smpd data during t_{see} and t_{cross} in the case that the robot is passive. The Wilcoxon signed-rank test was performed using Statistica v.8 54

A.1 Main technical features of Robulab10. 125

Introduction

FUTURISTIC visions of the world show humans and robots sharing the same environment at different levels of interaction. Fifty years ago the idea that autonomous systems could be active agents in the humans environment was just a dream realizable only in movies. However, in the last decades the scientific community has done huge improvements in this direction and robots are more and more integrated next to humans for supporting them in different kinds of tasks. Recently, the robotics community started to investigate what are the techniques to improve the performances of robots and, in particular, their acceptance in the human society. Probably inspired by the past science fictions, in which the robots had similar appearances and abilities than humans, scientists started to believe that one way to increase robot capabilities was to endorse them with human-like morphological characteristics and behaviors. For these reasons, an increasing number of studies focus on the analysis and the identification of principles, invariants and strategies used by a humans to daily interact with their environments. The development of robots is improved by the progressive evolution of technology, allowing the realization and control of more powerful and complex robots that look more and more like humans. Nowadays the design of humanoid robots, able to help humans and work with them in a real scenario, has became a very important scientific challenge.

The works described in this thesis are directed in such a direction. Assuming that the planning of human movements is optimal, we wanted to study human behaviors during walking tasks. Do we have implicit strategies when we interact with the surrounding environment? Do we act differently each time we have to avoid an obstacle or do we use implicit principles? What are the rules that drive us when we have to walk in a constrained environment like passing through a door? Can we identify and model them? When humans perform a simple action, is it really "simple" or is it made up with hierarchical sequence of sub-tasks? During this thesis we addressed these questions, basing our studies on the analysis of human walking behavior in different situations, with the aim of identifying the invariants of human movements and transfer them to robots.

A large part of the work done in this thesis was done within the framework of the European project KoroiBot. The aim of this project was to improve walking motions of humanoid robots in different scenarios, providing software tools based on mathematical models and methods, in particular optimization, and learning from human data. A more detailed description of the project is provided in the following section.

The European Project KoroiBot

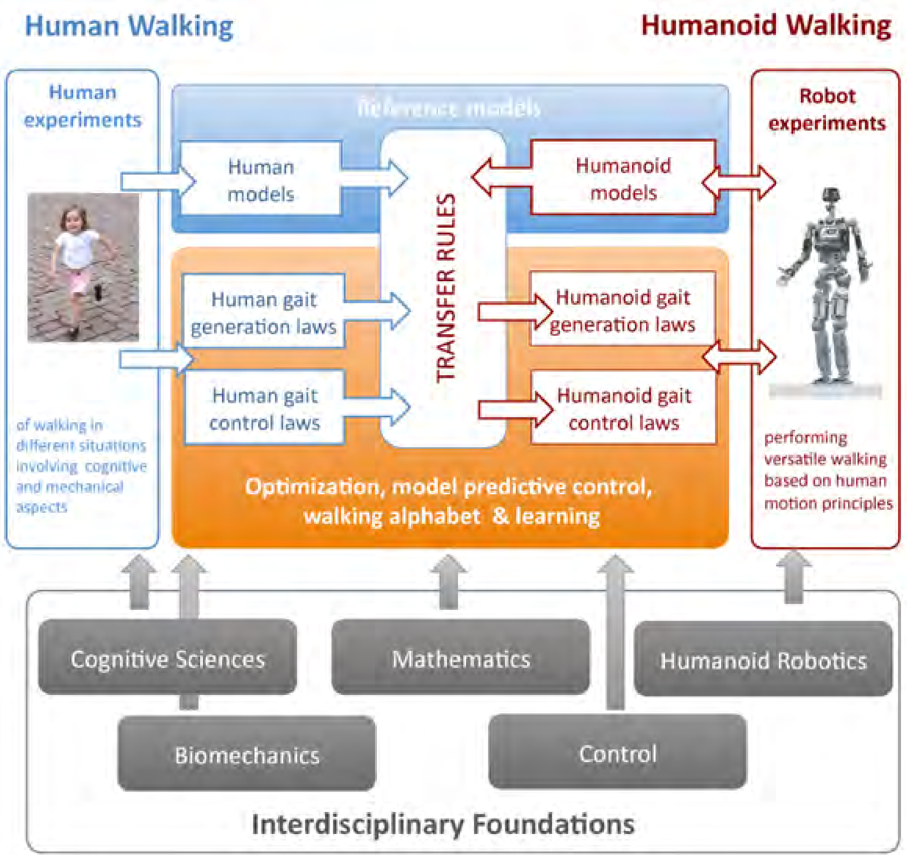
Human Walking
Humanoid Walking
Human experiments
Reference models
Human models
Humanoid models
Robot experiments
TRANSFER RULES
Human gait generation laws
Humanoid gait generation laws
Human gait control laws
Humanoid gait control laws
of walking in different situations involving cognitive and mechanical aspects
Optimization, model predictive control, walking alphabet & learning
performing versatile walking based on human motion principles
Cognitive Sciences
Mathematics
Humanoid Robotics
Biomechanics
Control
Interdisciplinary Foundations

Figure 1: Project components of KoroiBot and Interdisciplinary foundations.

The goal of the KoroiBot project is to enhance the ability of humanoid robots to walk in a dynamic and versatile fashion in the way humans do. Research and innovation work in KoroiBot mainly targets novel motion control methods for existing hardware, but also derives optimized design principles for next generation robots. The new software technologies are based on biological data, with the aim of increasing the performance of humanoid walking. Especially for humanoid robots with redundant degrees of freedom (DoF), optimization and learning might be solutions to make the redundancy a benefit rather than a burden. As depicted in Fig. 1, the project methodology can be divided into four pillars: (1) investigation of human walking by experiments, and related extraction of motion primitives by mathematical models and identification of walking principles; (2) development of adequate transfer rules; (3) development of novel optimization and learning based control approaches for humanoids walking, (4) integration of these algorithm on several robots (see Fig. 2). In order to test and evaluate the developed software, an interesting scenario consisting of different challenges for the humanoid robots was proposed (Fig. 3).

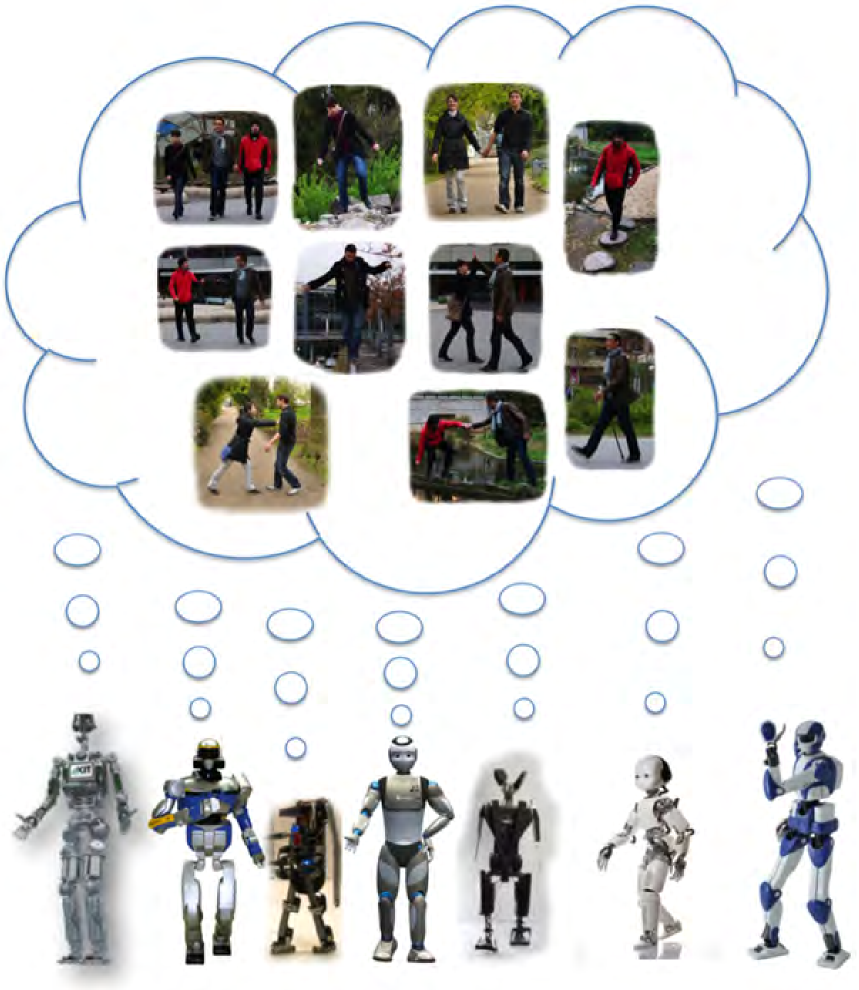
Figure 2: The seven humanoid robot platforms of the KoroiBot consortium dreaming of human walking capabilities.

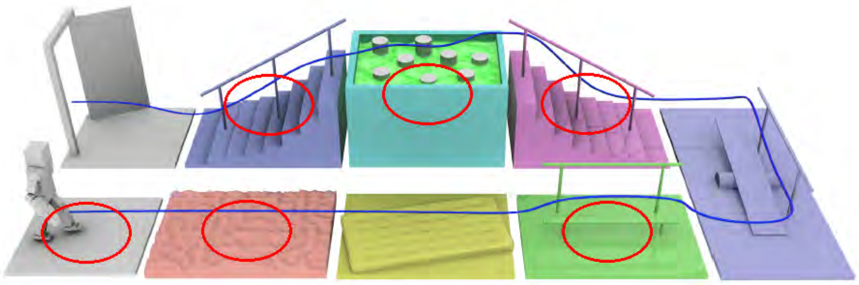
Figure 3: Challenges of the KoroiBot project. In red the challenges addressed by the LAAS-CNRS.

The work in the KoroiBot context

The European project KoroiBot is an interdisciplinary project. Each partner was assigned to different work packages (WP) focused on particular studies, as shown in Fig. 4. Among these WPs the work that I did during my thesis is related to WP1 and WP2. The former consisted to make different experiments for recording human walking data, aimed at the modeling and the developing of novel motion control laws inspired by biology. The latter targets to synthesize complex actions from sequences of elementary motor tasks and transfer them to the humanoid robots of the consortium.

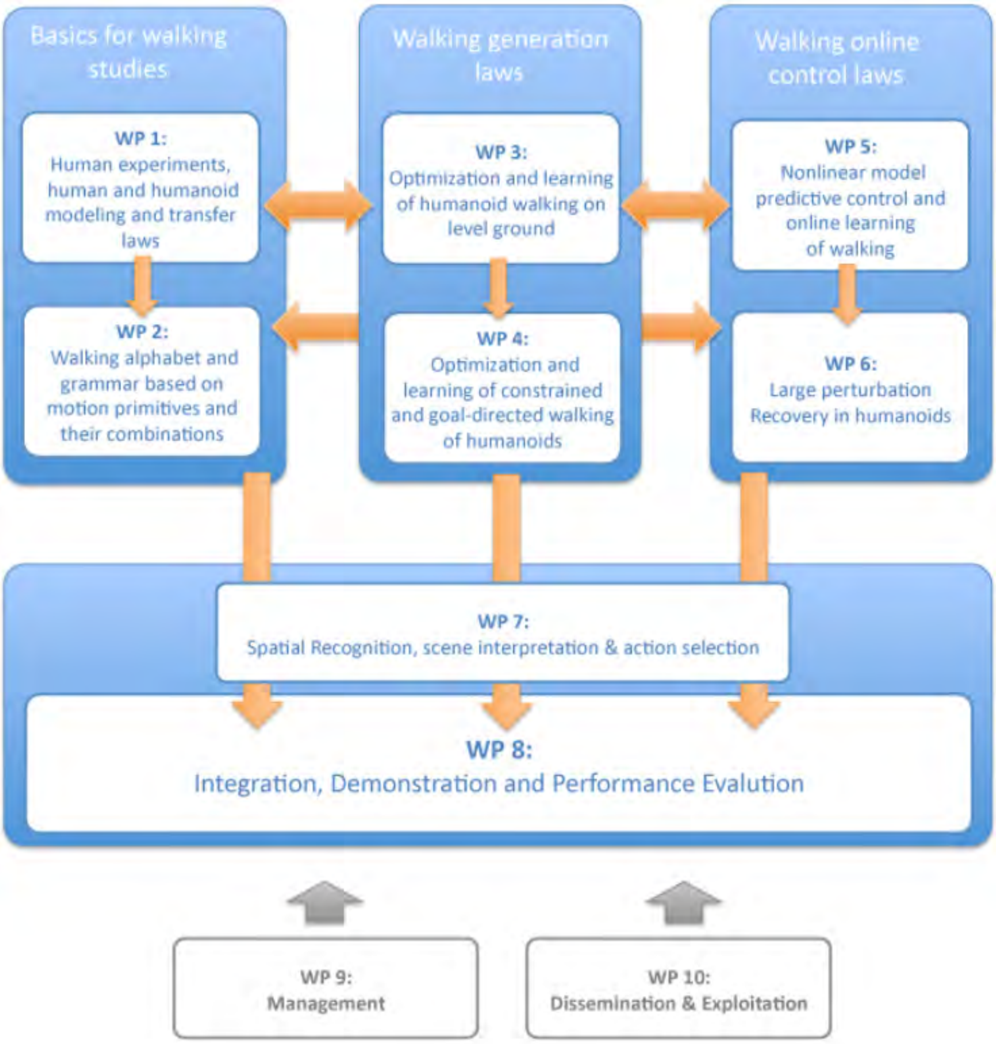
Basics for walking studies
WP 1: Human experiments, human and humanoid modeling and transfer laws
WP 2: Walking alphabet and grammar based on motion primitives and their combinations
Walking generation laws
WP 3: Optimization and learning of humanoid walking on level ground
WP 4: Optimization and learning of constrained and goal-directed walking of humanoids
Walking online control laws
WP 5: Nonlinear model predictive control and online learning of walking
WP 6: Large perturbation Recovery in humanoids
WP 7: Spatial Recognition, scene interpretation & action selection
WP 8: Integration, Demonstration and Performance Evalution
WP 9: Management
WP 10: Dissemination & Exploitation

Figure 4: Pert chart of the KoroiBot work packages and their interrelationships Our studies concerned WP1 and WP2.

Overview of the thesis

The work presented in this thesis is mainly focused on the analysis of human motion and the identification of human principles that can be transferred to robots for improving their capabilities. The manuscript can be roughly divided in two parts: the first one describes the studies that have been done in the context of the KoroiBot project. The second part presents a collaboration that has been done internally at LAAS-CNRS. The thesis is divided in four main chapters that can be summarized as follows:

- Chap. 1 and 2 : *Identification of walking strategies for avoiding a moving obstacle,*
- Chap. 3 : *Use of motion primitives to implement complex movements on humanoid robots,*
- Chap. 4 : *Vision-based control to pass through a door.*

An overview of each chapter is provided in the following sections.

Chapter 1

Title:	**How humans avoid moving obstacle crossing their way?**
Study:	*Identification of walking strategies for avoiding a moving obstacle*
Context:	KoroiBot project, WP1
Time:	during 1^{st} and 2^{nd} year
Collaborators:	INRIA-Rennes, MimeTIC research team and University of Rennes 2, M2S lab
People:	Anne-Hélène Olivier, Julien Pettré and Armel Crétual
Place:	LAAS-CNRS (Toulouse) and Campus de Ker Lann (Rennes)
Key Words:	Human direct-goal locomotion, Motion Capture System, Moving obstacle, Collision avoidance strategies, Passive Behavior

Summary

One of the first steps of this thesis was to analyze human walking motions during situations which could perturb the natural behavior of a person. With this aim, we decided to make experiments in which a pedestrian, that was walking calmly and naturally, was significantly disturbed. To this end, we wanted to introduce one or multiple external agents in the scenario, as obstacles, in order to record human reactions in terms of trajectory (speed and turning) and body organization (orientation of the feet, shoulders, head and the step frequency). In order to generate such a situation, the "obstacle" had to move. In particular, as we wanted to create precise and repeatable experiments, we chose to control a wheeled robot to impersonate the moving obstacle. Having in mind the related works on human locomotion, we found interesting the possibility to collaborate with specialists in this field. So, we started a productive partnership with researchers of INRIA-Rennes who, in their previous studies, had investigated the strategies set by two humans crossing each other or in a crowd scenario. In particular, the main idea was to compare the human strategies that our partners already identified, with the ones set to avoid a moving obstacle. Given their experience in human motion and our knowledge in robot control, we setup interesting experiments in which a moving obstacle had to perpendicularly cross the pedestrian path. The control algorithm allowed us to generate specific interactions that aimed to be as similar as possible to the ones observed between two humans. All the experiments took place in the Campus de Ker Lann which provides a huge gymnasium supplied with a motion capture system that perfectly matched our objectives. The recorded human data have been shared and uploaded in the KoroiBot database. After several tests we realized the ideal experimental setup: the robot starting position had to be hidden by some occluding walls otherwise the pedestrians were adapting too early; moreover, the wheeled robot had to be a fast and a robust object in order to perturb significantly the behavior of the participants. To help the reader to figure out the scenarios, an overview of them is shown in Fig. 5. In the following chapter, we will present experiments where the moving obstacle was controlled to behave passively (1). In this way, only the participant contributed to solve the collision.

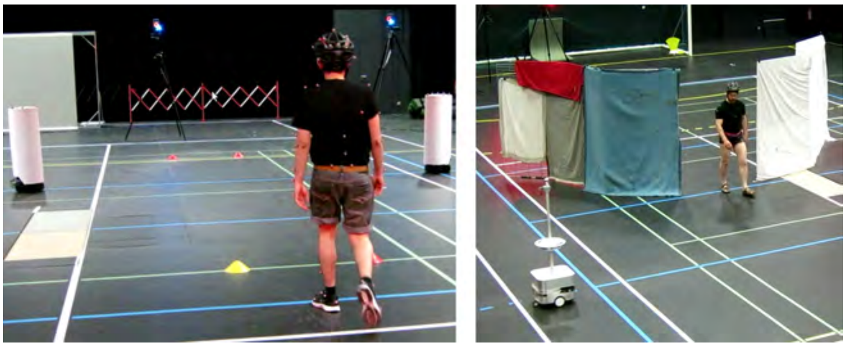

Figure 5: An overview of two different scenarios tested in this study. In the left picture, two TurtleBots dressed with some papers to make them look bigger. The participant had to walk straight and avoid them. In the right picture, we improved the experimental setup introducing some occluding walls and considering the wheeled robot Robulab that is faster and looks heavier. Each experimental setup, required at least one week of work to be realized and calibrated.

⚠ **Passive Behavior** (1)

In this manuscript we use the term "Passive Behavior" to indicate that the robot was controlled to move straight and at constant speed. The robot was not reacting to the adaptations performed by the participants.

Chapter 2

Title:	**Human and Robot interaction: cooperative strategies for collision avoidance.**
Study:	*Identification of walking strategies for avoiding a moving obstacle*
Context:	KoroiBot project, WP1
Time:	during 3^{rd} year
Collaborators:	INRIA-Rennes, MimeTIC research team and University of Rennes 2, M2S lab
People:	Anne-Hélène Olivier, Julien Pettré and Armel Crétual
Place:	LAAS-CNRS (Toulouse) and Campus de Ker Lann (Rennes)
Key Words:	Human direct-goal locomotion, Motion Capture System, Moving obstacle, Collision avoidance strategies, Reactive Behavior

Summary

Nowadays, the robotics community is putting a lot of effort on the development of robots that can perform tasks like humans and improve their capabilities in terms of energy consumption and precision. Clearly, in the future robots and humans will share the same spaces and they will have to adapt each others. Although humans adjust their behavior according the surrounding environment quite spontaneously, such a task is not trivial for robots. Moreover, ideally the movements of the robot should be optimized in order to make humans adapt more naturally. In this context, the study presented in this chapter is more based on the social aspects of human behavior. We believe that, in order to improve robot locomotion capabilities, it is important to analyze also the psychological aspects of the human behavior and not only the kinematic ones. In other word, we hypothesize that it is necessary to understand the rules behind the human strategies before transferring them. This could even help to simplify the modeling and the integration of human principles in complex systems as humanoid robots. Daily, walkers avoid each others in several different situations but they succeed such a task more or less in a similar way. We arose question like: are these strategies implicit? Can we define and transfer them? Can we optimize the way robots interact with humans? Can we make a walker behave more naturally in an environment in which there are autonomous system moving around him? This study aims to address these questions.

In the last year of this thesis, we decided to continue the previous collaboration with our partners of INRIA-Rennes. As already explained, in the previous experiments we controlled the robot to behave passively. However, we were interested to extend this work,

by controlling the robot in a more unpredictable way to perturb more considerably the innate walking of the pedestrians. To this end, in this second part we controlled the robot to behave reactively (2). We transferred the collision avoidance strategies observed in humans to the robot and we analyzed the human reactions. The main idea was to study the differences with respect to the case in which the robot behaves passively. Moreover, we wanted also to compare the avoidance strategies of the participants, in the case that the robot acts like a human, with respect to the ones observed between two pedestrians [Olivier 2013]. We reproduced the same experimental setup of the Chap. 1, improving the quality and the design of the experiments. We used the same robot platform. An overview of the scenario is shown in Fig. 6.

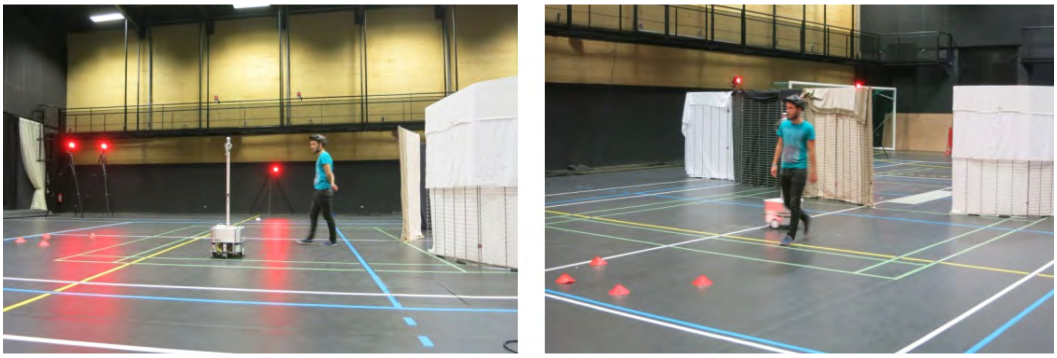

Figure 6: An overview of the experimental setup of the study presented in Chap. 2.

Reactive Behavior (2)

In this manuscript we use the term "Reactive Behavior" (or "Active Behavior") to indicate that the robot was controlled to positively contribute to the collision avoidance. In reactive mode, the robot predict human movements and it adapts its velocity and orientation in order to avoid the collision.

Chapter 3

Title:	**Learning Movement Primitives for the Humanoid Robot HRP-2**
Study:	*Use of motion primitives to implement complex movements on humanoid robots*
Context:	KoroiBot project, WP2
Time:	during 2^{nd} and 3^{rd} year
Partners:	University Clinic Tübingen, Department of Cognitive Neurology
People:	Albert Mukovskiy, Martin A. Giese
Place:	LAAS-CNRS (Toulouse)
Key Words:	Robotics, Goal-directed walking, Motion primitives, Walking pattern generator, Motor coordination, Action sequences

Humanoid robots are complex and redundant mechanical systems. One of the robotics community challenges is to create humanoid robots equipped with human features i.e. communication skills, walking capabilities, adaptation and reactive movements. However, humans and humanoid robots are really different in terms of size, geometrical proportions, velocity and acceleration limits, power and energy consumption. Human abilities are learned and improved by life experience and they are further improved everyday. For this reason, it is really challenging to find the way to transfer such advanced human capabilities to robots. However, recent studies on human motion have shown that complex actions can be represented as a sequence of motor primitives (3) [Flash 2005]. These motion primitives are hypothesized as being the "building bricks" of any action. Therefore, the main idea is that instead of analyzing and trying to reproduce human full-body complex motion, one should identify the "alphabet" of movements used by the brain. In other words, assuming that an alphabet of movements is known, it could be possible to compose any kind of complex movements as a sequence of contribution of simple letters that are the motion primitives.

In the framework of the KoroiBot project, the WP2 proposed to integrate complex motion strategies into locomotion control as simple sequences of individual steps or step phases, which mimic optimal behavior of humans. Based on some extracted primitives, techniques as machine learning and optimal control should be used to derive models and data, and transfer them to humanoid robots. In this context, we decided to consider walking-to-grasp movements and implement them on the humanoid robot HRP-2 at LAAS-CNRS.

In this chapter we will present a novel highly flexible approach to model complex movements based on an hierarchical use of motion primitives. These primitives can be combined in space and time and over multiple temporal scales. They are learned by biological kinematic data and then reformulated in a mathematical framework which allows their implementation in optimal control systems. The methods we used for learning the motion primitives are based on previous works done by our partners from Tübingen. They allow to decompose complex movements in terms of motion primitives, based on kinematic data [Giese 2009b, Mukovskiy 2013]. In this context, we proposed a whole body controller in which the upper-body movements are generated by a combination of such motion primitives whereas the lower body behavior is computed by a walking pattern generator.

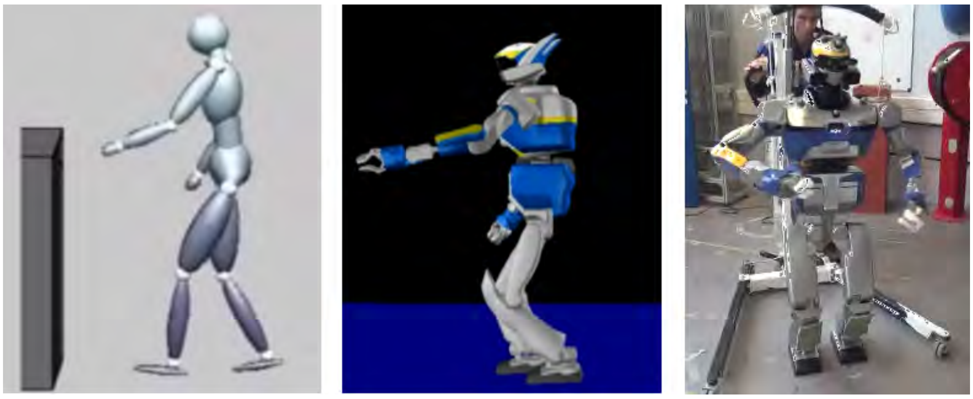

Figure 7: An illustrated overview of the work presented in Chap. 3. In the left, an avatar is reproducing some movements recorded from a human. In the center, an avatar of the humanoid robot HRP-2 is performing the same movements but in a realistic simulation. In the right, a snapshot of real experiments done with the robot HRP-2 at LAAS-CNRS.

Motion Primitives (3)

"Motion Primitives" (or "Motor Primitives") refer roughly to building blocks at different levels of the motor hierarchy. They do need to be universal and the same building block is not necessarily used for all the possible behaviors or tasks. Instead, they might be specific to only a particular representation of movements or tasks. The crucial feature is that many different movements can be derived from a limited number of motor primitives through appropriate operations and transformations, and that these movements can be combined through a well defined syntax of motion to generate more complex actions. An exhausting description of Motion Primitives, at different levels (behavioral, neural, muscle, kinematic and dynamic), has been provided by Tamara Flash [Flash 2005]

Chapter 4

Title:	**The geometry of confocal curves for passing through a door**
Study:	*Vision-based control to pass through a door*
Context:	Internal collaboration (LAAS-CNRS)
Time:	during 1^{st} and 2^{nd} year
Collaborator:	ERC Actanthrope
People:	Paolo Salaris, Jean-Paul Laumond
Place:	LAAS-CNRS (Toulouse)
Key Words:	Nonholonomic motion planning, Visual servoing, Wheeled robots

From the experience gained and the software developed to control a wheeled robot as a moving obstacle, we developed an internal collaboration at LAAS-CNRS within the framework of ERC Actanthrope. The aim of this work was to implement some vision-based control laws to steer a robot through a door by using advanced geometric parametrization provided by confocal curves. At the beginning we planned to implement this control on HRP-2, however given the difficulties to obtain accurate vision-based controls during walking on humanoid robots, we decided to initially test the algorithm into a nonholonomic wheeled robot equipped with a rigidly pinhole camera. We developed and implement control strategies to detect a door, identified by two landmarks attached to its vertical supports, and steer the vehicle to pass through it. We built around the door a planar geometry of bundles of hyperbolas, ellipses and orthogonal circles. The method is able to drive the robot to the goal by using static feedback control laws that are function of the current state of the system expressed in suitable coordinates. The originality of this work is that these new coordinates can be directly measured in the camera plane. Although the methods was implemented on a wheeled robot and not an anthropomorphic system, we found that the proposed approach had similarities with the strategy adopted by humans for passing through a door. An overview of the experimental setup is depicted in Fig. 8.

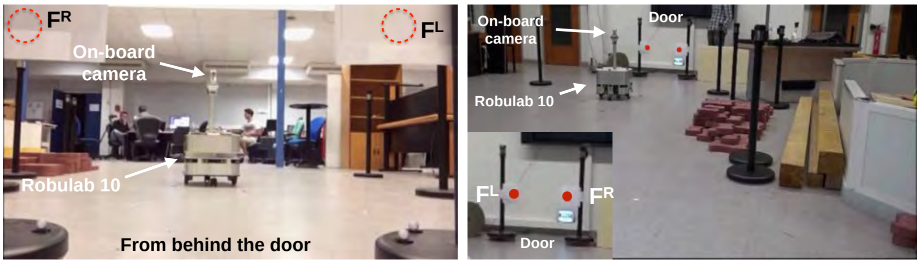

Figure 8: An overview of the experimental setup of the work shown in Chap. 4. The wheeled robot is the same as the one used for the works presented in Chap. 1– 2. The entire work was done at LAAS-CNRS.

Other contributions

During the three years of my thesis I also had some other minor contributions. They are rapidly described in this introduction but not further developed in the manuscript.

Recording human motion in the KoroiBot scenario

In the context of the Koroibot WP1, we participated with our project partners from University of Tübingen and University of Heidelberg to experiments for recording human movements in the KoroiBot scenario previously shown in Fig. 3. In all the experiments the body kinematics was recorded with 10 Vicon-MX cameras and the normal forces under the feed was collected with Pedar System. The participants were told to perform the following tasks: walking straight, walking stairs up and down forwards, walking on a soft mattress, walking on a beam forwards, walking on different slopes fast up and down, stepping stones with two different configurations, walking following a circular trajectory at different speed. An overview of the experiments is shown in the pictures above. An illustration of some experiments is provided in Fig. 9.

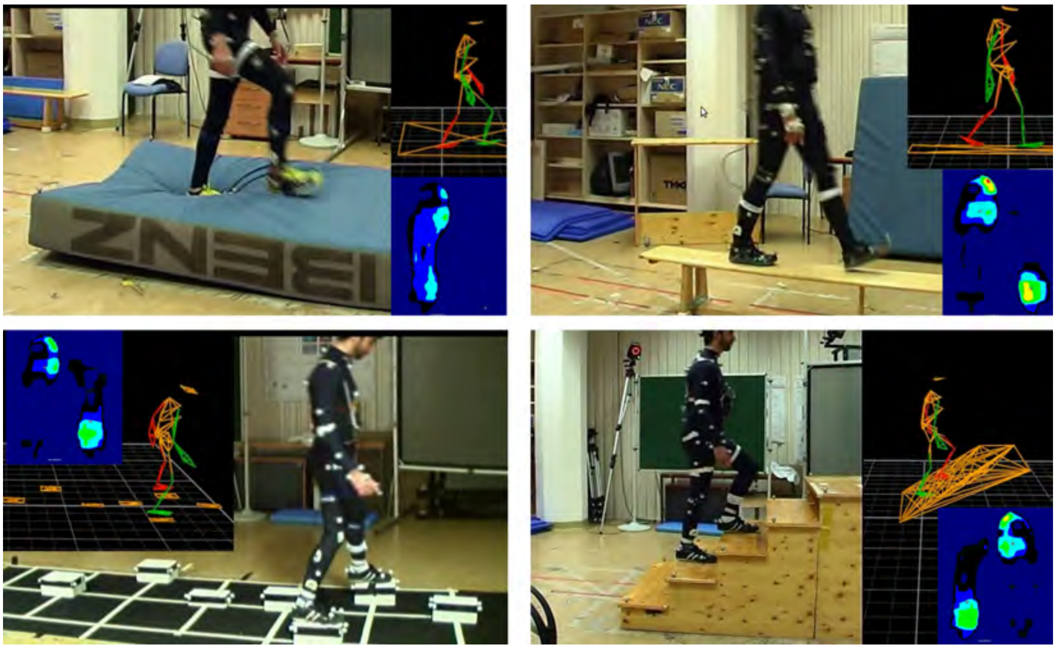

Figure 9: Illustration of four different tasks. From top-left to bottom-right: walking on a soft mattress, walking on a beam, stepping stones, walking stairs up. The kinematic data and the related normal forces are depicted in the smaller images.

A new tool for tracking HRP-2 with the motion capture system of LAAS-CNRS

Another minor contribution during this thesis has been done at the beginning of the first year. Supported by Airbus/Future of Aircraft Factory and CNRS, we presented a preliminary proof of concept aiming at introducing humanoid robots in an aircraft factory. The goal was to demonstrate the capabilities of HRP-2 to deal with three aspects needed in a factory: reactivity to the changes of the environment, visual feedback and on-line motion generation. In particular, the robot had to move from a random starting position to a predefined target, while avoiding a moving obstacle crossing its way (respectively the red pylon engine depicted in blue and the red moving toolbox in Fig. 10). In order to localize the position of the robot, the obstacle and the target in the environment, each of them were equipped with markers and tracked by a motion capture system (MoCap) in the area. My contribution was to find the transformation matrix that links the HRP-2 joint frames and the MoCap system. In other words, we determined a tool to express the position and the orientation of each joint frame of HRP-2 in the MoCap frame. Thanks to this tool, that it is still currently used, we have been able to make improvements for our laboratory setup. For example, it has been possible to implement an algorithm into the crane control system for an automatic tracking and following of the robot during the experiments in the area. Moreover, we used this tool also for the benchmark of KoroiBot. Through motion capture system, we evaluate the precision and the improvement of HRP-2 walking controls, comparing the expected configurations and the real ones in different trials of walking.

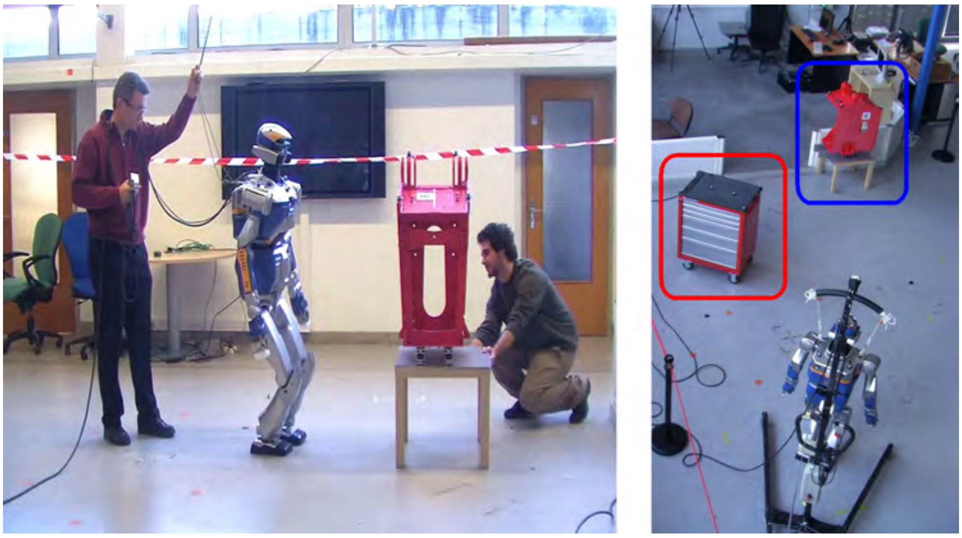

Figure 10: (Left) The robot is moving according to the position of the red pylon engine in order to maintain the same distance (1 meter). (Right) Situation of the experiment: the robot has to go in the vicinity of the pylon engine, depicted in blue, avoiding the red moving toolbox. The robot has to re-plan its path in real-time. In both cases, the robot is tracking the objects using the motion capture system.

Publications

Journal

Accepted

- C. Vassallo, AH. Olivier, P. Souères, A. Crétual, O. Stasse et Pettré J. *How do walkers avoid a mobile robot crossing their way?* Gate and Posture, vol. 51, pages 97 – 103, 2017

- P. Salaris, C. Vassallo, P. Souères et JP. Laumond. *The geometry of confocal curves for passing through a door*. IEEE Transactions on Robotics, vol. 31, no. 5, pages 1180–1193, 2015

Under review

- A. Mukovskiy, C. Vassallo, M. Naveau, O. Stasse, P. Souères et MA. Giese. *Adaptive synthesis of dynamically feasible full-body movements for the Humanoid Robot HRP-2 by flexible combination of learned dynamic movement primitives*. Robotics and Autonomous Systems, 2016. Corrected version under review

Conference

Accepted

- P. Salaris, C. Vassallo, P. Souères et J-P. Laumond. *Image-based control relying on conic curves foliation for passing through a gate*. In 2015 IEEE International Conference on Robotics and Automation (ICRA), pages 684–690. IEEE, 2015

- O. Stasse, F. Morsillo, M. Geisert, N. Mansard, M. Naveau et C. Vassallo. *Airbus/future of aircraft factory HRP-2 as universal worker proof of concept*. In 2014 IEEE-RAS International Conference on Humanoid Robots, pages 1014–1015. IEEE, 2014

- A Mukovskiy, C. Vassallo, M. Naveau, O. Stasse, P. Souères et Giese MA. *Learning Movement Primitives for the Humanoid Robot HRP-2*. In IEEE IROS 2015 Workshop on "Towards truly human-like bipedal locomotion: the role of optimization, learning and motor primitives". Hamburg, Germany, 2015

CHAPTER 1

How humans avoid moving obstacle crossing their way?

The work presented in this chapter was done in collaboration with biomechanists of the MimeTIC research team of Inria Rennes (French National Institute of Research in Computer Science and Control) and the "Movement, Sport and health Science" laboratory (M2S) in Rennes. A shorter description of this work can be found in [Vassallo 2017]. The aim of this collaboration was to analyze the human strategies to avoid collision with a moving obstacle. Having in mind previous results on human obstacle avoidance, as well as the main principles that they use for collision avoidance, we observe how humans adapt a goal-directed locomotion task when they have to interfere with a non collaborative mobile robot. Our results show differences in the strategy set by humans to avoid a robot in comparison with avoiding another human. The analysis is based on the concept of the risk of future collision distance estimated by the Minimal Predicted Distance, denoted by mpd [Olivier 2012]. mpd gives, for each time step, the future distance of closest approach between the human and the robot if both of them keep a constant speed and direction. Since the robot is controlled to move straight and at constant velocity, only the human walker is actively reacting to ensure collision avoidance. As an extension of this work, in the next chapter (Chap. 2), we will present experiments in which the robot is adapting its behavior to positively contribute to the collision avoidance.

1.1 Introduction

Robots and humans will share the same environment in a near future [Goodrich 2007, Kruse 2013]. To this end, roboticists must guarantee safe interactions between robots and humans during locomotion tasks. Our work goes a step further in this direction by studying how humans behave to avoid a moving robot.

There is an extensive literature describing how walkers avoid collisions. Several studies considered how walkers step over [Patla 2006] or circumvent [Vallis 2003] static obstacles. More recent ones focused on how humans avoid each other. It was shown that walkers are able to predict the risk of collision since they adapt their motion only if the future crossing distance is below a certain threshold [Olivier 2012]. This future distance is increased ahead of the crossing point and maintained constant during a regulation phase, demonstrating anticipation in avoidance [Olivier 2012]. Trajectory adaptations are performed both in speed and orientation [Huber 2014, Olivier 2012]: they depend on the crossing angle and the walking speed [Huber 2014]. These strategies do not maximize smoothness [Basili 2013], they result from a compromise between safety guarantee and energy minimization [Jansen 2011]. Moreover, these adaptations depend more on situations than personal characteristics [Knorr 2016].

The crossing order during collision avoidance is an interesting parameter to consider. Indeed, it has been shown that trajectory adaptations are collaboratively performed [Olivier 2012] but are role-dependent. The walker giving way (2nd at the crossing) contributes more than the one passing first. This role attribution appears to contribute positively before the interaction [Knorr 2016, Olivier 2013] and can be predicted with 95% confidence at almost 2.5m before crossing, even before any adaptation [Knorr 2016].

Studies resulted into simulation models of navigation and interaction. Warren and Fajen [Warren 2008] proposed to model the walker and the environment as coupled dynamical systems: the walker paths result from all the forces acting on them, where goals are considered as attractors and obstacles as repellors. This model is based on the distance to the goal and to the obstacles as well as the sign of change of the bearing angle. An integration of the bearing angle theory into some artificial vision system for crowd simulation was proposed by Ondrej et al. [Ondrej 2010].

These previous studies reached common conclusions about the human ability to accurately estimate the situation (crossing order, risk of collision, adaptations), and considered interactions with a moving objects. The kinematics of adaptations by a walker avoiding a moving obstacle (a mannequin mounted on a rail) are studied in [Cinelli 2007, Cinelli 2008, Gérin-Lajoie 2005]. Trajectories crossing at $45°$ resulted into adaptations both in the antero-posterior and medio-lateral planes, with successive anticipation and clearance phases [Gérin-Lajoie 2005]. Analysis is based on the notion of personal space modeled as a free elliptic area around each walker. When trajectories are colinear (the mannequin comes from the front), a 2-step avoidance strategy is observed: participants first adapt their locomotion in heading, then by speed [Cinelli 2008]. Moreover, the obstacle velocity influences the lateral rate of change of the walker trajectory [Cinelli 2007]; the slower the velocity, the lower the lateral rate of change. These experiments with mannequins were not designed to study the question of the crossing order. Other studies investigated human interactions with robots. It was shown that it is easier to understand and predict the behavior of robots if they are human-like [Carton 2013, Lichtenthäler 2013]. Some studies demonstrated that human-like behaviors [Dragan 2015, Kato 2015] improve on many levels the performance of human-robot collaboration. Nevertheless, the benefit of programming a robot with human-like capabilities to move and avoid collision with a human walker has not been demonstrated yet.

The chapter is structured as follows. Firstly, we recall the meaning of Minimal Predicted Distance. Then we present our approach in which a moving robot has to interfere with a pedestrian. The experimental setup is detailed in Section 1.3. In Section 1.4 we show how to control the robot to reproduce similar kinematic condition of interaction than the ones studied in [Olivier 2012] (in terms of relative angle, position, and velocities) and we apply a similar analysis in Section 1.5. While the nature of the interaction is changed, our results show differences in the strategy set by humans to avoid a robot in comparison with avoiding another human (Section 1.6 and Section 1.7). Finally we will see in Section 1.8 how humans prefer to give the way to the robot even when they are likely to pass first at the beginning of the interaction.

1.2 Minimal Predicted Distance

As explained before, the crossing configuration and the risk of future collision were estimated by the Minimal Predicted Distance, noted mpd [Olivier 2012]. In other world, the mpd functions provides information about the risk of collision: the smaller the mpd, the higher the risk of collision. For each time step, its value correspond to the future distance of closest approach if both the robot and the participant keep a constant speed and direction. Thus, as the robot is moving straight at constant speed (in the time phase of the experiments which are presented in this chapter), a variation of mpd means that the participant is performing adaptations. In other words, collision avoidance could be analyzed with respect to the variation of speed v and the orientation θ during the reaction phase (see Figure 1.1). In order to identify what were the main adaptations (accelerating/decelerating or turning), we partially derived the mpd function. Indeed, denoting by θ_1 and s_1 the instantaneous orientation and speed of participant #1 (θ_2 and s_2 for #2 respectively) and $X = (a, b)$ the relative position of participant #2 with respect to #1, the mpd turns on to be a function of all these variables:

$$mpd = f(a, b, \theta_1, s_1, \theta_2, s_2) \tag{1.1}$$

For any of the 6 parameters $\in \{a, b, \theta_1, s_1, \theta_2, s_2\}$, the instantaneous individual effect of p, in the mpd, can be expressed by the following partial derivative:

$$\varepsilon_p = \frac{\partial mpd}{\partial p} \cdot dp = \frac{\partial f}{\partial p} \cdot dp \tag{1.2}$$

The total instantaneous effect $\bigtriangledown f$ of the 6 parameters is then:

$$\bigtriangledown f = \varepsilon_a + \varepsilon_b + \varepsilon_{\theta_1} + \varepsilon_{\theta_2} + \varepsilon_{v_1} + \varepsilon_{v_2} \tag{1.3}$$

As an extension of the previous works [Olivier 2012, Olivier 2013], we introduced a signed definition of the mpd, noted smpd. The sign of this function depends on who, among the human and the robot, is likely to pass first or give way to the other participant. Further details will be treated in Section 1.5.

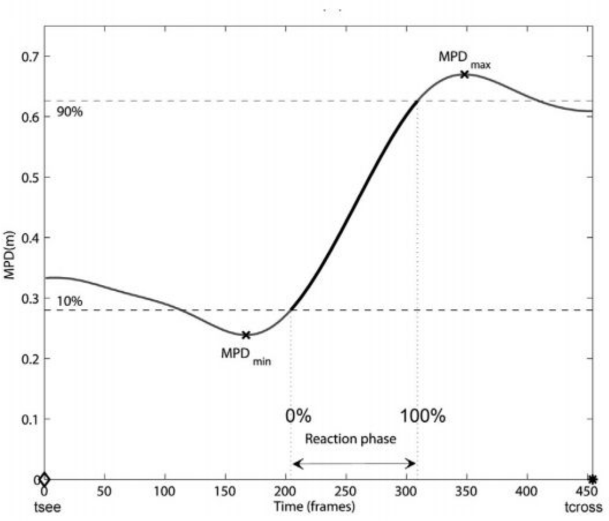

Figure 1.1: Illustration of the mpd evolution during the reaction phase between two humans crossing each other [Olivier 2012]. We defined t_{see} *as the instant of time in which the participant starts to see the other one, and* t_{cross} *as the crossing time. From the picture, we observe that the mpd at* t_{see} *is around 0.32m, that means the participants will not collide but they are going to pass near to each other. Once the Reaction phase starts, the mpd is increasing because one of the participants (or perhaps both of them) is reacting to increase the future distance at* t_{cross}*. In the end of the reaction phase, the mpd is around 0.7m.*

1.3 Materials and Methods

Participants

Seven volunteers participated in the experiment (1 woman and 6 men). They were 26.1 (± 5.4) years old and 1.78m tall (±0.21). They had no known vestibular, neurological or muscular pathology that would affect their locomotion. All of them had normal or corrected sight and hearing. Participants gave written and informed consent before their inclusion in the study. The experiments respect the standards of the Declaration of Helsinki (rev. 2013), with formal approval of the ethics evaluation committee Comitè d'Evaluation Ethique de l'Inserm (IRB00003888, Opinion number 13-124) of the Institut National de la Santé et de la Recherche Médicale, INSERM, Paris, France (IORG0003254, FWA00005831). All the participants were equipped with a full body marker set (53 markers) (see Figure 1.2a). They were located following the standard marker placement of Koroibot project [1].

---

[1] $https : //koroibot - motion - database.humanoids.kit.edu/marker_set/$

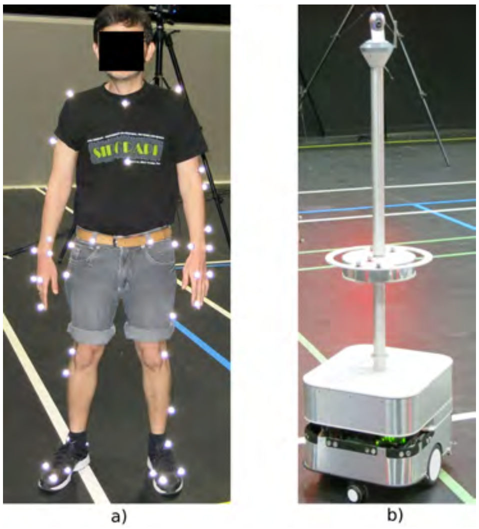

Figure 1.2: a) One of the participants equipped with the full body marker set. b) the mobile robot Robulab10.

Apparatus

The experiment took place in 50m x 25m gymnasium. The room was separated in two areas by 2m high occluding walls forming a gate in the middle. An overview of the experimental setup is shown in Figure 1.3. Four specific positions were identified: the participant starting position PSP, the participant target PT, and two robot starting positions RSP1 and RSP2. A specific zone between PSP and the gate is named Motion Estimation Zone MEZ. MEZ is far enough from PSP for the participants to reach their comfort velocity before entering the MEZ. The intersection point of the robot path [RSP1, RSP2] and the participant path [PSP, PT] is named Hypothetical Crossing Point HCP. It is computed hypothesizing that there is no adaptation of the participant trajectory.

Participant Task

Participants were asked to walk at their preferred speed from PSP to PT by passing through the gate. They were told that an obstacle will be moving over the gate and could interfere with them. One experimental trial corresponds to one travel from PSP to PT.

Recorded Data

3D kinematic data were recorded using the motion capture Vicon-MX system (120Hz). Reconstruction was performed using Vicon-Blade and computations using Matlab (Mathworks ®). The experimental area was covered by 15 infrared cameras. The global position of participants was estimated as the middle point of reflective markers set on the shoulders

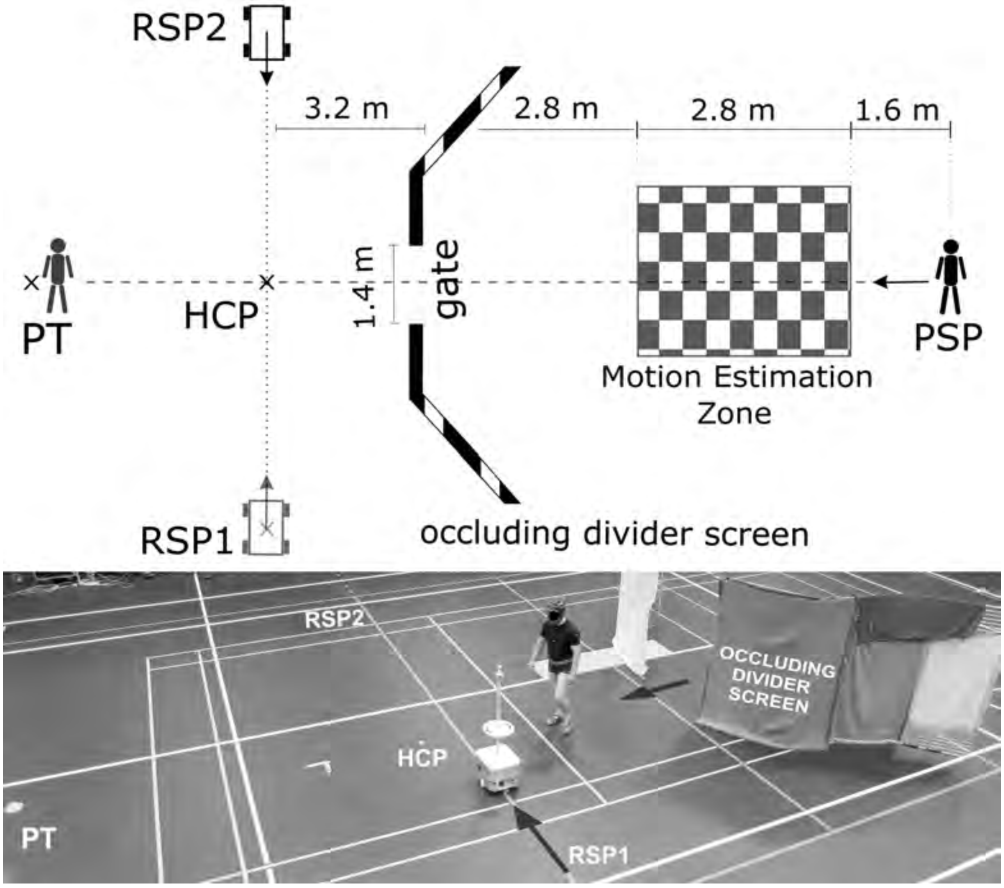
RSP2
3.2 m
2.8 m
2.8 m
1.6 m
1.4 m
gate
PT
HCP
PSP
Motion Estimation Zone
RSP1
occluding divider screen
RSP2
OCCLUDING DIVIDER SCREEN
HCP
PT
RSP1

Figure 1.3: Experimental apparatus and task. In this trial the robot was moving from RSP1 to RSP2. Participant decided to pass behind the robot.

(acromion anatomical landmark, LSHO-RSHO). The stepping oscillations were filtered out by applying a Butterworth low-pass filter (2nd order, dual pass, 0.5Hz cut-off frequency).

Experimental plan

Each participant performed 40 trials (see Table 1.1). Robot starting position (50% in RSP1, 50% in RSP2) was randomized among the trials. To introduce a bit of variability, in 4 trials the robot did not move and the participant did not have to react. Only the 36 trials with potential interaction were analyzed.

Robot Behavior

We used a prototype of RobuLAB10 wheeled robot from the Robosoft company (dimension: 0.45 x 0.40 x 1.42m, weight 25 Kg, maximal speed around 3 m/s) (see Figure 1.2b). The robot position was detected as the center point in its base (more details are given in

Table 1.1: Organization of the trials.

Trial	Robot Moving	RSP	MPD	Trial	Robot Moving	RSP	SMPD
1	Yes	Right	0.8	21	Yes	Left	-0.1
2	Yes	Left	0.8	22	No	Left	– –
3	Yes	Right	0	23	Yes	Right	0.1
4	Yes	Right	0.1	24	Yes	Left	0.1
5	Yes	Right	1.2	25	Yes	Left	-0.8
6	No	Right	– –	26	Yes	Left	1.2
7	Yes	Left	0.1	27	Yes	Left	-0.3
8	No	Right	– –	28	Yes	Left	1.2
9	Yes	Right	-0.3	29	Yes	Right	0.8
10	Yes	Left	0.3	30	Yes	Right	0.3
11	Yes	Left	-0.3	31	Yes	Right	-0.1
12	Yes	Left	0	32	Yes	Left	0
13	Yes	Left	0.8	33	Yes	Left	-0.1
14	Yes	Right	0	34	Yes	Right	1.2
15	Yes	Left	-1.2	35	Yes	Right	0.3
16	Yes	Left	-1.2	36	Yes	Left	0.3
17	Yes	Right	-1.2	37	Yes	Left	-0.8
18	No	Left	– –	38	Yes	Right	-0.8
19	Yes	Right	-0.8	39	Yes	Right	-0.1
20	Yes	Right	-0.3	40	Yes	Right	-1.2

Section 1.4). We programmed the robot to execute a straight trajectory between RSP1 and RSP2 at constant speed (1.4 m/s). The robot was controlled to generate specific interactions with the participant. In particular, the robot was either: a) on a full collision course (reach HCP at the same time than the participant), b) on a partial collision course (the robot reaches HCP slightly before or after the participant), or c) not on a collision course. To this end, we measured the participants speed through MEZ and estimated the time t_{hcp} at which HCP was reached. We deduced the time t_{rs} at which the robot should start to reach HCP at t_{hcp}. We finally added an offset $\triangle t$ to t_{rs} in order to obtain the desired interactions based on mpd values selected from the range [-1.2m, 1.2m]. Although the sequence of interactions was pre-defined in the remote control station (see Table 1.1), the participants were unaware about it. Each trial was repeated twice.

At the beginning of each trial, the software read the respective line of the table above. The robot starting position was initialized based on the robot velocity (set as constant) and the walker speed. To estimate the latter we used a Kalman Filter, modeling the walker as a material point moving along a line at constant speed (no acceleration). Tests have shown that participant velocity was almost constant in MEZ, then such an approximation was sufficient to reliably estimate the gait speed.

1.4 Obstacle Control

The robot position was tracked using a Vicon motion capture system. The robot position was computed as the centroid of seven markers fixed on its base. The remote control station was an external computer, communicating with the robot platform and the motion capture software through Wi-Fi. The exchange of data between the control station and the Vicon system was established by the ROS Hydro package *vicon_bridge* [2] which contains the driver needed for the communication. The robot was controlled by the remote station though an UDP connection. Further details about the low-level control of the robot Robulab are provided in Appendix A.

An overview of the experiment was shown in the previous section. The participant had to walk straight, from PSP to PT, pass through the gate and avoid a moving obstacle. The middleware ROS Hydro was used to interface the robot with the motion capture system and the remote control station. In order to guarantee accuracy and reliability of the experiments, a virtual robot with reference behavior was defined to plan the collision. Since obstacle velocity was set as constant (1.4 m/s), the initial position of the virtual robot changed according to the walker gait speed. In other words, the mobile obstacle was controlled in order to follow precisely the behavior of a virtual robot designed to obtain the desired crossing situation. Tracking control was considered for this task.

A right-handed reference frame *W* with origin in O_w and axes X_w and Y_w is attached to the plane of the robot motion. The configuration of the vehicle is described by $q(t) = (x(t), y(t), \theta(t))$, where $(x(t), y(t))$ is the position in *W* of a reference point of the vehicle and $\theta(t)$ is the orientation with respect to X_w. Denoting by $v(t)$ and $\omega(t)$ the forward and angular velocities, the kinematics is:

$$\begin{pmatrix} \dot{x} \\ \dot{y} \\ \dot{\theta} \end{pmatrix} = \begin{pmatrix} cos\theta & 0 \\ sin\theta & 0 \\ 0 & 1 \end{pmatrix} \begin{pmatrix} v \\ \omega \end{pmatrix} \tag{1.4}$$

The tracking problem, under the assumption that the robot velocity never vanishes, is to find a feedback control law such that the configuration $q(t)$ of the real robot matches the one $q_r(t)$ of the virtual robot. The error $e(t) = q(t) - q_r(t)$ can be written as:

$$e = \begin{pmatrix} e_1 \\ e_2 \\ e_3 \end{pmatrix} = \begin{pmatrix} cos\theta & sin\theta & 0 \\ -sin\theta & cos\theta & 0 \\ 0 & 0 & 1 \end{pmatrix} \begin{pmatrix} x_r - x \\ y_r - y \\ \theta_r - \theta \end{pmatrix} \tag{1.5}$$

---

[2] $http://wiki.ros.org/vicon\_bridge$

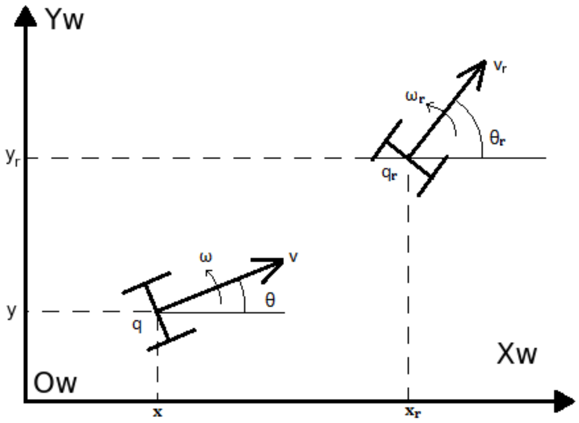

Figure 1.4: Representation of the tracking problem.

In [Zheng 1994] the authors have proposed the follows change of inputs

$$u_1 = -v + v_r \cos e_3$$
$$u_2 = \omega_r - \omega$$

and proved that the following nonlinear feedbacks make the error $q(t) - q_r(t)$ converge to zero

$$u_1 = -k_1(v_r, \omega_r)e_1$$
$$u_2 = -k_4 v_r \frac{\sin e_3}{e_3} e_2 - k_3(v_r, \omega_r)e_3$$

where k_4 is a positive constant and k_1, k_3 are continuous functions of v_r and ω_r, strictly positive. The starting point of the virtual robot changed according to the gait speed of the actor. Considering s as the distance between RSP and HCP, and v_g as the average walking speed of the participant, it is possible to determine the time needed by the walker to reach HCP (t_{cross}). Defining this interval as Time To Contact TTC, we obtain:

$$TTC = \frac{s + mpd}{v_g} \tag{1.6}$$

Since the robot needs time to reach a constant velocity, it was starting to move before the participant crossed the gate. In this way, the obstacle was perceived to move at constant speed. In order to guarantee that the tracking was feasible, the following condition needed to be satisfied: if the virtual robot was slightly ahead to the real one, the latter started to follow the former. Without this control, the real robot was moving backward. However, a considerable acceleration was required at the beginning to quickly minimize the error components e_1 and e_2.

1.5 Analysis

Signed Minimal Predicted Distance

As an extension of the previous works [Olivier 2012, Olivier 2013], we introduced a signed definition of the mpd, noted smpd. The sign of this function depends on who, among the participant and the robot, is likely to reach HCP first (still assuming constant motion). smpd is positive if the participant should arrive first or negative otherwise. A change of sign of smpd means that the future crossing order between the robot and the participant is switched. Our study focuses on the section of data when adaptations are performed: smpd is normalized in time by resampling the function at 100 intervals between t_{rob} (time 0%) and t_{cross} (time 100%). Quantity of adaptation is computed as the absolute value of the difference between smpd(t_{rob}) and smpd(t_{cross}). This extension was needed because it was observed that in human-human interaction the participants were always respecting the crossing order and no switch of mpd sign occurred.

Kinematic data

For each trial we computed t_{rob}, the time at which the robot reaches its constant cruise speed (when the acceleration amplitude was below a fixed threshold, 0.003 m/s^2), and t_{cross}, the time of closest approach between the participant and the robot. We decided to consider t_{rob} instead of t_{see} (the instant of time in which the participant crossed the gate) because of the robot did not reach its steady state velocity at t_{see} yet. Such a variation of velocity influenced too much the initial value of mpd, entailing wrong results. An example of the kinematic data for one of the trials is shown in Figure 1.5. By combining the trajectories shown in Figure 1.5a and the velocity profiles in Figure 1.5b, it is possible to deduce that the participant decided to decelerate and turn left, giving way to the robot. This hypothesis is confirmed by Figure 1.5c in which the mpd components gave us information about the main strategy adopted. Since the robot is moving straight at constant velocity, its components are almost equal to zero (no contribution). Analyzing the pedestrian ones, we deduce that the pedestrian mainly solves the collision by firstly decelerating (velocity component), then turning. From Figure 1.5d, we can conclude that the participant was slightly in advance with respect to the obstacle (smpd(t_{trob})= 0.12), however he decided to decelerate and after turning to give way to the robot and pass behind with a distance of 0.49 meter (smpd(t_{cross}) $\backsimeq$ -0.48). The hypothetical smpd was 0.1. Another example of the kinematic data is reported in Figure 1.6. In this trial, the actor is in advance with respect to the robot. Indeed, smpd at time t_{cross} is 0.78m (hypothetical smpd equal to 0.8m). During the reaction phase, the participant decides to keep the crossing order and then pass

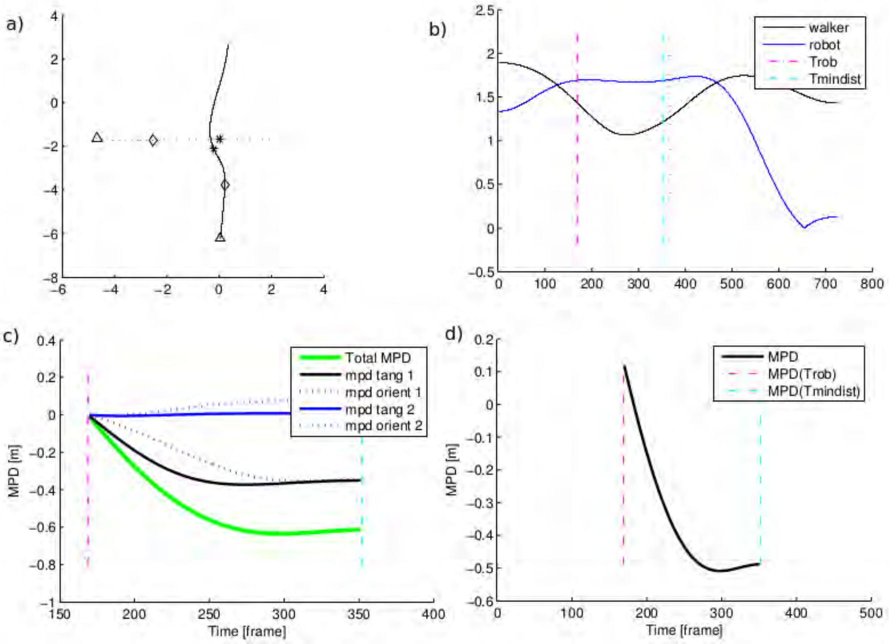

Figure 1.5: Example of the analysis of one trial in which a switch of mpd sign occurred. a) robot and pedestrian trajectories during the trial: triangles and star points are their position at t_{rob} and t_{cross} respectively. b) velocity profile of the walker and the obstacle. c) mpd components. d) mpd evolution during reaction phase (between t_{rob} and t_{cross}).

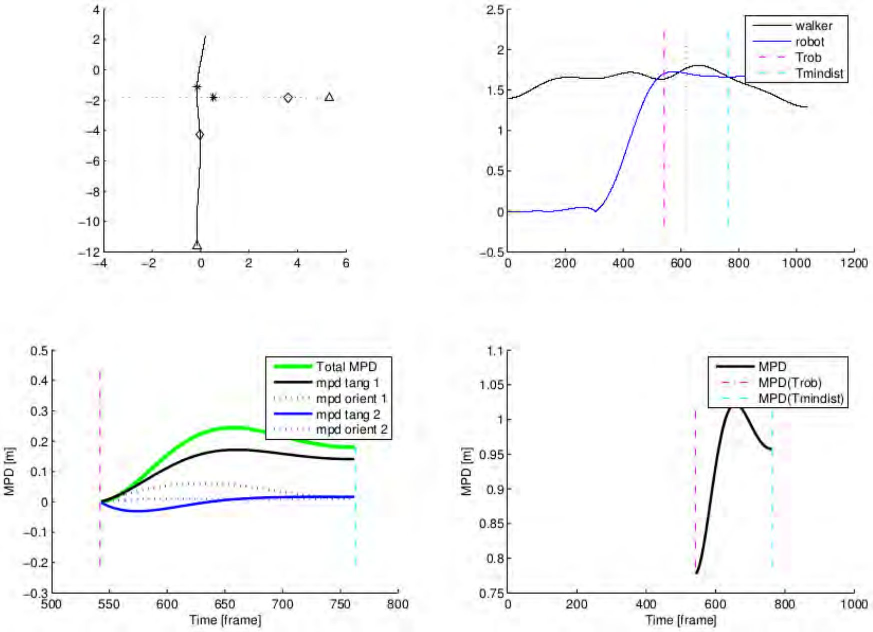

Figure 1.6: Example of the analysis of one of PosPos trials.

in front of the robot. Although the participant is sufficiently in advance to keep constant his strategy, he decided to accelerate and slightly turn in order to increase the crossing distance to 0.96m. In almost all the trials PosPos in which smpd(t_{cross}) is lesser than one meter, we observed such kind of reaction to increase the future distance. This aspect will be further analyzed in the discussion section.

Statistics

Statistics were performed using Statistica (Statsoft ®). All effects were reported at p<0.05. Normality was assessed using a Kolmogorov-Smirnov test. Depending on the normality, values are expressed as median (M) or mean ± SD. Wilcoxon signed-rank tests were used to determine differences between values of mpd at t_{rob} and t_{cross}. The influence of the crossing order evolution on the smpd values was assessed using a Kruskal-Wallis test with post hoc Mann-Whitney tests for which a Bonferroni correction was applied: all effects are reported at a 0.016 level of significance (0.05/3). Finally, we used a Mann-Whitney test to compare the crossing distance depending on the final crossing order.

1.6 Results

We considered 243 trials because 9 of the 252 were removed, as the robot failed to start. Figure 1.7 depicts the evolution of smpd for all trials. The sign of smpd at t_{cross} shows that the participants passed first in 42% of all the trials, they gave way in the 58% of other

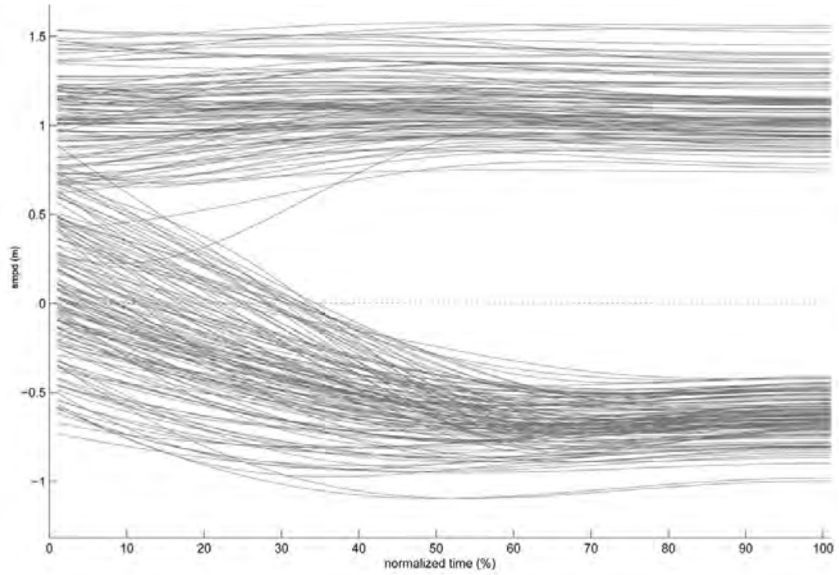

Figure 1.7: smpd plots for all the 243 trials, after resampling over the interaction time [t_{rob}, t_{cross}].

cases. Combining this information with the sign of smpd at t_{rob} (beginning of interaction), we could evaluate if participants switched their role during interaction, i.e., change the crossing order. We divided trials into four categories depending on the sign of smpd at t_{rob} and at t_{cross}: PosPos, NegNeg, PosNeg and NegPos. For example, the PosNeg category is for trials with smpd(t_{rob})>0 and smpd(t_{cross})<0.

All the trials are distributed among those categories in the following way: PosPos=104 trials (43%), NegNeg=69 trials (28%), PosNeg=70 trials (29%), NegPos=0 trials (0%). Examples of corresponding trajectories for each category are illustrated in Figure 1.8. In 29% of cases, participants were likely to pass first at the crossing point but adapted their trajec-

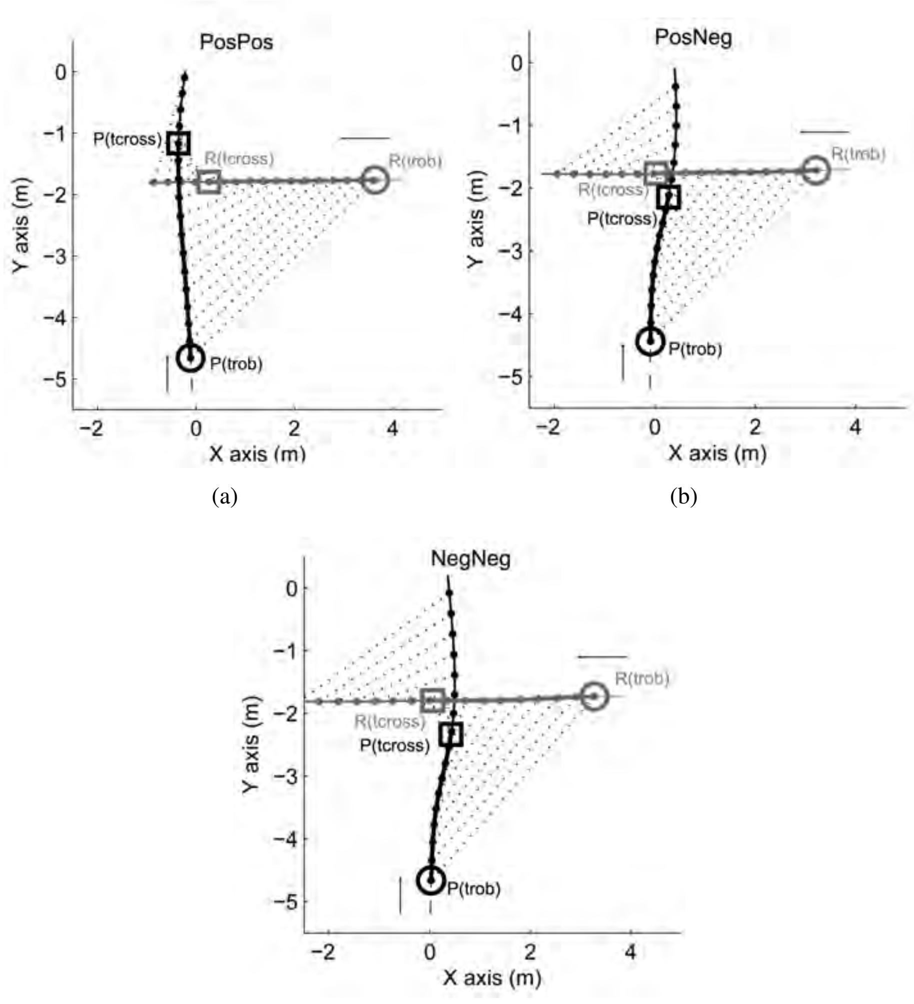

(a)

(b)

(c)

Figure 1.8: Three examples of participant-robot trajectories, for PosPos (a), PosNeg (b) and NegNeg (c) category of trial. The part of the trajectory corresponding to the interaction [t_{rob}, t_{cross}] is bold. Time equivalent participant-robot positions are linked by dotted line.

tory to finally give way to the robot. However, the opposite case for which the participant would be likely to give way and finally would pass first was never observed. The mean evolution of smpd in each category is shown in Figure 1.9a and its time derivative in Figure 1.9b. From these curves we can distinguish the reaction period from the regulation one as defined by [Olivier 2012]. They respectively correspond to periods during which participants perform adaptations (smpd varies) or consider collision to be avoided (the derivative

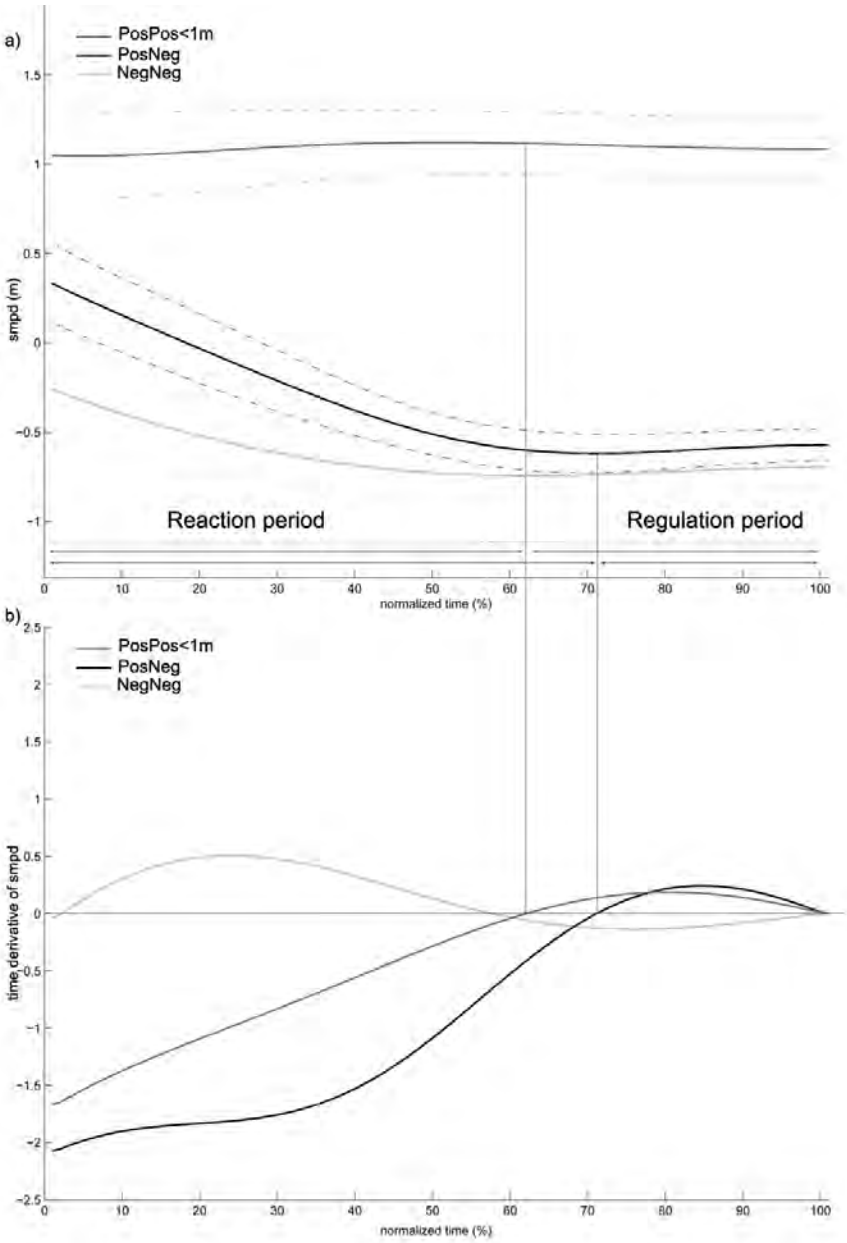

Figure 1.9: (a) Mean evolution of smpd for each category of trial ±1 SD. (b) Time derivative of the mean smpd.

is null, and may even variate in the opposite direction).

Figure 1.10 shows comparisons between smpd(t_{rob}) and smpd(t_{cross}), as well as distances of closest approach with respect to each of the three non-empty categories, and the crossing distance depending on the crossing order.

PosPos Trials

Difference between smpd at t_{rob} (1.05m) and at t_{cross} (1.04m) is at the limit of significance (p=0.052) (cf Figure 1.10-a). Participants performed no or few adaptations to their trajectory. We detail this result by ordering PosPos trials by increasing smpd(t_{rob}) value and dividing them into 5 subgroups of the same size (cf Figure 1.10-b). Results show that there was a significant increase of smpd between t_{rob} and t_{cross} for subgroups 1 and 2 (respectively Msmpdtrob=0.73m, Msmpdtcross=0.89m, Z=3.92, p<0.0001,

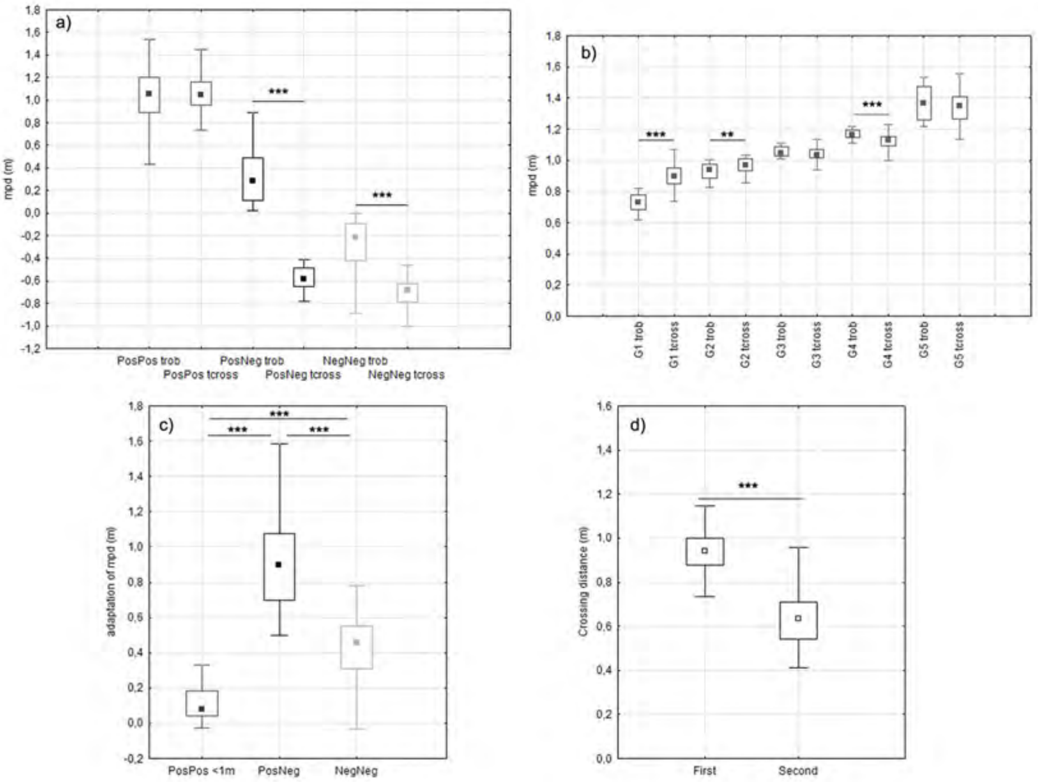

*Figure 1.10: a) Comparison between initial and final values of smpd at t_{rob} and t_{cross} for all trials of each non-empty category (PosPos, PosNeg, NegNeg). A significant difference in values means that adaptations were made to the trajectory by the participant (**p<0.01, ***p<0.001). b) Comparison between initial and final values of smpd at t_{rob} and t_{cross} for all the trials of each subgroup of the PosPos category. c) Total variation for smpd over the interaction. d) Minimum distance observed between the robot and the participant at t_{cross}, with trial grouped by passing order of the participant.*

r=0.88 and Msmpdtrob=0.94m, Msmpdtcross=0.97m, Z=3.17, p<0.01, r=0.71). For subgroups 3 and 5, there was no significant mpd variation between t_{rob} and t_{cross} (respectively Msmpdtrob=1.05m, Msmpdtcross=1.04m, p=0.14 and Msmpdtrob=1.37m, Msmpdtcross=1.35m, p=0.11). For subgroup 4 there was a significant decrease of smpd between trob and tcross (Msmpdtrob=1.18m, Msmpdtcross=1.16m, Z=2.42, p<0.05, r=0.54). This result suggests that when the initial value of smpd(t_{rob}) is lower than 1m, participants significantly adapted their trajectory. Considering the previous example of PosPos trial in Figure 1.6, we can confirm that the obtained results actually reflect the general behavior of the participants. In addition, it was observed that when the pedestrian pass in front of the obstacle, the distance between them is around 1 meter.

In the sequel we neglected subgroups 3, 4 and 5 since they do not capture avoidance adaptations. The updated Pos-Pos group is then named PosPos<1m. Its median values of smpd(t_{rob}) and smpd(t_{cross}) were respectively 0.81m and 0.94m.

PosNeg Trials

Results show a significant difference of smpd between t_{rob} and t_{cross} (Msmpdtrob=0.29m, Msmpdtcross=-0.58m, Z=7.23, p<0.0001, r=0.86). When participants initially were likely to pass first with an existing risk of collision, they finally decided to give way. Moreover, it was observed that the distance between the obstacle and the walker at the crossing time was around 0.5m.

NegNeg Trials

Results show a significant difference of smpd between t_{rob} and t_{cross} (Msmpdtrob=-0.22m, Msmpdtcross=-0.68m, Z=7.21, p<0.0001, r=0.87). When participants were likely to give way, still with an existing risk of collision, they increased the future distance of closest approach while maintaining the crossing order.

Quantity of adaptation

The more smpd variation, the more adaptation performed (Figure 1.10c). By Kruskal-Wallis test, it results that there is an influence of the group on the quantity of adaptation: H(2,180)=132.17, p<0.0001). Post hoc test showed that more adaptation are performed for trials of the PosNeg group (M=0.90m) than for NegNeg (M=0.46m). Both show more adaptation than for PosPos<1m (M=0.07mn), p<0.001.

Crossing distance

The average distance of closest approach was 0.83m (± 0.27m). The crossing order influenced this distance (Figure 1.10d). It was higher when participants passed first (M=0.94m) (U=175, Z=-9.03, p<0.0001).

1.7 Discussion

We studied how humans adapt their trajectory to avoid collision with a moving robot. We considered situations which are similar to previous studies on human-human collision avoidance and our analysis was based on concept of smpd to enable comparisons.

Results show that, concerning some aspects, humans have similar behavior when avoiding a robot or another human [Olivier 2012]. They accurately estimate the future risk of collision: they do not perform adaptations when smpd is initially high (smpd(t_{rob})>1m). They also solve collision avoidance with anticipation. Figure 1.9 shows that smpd plateaus in the latter period of interaction, called the regulation phase. A constant smpd indicates that the avoidance maneuvers are over, and this happens significantly before t_{cross}.

A significant difference about crossing configuration concerns the crossing order inversions that was observed in 29% of the trials: participants were initially likely to pass first but adapted their trajectory to finally give way to the robot. This threshold can be defined so that smpd(t_{rob}) is around 0.8m, which is the value of smpd(t_{rob}) for the Pos-Pos<1m group: above this threshold, participants remain first, otherwise they change the crossing order to give way to the robot. There was an overlapping in the smpd(t_{rob}) values between Pos-Pos<1m and Pos-Neg groups. To confirm such a threshold, we compared these smpd(t_{rob}) values using a Mann-Whitney test. Results showed that smpd(t_{rob}) for Pos-Pos<1m trials (M=0.81m) was higher than for the Pos-Neg trials (M=0.30m) (U=104, Z=7.69, p<0.0001). We can link this 0.8m threshold to the crossing distance observed between two pedestrians in similar conditions [Olivier 2012] that was 0.81m. Moreover, it was observed that when participants decide to pass in front of the robot, the distance at the crossing time is around 1m while, in the case of PosNeg trials, such distance is around 0.5m. We correlated this difference to the concept of personal space and safer behavior.

The absence of inversion NegPos was also similarly observed and modeled by the bearing angle theory [Kruse 2013]. Assuming that the robot obeys the bearing angle model and the pedestrian contradicts it by re-inverting the sign of the bearing angle change, the two adaptations could cancel each other out, ending into failure.

Which factors may explain such an inversion of role? We can assume that changing role in the crossing order is somehow inefficient: no physiological or kinematic factor explains this observation. It is not relevant to explain this based on perceptual factors (can humans early perceive the role they are likely to have?). Indeed, inversion is observed in only one direction (Pos-Neg), and we observed that the risk of collision is correctly perceived. We interpret the role inversion as an extreme adaptation to preserve the personal space, directly related to the perceived risk of collision. Passing in front of the robot may be perceived as more dangerous. We suggest the following hypotheses to explain this feeling of danger. First, humans ignored how the robot was controlled and its goal. The ongoing situation cannot be easily predicted by pedestrians during short interactions. Even though we would have instructed participants that the robot would not react to them, they may fear that the robot would have unexpected motion changes. Our second hypothesis deals with the lack of experience of participants to interact with an autonomous system. Humans perform collision avoidance with other humans daily and they may expect collaboration from them. Human-Robot collisions occur very rarely in real life. Our third hypothesis is about the fear of getting hurt: visually the robot looks quite heavy, metallic and compact. Colliding with it could certainly hurt legs which makes reasonable that participants prefer to adopt a safer behavior than when crossing a human.

1.8 Conclusion

In the work described in this chapter, we reproduce the experimental protocol proposed by Olivier et al. [Olivier 2013] in order to compare the differences between human-human and human-robot collision avoidance. We programmed a moving robot to cross the path of a walker in different ways: a) on a full collision course, b) on a partial collision course (the robot was slightly in advance or late with respect to the participant), or c) not on a collision course. In order to control the robot to obtain these configurations, the walking speed of the participants was estimated once they reached their comfort speed. Results showed that the strategies to avoid a moving obstacle have similarities with human-human interactions (estimation of collision risk, anticipation) but also leads to some major differences. Humans preferentially give way to the robot, even though this choice is not optimal to avoid collision. Moreover, humans never decided, in the cases in which they were second in the crossing order, to accelerate and pass as first. We interpret this behavior based on the notion of perceived danger and safety. This conservative strategy could be due to the lack of understanding of how the robot behaves and the lack of experience of such an interaction with an autonomous system. However, human always succeeded in avoiding the robot with anticipation and without aberrant reaction. We also raised questions about humans reactions facing a robot programmed to behave as a human. Would humans understand that the robot cooperates and adapt their own strategy accordingly?

The conclusion of this study opens paths for future research. A first direction is to better understand the possible effect of this notion of danger during human-robot interactions. What are the aspects that influence more human perception (velocity, shape, size)? A second direction is the design of safe robot motion amidst human walkers. How should the robot adapt to humans? Should it be collaborative with the risk of compensating human avoidance strategies? Should it be passive? We believe that robots should be first equipped with human abilities to early detect human avoidance strategy and adapt to it.

In the next chapter, we will extend this study of human-robot crossing interaction: the robot will be equipped with collision avoidance capabilities, imitating human strategies. The idea is to investigate the differences on strategies set by participants if the robot is cooperative instead of passive.

CHAPTER 2

Human and Robot interaction: cooperative strategies for collision avoidance

In the previous chapter we analyzed the human strategies to avoid an obstacle which moves straight and at constant velocity. Tests showed that the participants preferred to give way to the robot even if this solution was not optimal to avoid the obstacle. We hypothesized that the lack of experience of the participants to interact with this kind of autonomous systems implicate insecurity, and then they adopt a safer approach. In particular, we interpreted such a situation as a passive interaction: since the robot is not reacting but still moving, the participant could actually be surprised. Moreover, they adopt strategies that are less performing with respect to the ones that they apply when they cross another human. Therefore, our guess is that pedestrians would consider the robot as a non collaborative agent or an unpredictable moving obstacle. This seems reasonable since humans are sharing their environment daily with other humans, which lead them to develop implicit and cooperative strategies based on the respect of social rules. Considering all these aspects, in this chapter we present a new study in which the moving obstacle is now cooperative and reactive in order to avoid the collision with the walker. The aim of this study is to understand if the comfort[1] of the pedestrian to share the environment with an autonomous system can be improved if the robot behaves like a human.

2.1 Introduction

Since robots are progressively leaving their security cage to move in human populated environment, for applications such as service robotics or the factory of the future, social aspects have to be considered to drive their behavior. Previous works have shown that the compliance of the social aspects improve the acceptance, comfort and perceived safety of robots when they share the environment with other humans [Buss 2011, Carton 2013, Lichtenthäler 2012]. Nowadays, social aspects are typically taken into account to develop robot features inspired from humans [Breazeal 2005]. Readability, legibility and predictability are terms widely used in this research area. In fact, they describe the effect that it is easier for human to predict and understand the purpose of motions if they are human-like [Carton 2013, Dragan 2013, Lichtenthäler 2013]. However, it has not been defined yet whether human get used faster to interact with robots if they behave in a human-like way. Our work analyzes how humans react with a mobile robot that behaves as a human. In particular, we focus on a collision avoidance task. Avoidance strategies have been studied widely by psychologists, sociologists and in robotics. The general goal is to avoid collision in accordance with a minimum effort principle and by preserving the personal space. Several theories regarding the effectiveness of readable locomotion are provided in literature about the behavior of pedestrians. The sociologist Erving Goffman observed in his studies that humans externalize themselves that means to make their desired future motion predictable and clearer in a nonverbal way [Goffman 1971]. In his theory, humans are consistently scanning the environment, especially the area in front of them, when they walk towards and also expect others to act similarly. Moreover, pedestrians scan the area mainly to perceive nonverbal signals from others to mutually avoid collisions. Virtualization of avoidance behavior is widely studied in literature. Van Basten et al. [van Basten 2009] synthesized human behavior for virtual characters in computer games but without transferring rules about human-robot interactions. They based their work on the concept of collaboration, anticipation, clearance and synchronization, by examining the contribution of each agent to avoid collision. Reliastic collision avoidance for virtual characters is also studied in [Karamouzas 2010]. One of the fundamental works in the human locomotion behavior has been provided by Fajen et al. [Fajen 2003]. They propose a steering model to avoid collision at constant velocity, derived by human data. They also compare the difference between the strategies set in real and in virtual environments. Experiments in which two pedestrians are crossing each other (usually perpendicularly) are considered by many studies [Albrecht 2012, Basili 2013, Huber 2014, Olivier 2013]. The authors focus on personal behavior and respective adaptations. A specific common principle is hard to find since several factors influence the results. Some approaches classified velocity adaptation as the main strategies [Basili 2013] whereas others sustain that collision avoidance is performed both in velocity and path adaptation (orientation) [Olivier 2012]. Recently, Carton et al. [Carton 2016] studies the differences between Human-Human and Human-Robot moving face-to-face and the relative strategies to avoid collision. In order to evaluate the effectiveness of readability for humans and robot, they compare the adaptation in terms of path variation and velocity. Their experimental results show that readable locomotion positively contribute to the locomotion planning of the other agent sharing the same environment. Moreover, their study confirm that humans apply the same behaviors for locomotion planning with humans and with robots. Human strategies to avoid a moving obstacle that imitates a pedestrian behavior, in a real scenario and in a 90° crossing configuration has not still been considered. Our work moves forward in this direction. We reproduced the same experimental setup than previous studies ([Olivier 2013], [Vassallo 2017]) in order to understand the different reactions of a walker avoiding another human walker, a passive moving obstacle and a cooperative robot. Comparisons are based on the concept of smpd introduced in the previous chapter.

---

[1] In the sequel of this manuscript we will use the term "comfort" to indicate the natural behavior of a walker. In particular, "to improve the comfort" it means that the participant behaves smoother and more calmly.

The chapter is structured as follows. The experimental setup and the apparatus are explained in Section 2.2. In particular, we highlight the improvements made in this context, in order to improve the quality of the results. The way how we control the robot to behave as human is presented in Section 2.3. Follows the relative analysis based on smpd and then the discussion. We also compared the avoidance strategies when the robot is active with respect to the passive one previously studied. A conclusive section ends the chapter.

2.2 Materials and Methods

2.2.1 Participants

Ten volunteers participated in the experiment (2 women and 8 men). They were 29.2 (± 8.4) years old and 1.74m tall (±0.11m). They had no known vestibular, neurological or muscular pathology that would affect their locomotion. All of them had normal or corrected sight and hearing. Participants gave written and informed consent before their inclusion in the study. The experiments respect the standards of the Declaration of Helsinki (rev. 2013), with formal approval of the ethics evaluation committee Comitè d'Evaluation Ethique de l'Inserm (IRB00003888, Opinion number 13-124) of the Institut National de la Santé et de la Recherche Médicale, INSERM, Paris, France (IORG0003254, FWA00005831). All the participants were equipped with 6 markers fixed to a helmet that they were wearing.

2.2.2 Apparatus

The experimental setup was almost identical to the one already presented in Section 1.3. The experiments took place in 50m x 25m gymnasium. Two areas were defined and separated by 2m high occluding walls, forming a gate in the middle. One of the problems of the previous experiment was that the lateral area of the gymnasium was not sufficiently covered by the cameras field of view. To this end, the devices were reorganized such that the robot starting position could be farther (around 2 meters more for each side). Thereby, the accuracy of the tracking was improved since the starting position of the real robot and the virtual one was almost the same or really near. An overview of the experimental setup is shown in Figure 2.1. Four specific positions were identified: the participant starting position PSP, the participant target position PT, and two robot starting positions RSP1 and RSP2. The walking speed was measured in the Motion Estimation Zone area (MEZ). With respect to the previous chapter, the participant were starting to move from farther, in the uncovered area. We improved the system in order to identify and track the actor position in a faster way. To this end, the distance between PT and MEZ was increased from 1.6m to 4m, allowing participants to reach their cruise speed more comfortably. The length of the MEZ area was extended too, from 2.8m to 3.5m. The intersection point of the robot path [RSP1, RSP2] and the participant path [PSP, PT] is named Hypothetical Crossing Point HCP. In this experimental setup we added two new positions next to HCP: the via points

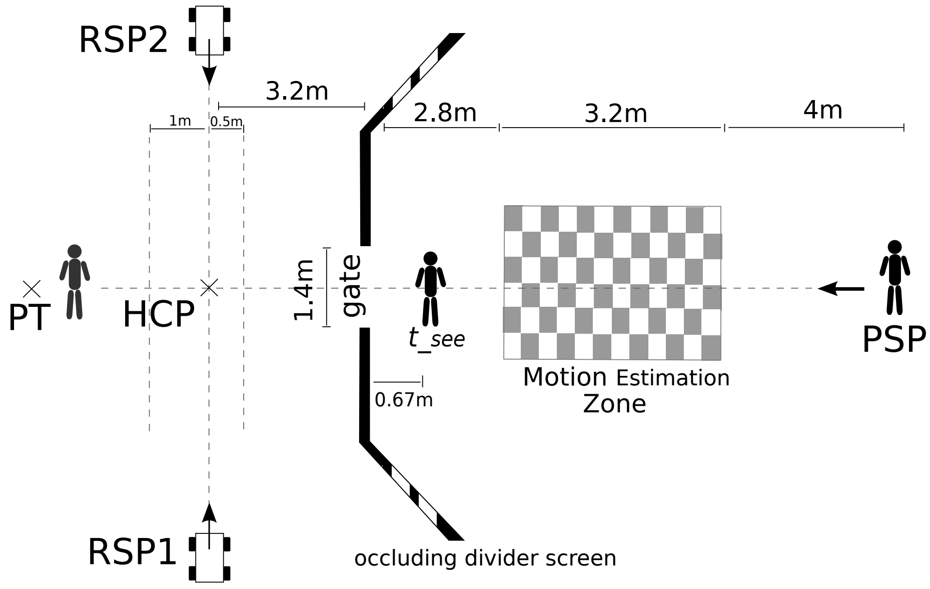

Figure 2.1: Experimental apparatus and task. The covered area was extended with respect to the previous work.

VP1 and VP2. They are defined as intermediate waypoints in the robot trajectory to pass behind or in front of the participant (more details in Section 2.3.2).

2.2.3 Participant Task

Participants were asked to walk at their preferred speed from PSP to PT by passing through the gate. They were told that an obstacle will be moving over the gate and could interfere with them. Participants were completely unaware about the robot behavior. One experimental trial corresponds to one travel from PSP to PT.

2.2.4 Recorded Data

3D kinematic data were recorded using the motion capture Vicon-MX system (100Hz). Reconstruction was performed using Vicon-Blade and computations using Matlab (Mathworks ®). The experimental area was covered by 15 infrared cameras. Contrary to previous experiments, we estimated the global position of participants as the centroid of reflective markers set on the helmet that they were wearing, because it was less subjected to noise, especially during the crossing through the door. The stepping oscillations were filtered out by applying a Butterworth low-pass filter (2nd order, dual pass, 0.5Hz cut-off frequency).

ID Trial	Cooperative Behavior	RSP Side	SMPD	ID Trial	Cooperative Behavior	RSP Side	SMPD
1	Yes	Left	-0.6	31	No	Left	0
2	Yes	Right	0	32	Yes	Right	0.3
3	Yes	Right	0.6	33	No	Left	0.6
4	No	Right	-0.9	34	Yes	Left	0.9
5	Yes	Left	-0.3	35	No	Right	– –
6	No	Right	0.9	36	No	Left	-0.3
7	Yes	Left	-0.3	37	Yes	Left	-0.9
8	No	Right	0.6	38	No	Left	0.9
9	No	Right	-0.6	39	Yes	Left	0.6
10	Yes	Right	0.9	40	Yes	Right	0.9
11	No	Right	-0.9	41	Yes	Left	0
12	Yes	Left	0.3	42	Yes	Right	-0.6
13	Yes	Left	0	43	Yes	Left	-0.9
14	No	Right	0.3	44	No	Right	0
15	Yes	Right	0.6	45	No	Right	-0.3
16	No	Right	– –	46	No	Left	-0.6
17	Yes	Right	-0.3	47	Yes	Left	0.3
18	Yes	Right	0.3	48	No	Left	0.6
19	No	Right	-0.3	49	Yes	Right	0
20	No	Left	0.9	50	No	Right	0.9
21	No	Left	– –	51	Yes	Right	-0.6
22	Yes	Left	0.9	52	Yes	Right	-0.3
23	No	Left	0.3	53	No	Left	-0.3
24	No	Right	0.6	54	No	Left	– –
25	No	Right	0	55	No	Left	-0.6
26	No	Left	0	56	No	Left	0.3
27	No	Right	0.3	57	Yes	R	-0.9
28	Yes	Right	-0.9	58	Yes	Left	-0.6
29	Yes	Left	0.6	59	No	Left	-0.9
30	No	Left	-0.9	60	No	Right	-0.6

Table 2.1: Organization of the trials

2.2.5 Experimental plan

Each participant performed 60 trials (see Table 2.1). The robot starting position (50% in RSP1, 50% in RSP2) was randomized among the trials. To introduce a bit of variability, in 4 trials the robot did not move and so the participant did not have to react. Only the 56 trials with potential interaction were analyzed.

2.3 Robot Behavior

We used a prototype of RobuLAB10 wheeled robot from the Robosoft company (dimension: 0.45 x 0.40 x 1.42m, weight 25 Kg, maximal speed around 3 m/s) (see Figure 1.2b). The robot position was detected as the center point in its base. Despite previous work, we limited the smpd trials in the range [-0.9m, 0.9m] since it was observed that over this range the interactions were not significant. We control the robot to behave either cooperatively or passive (50$\%$ passive and 50$\%$ active). In the cases in which the robot was active, in function of smpd sign, it decided to move in such a way to maintain its role (even if this choice was not optimal). The two behaviors were randomized among the trials.

2.3.1 Passive Behavior

In this work we also replicated the robot passive behavior in order to confirm the previous results and compare them with the new ones. The robot was controlled to generate specific interactions with the participant; the robot was either: a) on a full collision course (reach HCP at the same time than the participant), b) on a partial collision course (the robot reaches HCP slightly before or after the participant), or c) not on a collision course. Walking speed was measured in MEZ and the crossing configuration was computed as a function of the desired smpd, exactly as in the previous work. Each trial was repeated twice.

2.3.2 Cooperative Behavior

In the previous chapter, we observed that humans behave differently depending on whether they have to pass in front of the obstacle or behind. In particular, it emerged that if they pass ahead the obstacle, the distance is greater than when passing behind. In fact, the distance are respectively around 1m and 0.5m. Moreover, participants were used to accelerate to pass as first or decelerate to give way. Based on these observations, in the new experiments the robot is controlled in order to behave as a human. Initially its velocity is regulated to be equal to the one of the participant.

Once the interaction phase begins (the walker had almost crossed the door and the robot is visible at t_{see}) (see Figure 2.2), we generate specific reactive movements of the robot based on the value of smpd:

- when robot is late (smpd > 0): the vehicle is controlled to first decelerate and then turn to pass behind the human, see Figure 2.2, 2.3(a);
- when the human is late (smpd < 0): the vehicle is controlled to first accelerate and then turn to pass in front of the human, see Figure 2.3(b), 2.3(c);
- in case of full collision course (smpd = 0): given the actor position and the relative velocity, the robot estimates at t_{see} who is reaching HCP as first. Then it reacts to pass as first or to give way, as in the cases of smpd<0 or smpd>0 respectively.

At the beginning of each trial, the software read the relative trial configuration (Table 2.1). The robot starting position was computed in real time, based on the actor velocity. Once the actor was over the MEZ area, the robot started to move at the same speed as the pedestrian. We estimate this velocity as in the previous study (Kalman Filter, material point moving along a line, no acceleration).

2.4 Analysis

2.4.1 Kinematic data

The analysis of the data for the trials in which the robot as a passive behavior was the same as in the previous chapter. We computed t_{rob}, the time at which the robot reaches its constant cruise speed (acceleration below a fixed threshold, 0.003 m/s^2), and t_{cross}, the time of closest approach between the participant and the robot. However, for the trials in which the robot is active, we cannot define t_{rob} since the reactive behavior of the robot implies several variations of its velocity. Moreover, in the previous chapter, we considered t_{rob} instead of t_{see} because the aim of the work was to analyze the human strategies to avoid a passive obstacle. The smpd components relative to the robot were minimized and the participants mainly contributed to change the smpd. However, in the following work,

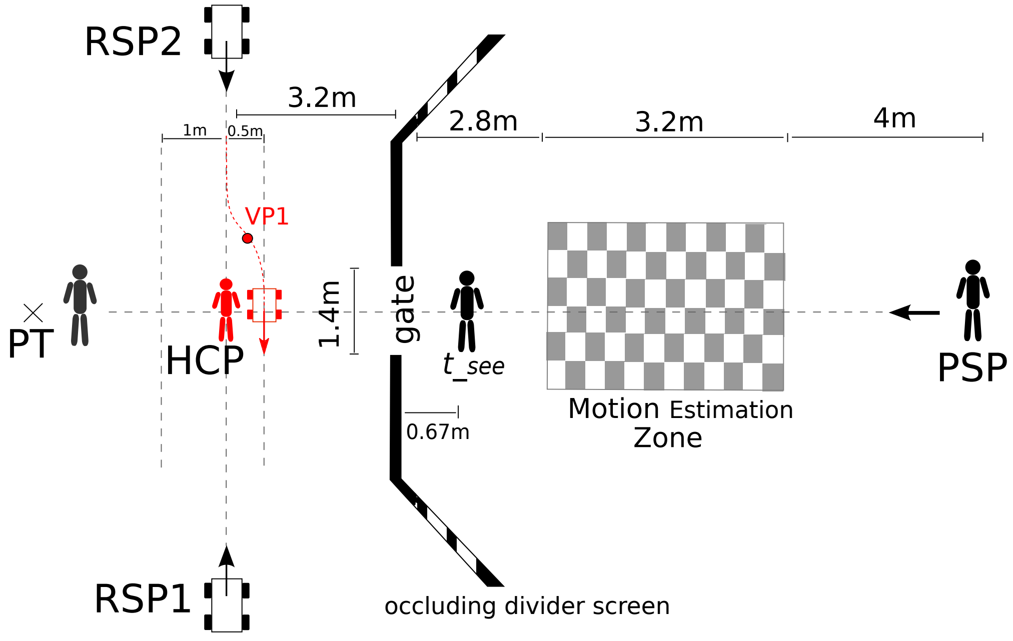

Figure 2.2: Experimental setup when robot is cooperative. The pedestrian moves from PSP to the gate through the MEZ. At 0.67m before crossing the gate, the actor is able to see the robot (t_{see}). In the following trial, the robot decelerates and passes behind the actor, going through VP1. The red robot and the red actor illustrate the hypothetical crossing configuration.

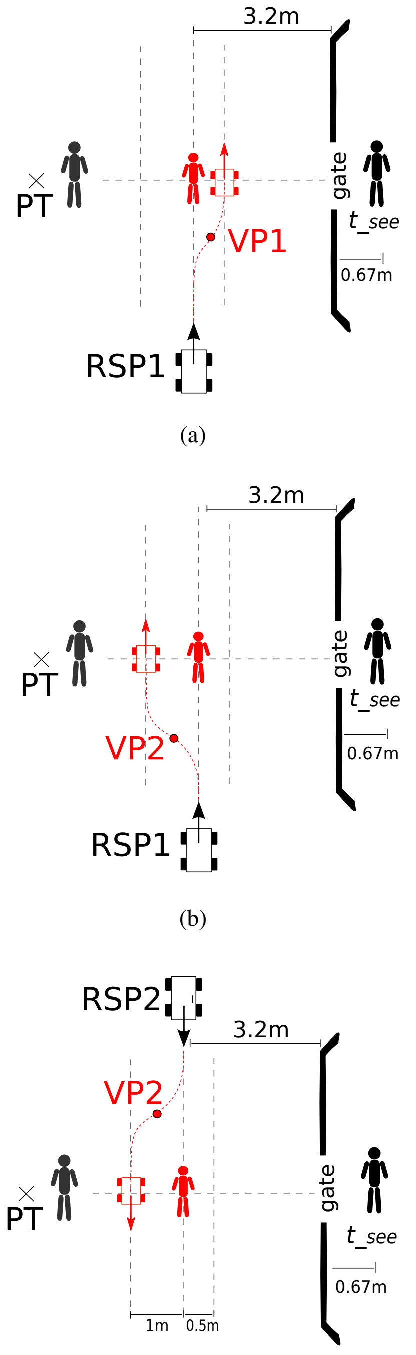
3.2m
PT
gate
t_see
VP1
0.67m
RSP1
3.2m
PT
gate
t_see
VP2
0.67m
RSP1
RSP2
3.2m
VP2
PT
gate
t_see
0.67m
1m
0.5m

(a)

(b)

(c)

Figure 2.3: (a) smpd>0: The robot starts from RPS1, decelerates and turns right. (b) smpd<0: the robot starts from RPS1, accelerates and turns left. (b) smpd<0: the robot starts from RPS2, accelerates and turns right.

we control the robot to be either passive or active. Therefore, when the robot is active, the smpd is influenced both by the robot and the participant. So that, we consider the interaction phase starting at t_{see}, the time in which the participant was approaching the gate. The general profile of the smpd was tested with different distances from the door, from which we supposed that the person could start seeing the robot. In particular we compare the general behavior when the participant was before, exactly and slightly over the door line. Tests showed that reliable results are obtained if we consider t_{see} as the instant of time where the participant passed the door of 0.2 meter. This is due to the high variation of the mobile robot velocity at its start. Similarly to the previous chapter (see page 33) four different groups of trials were considered, according to the sign of mpd at the beginning and at the end of the interaction: PosPos, PosNeg, NegPos and NegNeg. We considered t_{rob} for the trials in which the robot is passive and t_{see} for the ones in which it is active.

2.4.2 Statistics

All the statistical analyzes were performed using Statistica (Statsoft ®). All effects were reported at p<0.05. We normalized all the data by using a Kolmogorov-Smirnov test. Based on the normality, the values are expressed as median (M) or mean ±SD. The variation of smpd sign during the interaction time was determined by Wilcoxon signed-rank tests. To compare the crossing distance depending on the final crossing order, we used a Mann-Whitney test.

2.5 Results

We considered 552 trials because 8 of the 560 initial trials were removed, as the robot failed to start. Each participant performed 60 trials of which 4 were not considered because the robot did not move and so there was no interaction. In each experience, the robot was active for 50% of the trials and passive for the remaining 50%. In total, we had 274 trials where the robot was active and 278 where it was passive. The analysis and the results have been divided for the two cases. At the end of the chapter, based on the behavior of the participants, these two cases will be compared with each other. Statistical results were computed considering 280 trials.

2.5.1 Passive Robot

We based our analysis on the concept of smpd. In particular, we investigated the smpd values at t_{rob} and t_{cross}. It resulted that, at the beginning of the interaction, the participants were first in the crossing order in 38.41% of all cases. However, they decided to give way

in 15.22% of trials. Globally, it emerges that the smpd categories are distributed among the trials in the following way: PosPos=64 trials (23.18%), NegNeg=169 trials (61.23%), PosNeg=42 trials (15.22%), NegPos=1 trial (0.36%). Clearly, this last category won't be considered in the future analysis. The evolution of the smpd for all the trials is depicted in Figure 2.4.
Comparing these results with the one of the previous chapter (Figure 1.9, page 32), it emerges that the general behavior is almost identical. Examples of corresponding trajectories are illustrated in Figure 2.5. The mean evolution of the smpd for each category is shown in Figure 2.6.

Statistical Results

Since we reduced the smpd range (from [-1.2m,1.2m] to [-0.9m,0.9m]) we did not observe too many trails in which there is no interaction for PosPos and NegNeg groups. For this reason, we did not subdivided these two groups into subgroups for further analysis. From the statistical analysis of the variation of the smpd between t_{rob} and t_{cross} , it results that participants performed significant adaptations in all the groups.

Table 2.2 shows the median value of smpd at t_{rob}, **Msmpdtrob**, and at t_{rob}, **Msmpdtcross**.

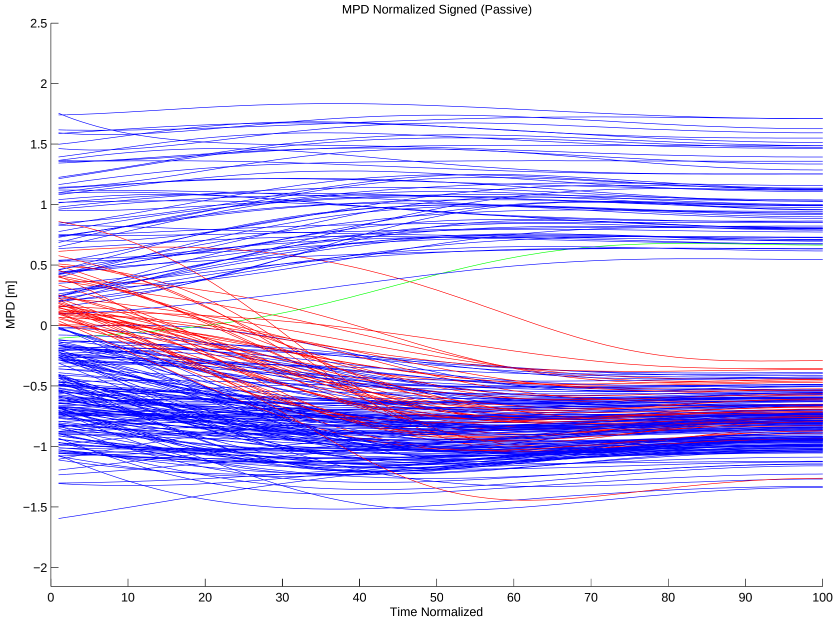

Figure 2.4: smpd plots for all the 278 trials, after resampling over the interaction time [t_{rob},t_{cross}].

From Statistica, we report the Wilcoxon signed-rank test using the **Z** parameter (**r** represents the reliability of the test). The reader is invited to give a look at Figure 2.6 to better understand the results described below.

Table 2.2: Statistical analysis results of the smpd data during t_{rob} *and* t_{cross} *in the case that the robot is passive. The Wilcoxon signed-rank test was performed using Statistica v.8 .*

Category	Msmpdtrob	Msmpdtcross	Z	r
PosPos	0.73m	1.05m	4.04	0.7379
PosNeg	0.41m	-0.83m	5.23	0.8719
NegNeg	-0.58m	-0.84m	4.69	0.5739

PosPos Trials

Results show a significant difference of smpd between t_{rob} and t_{cross} and they confirm the ones presented in the previous chapter. Participants adapted their trajectory to pass first if the smpd(t_{rob}) was less than 1 meter, otherwise no adaptation was noticed.

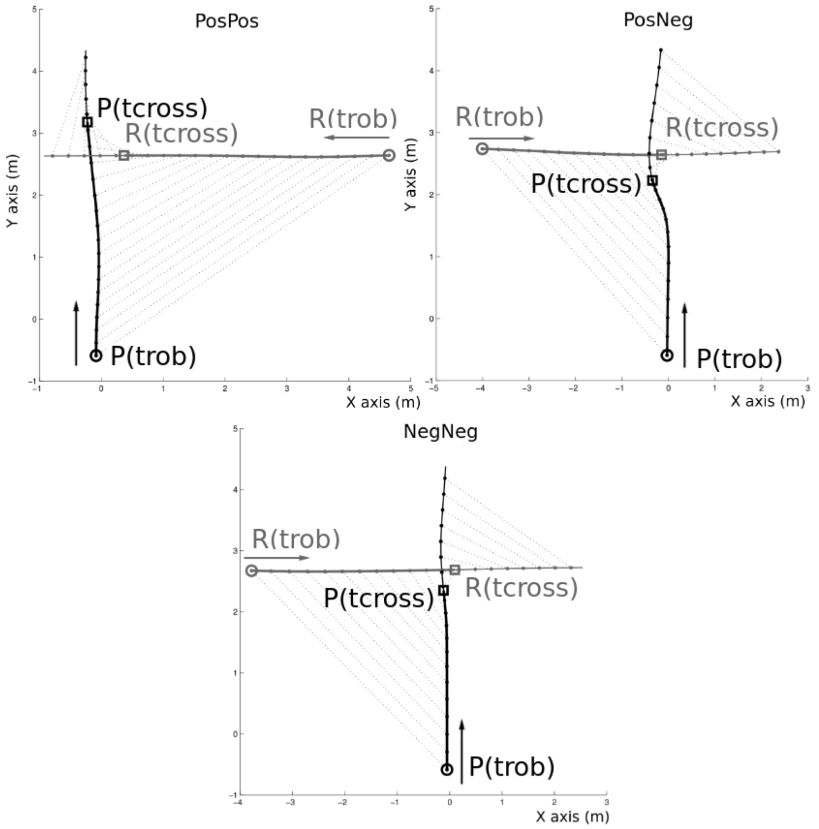

Figure 2.5: Examples of participant and robot trajectories for each category of trial. The bold trajectory represents the interaction time [t_{rob}, t_{cross}*].*

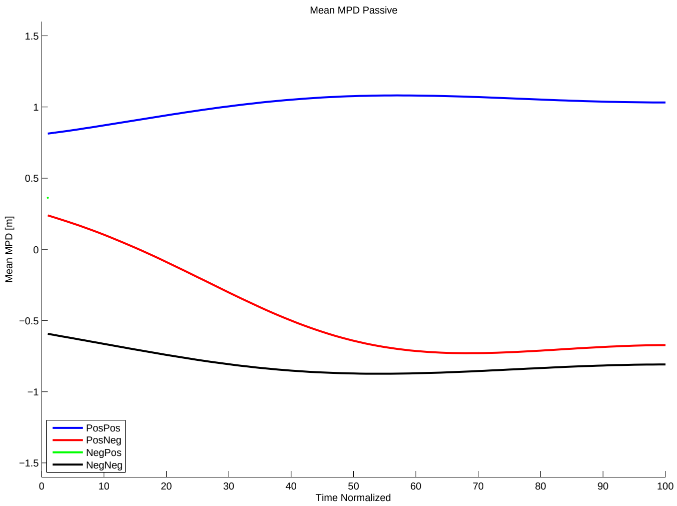

(a) Mean evolution of smpd for each category of trial.

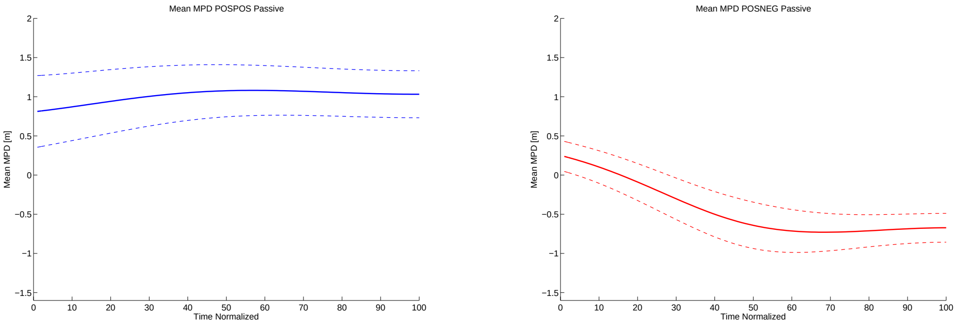

(b) PosPos

(c) PosNeg

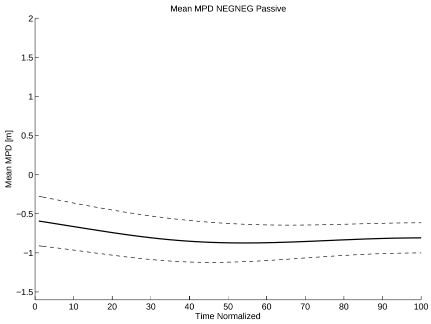

(d) NegNeg

Figure 2.6: Mean evolution of smpd ±1 Standard Deviation for the three categories where the robot is passive.

PosNeg Trials

Results show a significant difference of smpd between t_{rob} and t_{cross} and they confirm the ones presented in the previous chapter. When participants initially were likely to pass first with a possible risk of collision, they decided to give way to the robot. Such a behavior is observed if there exists an high risk of collision (future crossing distance around 0.5 meter).

NegNeg Trials

Results show a significant difference of smpd between t_{rob} and t_{cross} and they confirm the ones presented in the previous chapter. Participants maintained the crossing order by giving way to the robot. If the future crossing distance was small enough to be considered as risky, participants also adapted their trajectory to increment it.

2.5.2 Cooperative Robot

As previously explained, we consider t_{see} as the instant of time at which the reaction phase begins. The sign of mpd at t_{see} shows that the participant passed first in 52% of all cases and gave way in the other 48%. Combining this information with the sign of mpd at t_{cross}, it turns on that the smpd categories are distributed among the trials in the following way: PosPos=140 trials (50.91%), NegNeg=110 trials (40%), PosNeg=22 trials (8%), NegPos=3 trials (1.09%). The evolution of the smpd for all the trials is depicted in Figure 2.7. Since NegPos group is composed by only 3 trails that are mainly outliers, we will not consider them in the future analysis.

If we compare these results with the ones observed in the previous chapter (Figure 2.4, page 50), it appears that the general behavior is slightly changed. In fact, we still have PosNeg trials but the crossing order is mainly preserved. Such preservation of the roles reflects more the behavior observed by Olivier et al. [Olivier 2013] with two humans crossing each other. The mean evolution of the smpd for each category is shown in Figure 2.8. Examples of corresponding trajectories are illustrated in Figure 2.9.

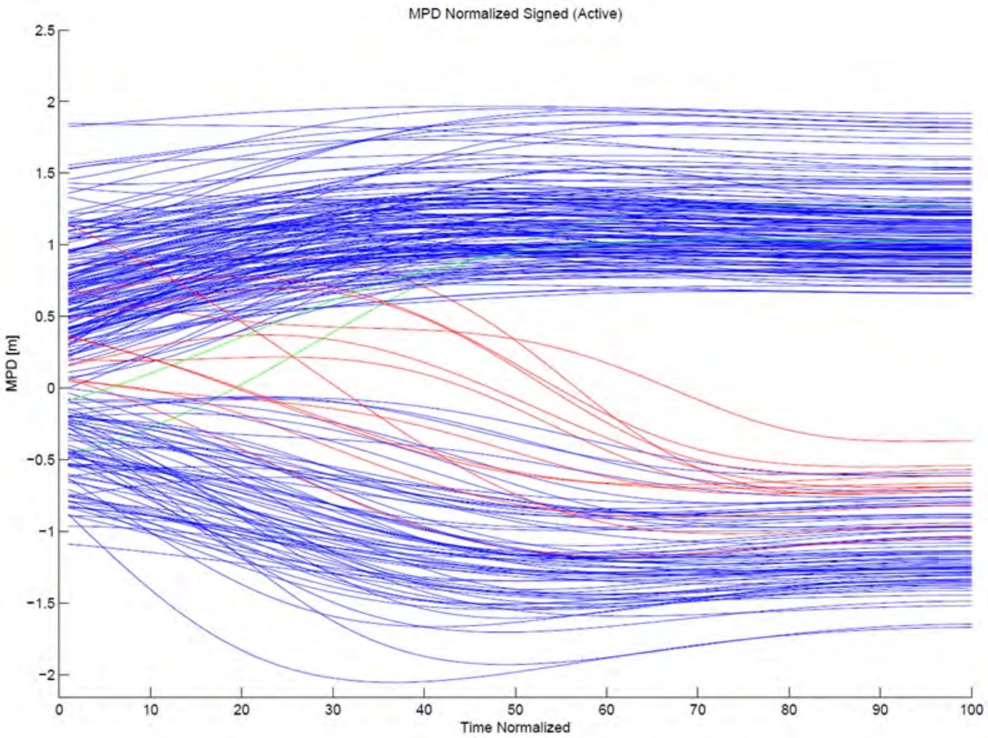

Figure 2.7: smpd plots for all the 278 trials, after resampling over the interaction time [t_{see},t_{cross}].

Statistical Results

In the experiments with a cooperative robot, the average behavior of the smpd for all the categories is more uniformly distributed among all the trials. In particular, we notice that the switch of roles PosNeg is more sporadic (only 8% of trials). We statistically analyzed the smpd at t_{see} and t_{cross} in order to understand if there is a significant variation: participants performed considerable adaptations in all the groups. Results are shown in Table 2.3, where **Msmpdsee** and **Msmpdtcross** are respectively the medium value of smpd at t_{see} and t_{cross}. Also in this case, the reader is invited to give a look at Figure 2.8 to better understand the following results.

Category	Msmpdtsee	Msmpdtcross	Z	r
PosPos	0.71m	1.08m	9.17	0.7863
PosNeg	0.29m	-0.71m	8.98	0.8748
NegNeg	-0.46m	-1.14m	4.11	0.8711

Table 2.3: Statistical analysis results of the smpd data during t_{see} and t_{cross} in the case that the robot is passive. The Wilcoxon signed-rank test was performed using Statistica v.8 .

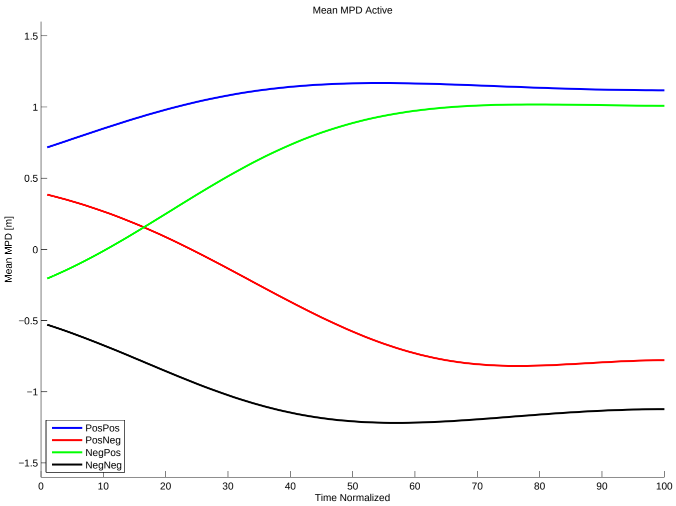

(a) Mean evolution of smpd for each category of trial.

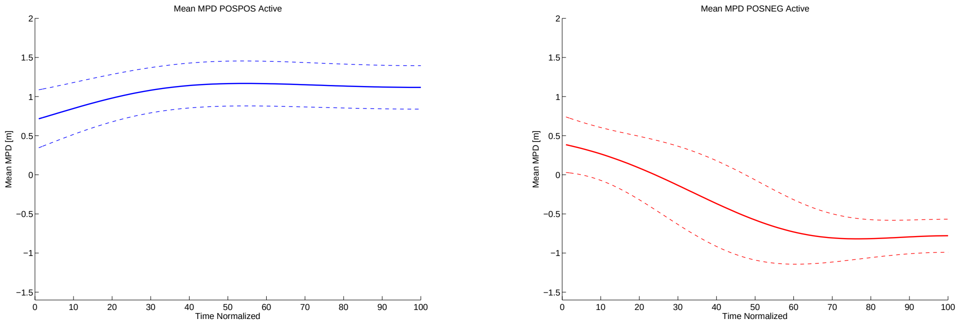

(b) PosPos (c) PosNeg

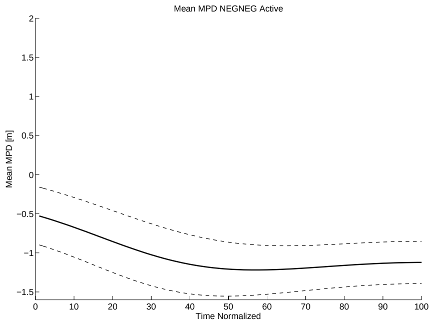

(d) NegNeg

Figure 2.8: Mean evolution of smpd ±1 the Standard Deviation (SD) for the three categories where the robot is cooperative. The category NegPos was not considered.

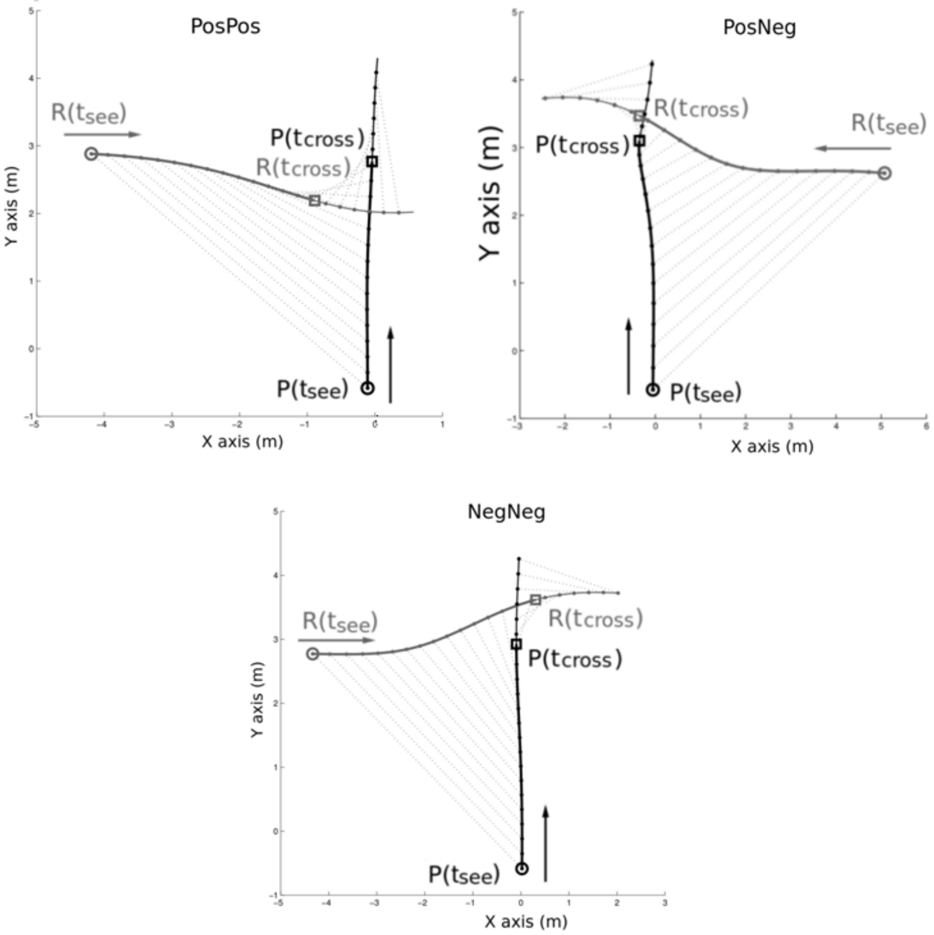

Figure 2.9: Examples of participant and robot trajectories for each category of trial. The bold trajectory represents the interaction time [t_{see},t_{cross}].

PosPos Trials

Results show a significant difference of smpd between t_{see} and t_{cross}. Participants preserved the crossing order if the smpd(t_{see}) was around 0.65m. In contrast to the previous results, the average behavior is shifted toward the zero of around 0.2m. It means that, even if the risk of collision was high (0.1m), there was no an arbitrary switch of roles.

PosNeg Trials

Results show a significant difference of smpd between t_{see} and t_{cross}. Similarly to the previous experiments, the participant decided to give way to the robot if significant risk of collision existed (future distance around 0.35m). However the PosNeg trials are few with respect to the experiments where the robot was behaving passively (8% versus 15.21%).

NegNeg Trials

Results show a significant difference of smpd between t_{see} and t_{cross}. During NegNeg trials, both the actor and the robot were positively contributing to maintain the crossing order. Indeed, by comparing Figure 2.8(d) and Figure 2.6(d) it can be noticed that there is an increment of smpd. This variation is bigger than for the PosPos group, because the actors behaved in order to maintain a larger distance from the robot, compared with the case in which they pass behind. This results is coherent with the one observed in the previous experiments: participants passed closer to the robot closer when passed behind.

2.5.3 Crossing Distance

The average distance of closest approach for PosPos and NegNeg group is 1.13m ($\pm$ 0.3m). It is 1.10m ($\pm$ 0.31m) for the PosNeg group.

2.6 Discussion

We investigated the strategies set by humans to avoid a moving robot. We considered a situation similar to the one of previous studies on collision avoidance between two humans [Olivier 2013] and collision avoidance between a human and a robot moving straight at constant speed (Chapter 1). The analysis was based on smpd (Section 1.5) to enable comparison. We programmed the robot to be either passive or cooperative. In the first case, we confirmed the previous results: participants do not perform adaptation if the smpd is initially high (smpd(t_{rob}>1m) and the collision avoidance is performed with anticipation. Moreover, participants preferred to give way to the robot although they were likely to pass first. It results that in most of the cases (76.45%), the participants pass second. Considering the trials in which the robot was active, we observed similarities but major differences. Similarly to human-human interaction, the crossing order is mainly respected (around 90% of all cases). However, we still observe a tendency of actors to give way to the robot (PosNeg group corresponds to 8% of trails). The switch of roles NegPos was not observed.

Which factors may explain such a change of behavior between passive and cooperative cases? It appears that the inactive behavior of the robot is somehow counterproductive. Humans daily set implicit strategies when they have to cross each other. When pedestrians have to interact with an autonomous system, the feeling of insecurity and danger may be natural because they are not used to share their environment with robots. In the previous discussion, we hypothesized that participants preferred to preserve their personal space rather than succeeding the collision avoidance task quickly and smoothly. However, in view of the last results, it appears that when the robot applies the observed human avoidance strategies, the comfort of the pedestrians is eased. Considering the number of trials in which the crossing order is preserved, we clearly observed that the robot behavior successfully suggests the future crossing order to the human. In the previous work [Olivier 2013], our partners found out that the participant giving way (#2) was contributing more than the one passing first (#1). Moreover, it resulted that the participant #2 preferred to adapt mainly his speed during at the beginning of the interaction and, in turn, both participants were adapting their orientation. This behavior was similarly observed in the last experiments: the robot was initially accelerating or decelerating and then it slightly turned. Although such a behavior was not really evident, it was sufficient for the pedestrians to understand the intentions of the robot and then, in turn, their own role on the crossing order.

2.7 Conclusion

In this chapter, we used the experimental protocol proposed by Olivier et al. [Olivier 2013] and Vassallo et al. [Vassallo 2017]. We based our analysis on the concept of smpd introduced in Section 1.5. In these last experiments we programmed a wheeled robot to move either passively (as well as in the previous chapter) or in a cooperative way. In order to be cooperative, the robot follows simplified observed strategies that were identified in humans: it accelerates and turns to pass ahead the participant or it decelerates and turns to pass behind. Since the study of this work is divided in two parts, we obtained several results that could have compared. Firstly, we confirm the observations previously presented: humans do not behave optimally in terms of time and energy when they have to interact with a passive robot. They prefer to preserve their personal space. Secondly, we observe how humans react if the robot cooperates to avoid the collision. Results show that walkers behave more naturally: the crossing order is respected in most of cases and the adaptations, in terms of speed variation, are smoother. Although we observed a change of roles (8% of cases), we related this phenomenon to the fact that pedestrians have still a tendency to give way to the robot. We hypothesize that, with appropriate analysis and improvements of the observed strategies, the percentage of change of roles could be further decreased. Therefore we conclude that, in terms of safety and efficiency, the performance of human-robot collaboration is improved if the robot behaves in a human-like way. This result was already observed in literature by many authors [Kato 2015, Dragan 2015]. In addition, we proved the veracity of the hypothesis, proposed by [Carton 2013, Dragan 2013, Lichtenthäler 2013]: it is easier for humans to predict and understand the purpose of the robot motions if they are human-like.

CHAPTER 3

Learning Movement Primitives for the Humanoid Robot HRP2

The modeling of online reactive motion is an important challenge in humanoid robotics. In particular, the generation of complex full-body movement, maintaining the dynamic stability of the gait, is an extreme difficult task, although it is a natural behavior for humans. Therefore, walking pattern generators have to consider online-reactive motion of both low-body and upper-body part. The work presented in this chapter provides a new step in this direction. It has been done in collaboration with computational neuroscientists of the University Clinic Tubingen, within the framework of the European project Koroibot. We propose a new approach to synthesize realistic complex humanoid robot movements with motion primitives. The control framework proposed combines biologically-inspired online planning for the upper body and model predictive control for the lower body. The upper-body movements are generated via a coupled dynamical motion primitives. Such primitives are learned from human data recorded with a motion capture system, after appropriate retargeting and adjustment in order to respect the constraints of the robot. The lower body is controlled by the walking pattern generator developed al LAAS-CNRS by Naveau et al. [Naveau 2017].

3.1 Introduction

The planning of flexible and adaptive behavior for humanoid robots cannot be accomplished satisfactorily by the off-line synthesis of dynamically stable behaviors. The reason for that is the continuous change of the environment and the error in state estimations. Moreover, the optimal control of human-like multi-joint systems is a computationally challenging problem. Current solutions involve near real-time whole body Model Predictive Control with regularized modeling of contacts in order to decrease the associated computational cost [Tassa 2012, Koenemann 2015]. A precise modeling of contact phases requires hours of offline computation time [Koschorreck 2012]. Another challenging issue for the generation of human-like behaviors is the sequential planning of multi-step sequences, where individual steps can be associated with different sub-goals or constraints (like contact with goal objects or step-length constraints). This problem being multidisciplinary, we quickly review associated work in computer graphics, biological motor control, and humanoid robotics.

3.1.1 Modeling of whole-body movements in computer graphics

Synthesizing complex whole body movements is a problem widely addressed in computer graphics, e.g. [Levine 2012], and many learning-based approaches have been proposed that provide low-dimensional parametrization of classes of whole body motion

[Hsu 2005, Wang 2008]. In particular, recent works focused on methods for the blending of learned motion primitives, whose concatenations over time have to satisfy additional task constraints. For example, in [Feng 2012] captured motion samples were blended exploiting a "prioritized stack of controllers". In [Shoulson 2014] the instantaneous blending weights of controllers were prioritized by their serial order. In [Huang 2014] the coordination between locomotion and arm pointing in the last step was modeled by blending and selecting arm pointing primitives dependent on the gait phase.

3.1.2 Biological motor control of multi-step sequences

Human motor behavior including action sequences has been shown to be highly predictive. This has been investigated, for example, in a recent study on the coordination of walking and reaching [Land 2013]. Human subjects had to walk towards a drawer and to grasp an object, which was located at different positions in the drawer. Participants optimized their behavioral from multiple steps before the object contact, predicting the maximum end-state comfort during the reaching action [Weigelt 2010, Rosenbaum 2008]. This means that the steps prior to the reaching were modulated in a way that optimizes the distance for the reaching action [Land 2013]. In [Mukovskiy 2015a], our KoroiBot partners have proposed a learning-based framework that is based on movement primitives, learned from motion capture data. They are able to reproduce such human planning strategies in computer animation. The underlying architecture is simple and approximates complex full-body movements by dynamic movement primitives that are modeled by nonlinear dynamical systems. These primitives are constructed from kinematic primitives that are learned from trajectory sets by an anechoic demixing. Similarly to previous works [Gams 2008, Buchli 2006], the proposed method generates complex movements by combination of a small number of learned dynamical movement primitives. [Mukovskiy 2015a, Giese 2009a] have previously demonstrated the advantages of this approach for the adaptive online generation of multi-step sequences with coordinated arm movements.

3.1.3 Related approaches in humanoid robotics

Several approaches have been proposed in robotics for the synthesis of walking combined with grasping movements. Indeed, the DARPA robotics challenge valve manipulation task forced the researchers to find efficient and robust methods to perform reaching and manipulation tasks. [Ajoudani 2014] proposed a hybrid controller, where the robot is using a goal-driven fast foot step planner in combination with visual servoing for the reaching and grasp of the valve. [Kuindersma 2015] proposed a complete control architecture for the humanoid robot Atlas that is able to localize the robot and automatically find foot steps around or over obstacles in order to reach a user-defined goal. The architecture contains also a whole-body controller which allows the robot to get up from a lying down position, or to do complex tasks like turning the valve. Another team (IHMC) presented an architecture in [Johnson 2015] with a more sophisticated control of the locomotion [Englsberger 2014]. All three mentioned control architectures can make a humanoid robot reach, and then grasp or manipulate objects as required for the robotics challenge. Walking to grasp and manipulation tasks are usually subdivided in two different sub-tasks and, to our knowledge, a simultaneous coordination of both tasks has not been demonstrated so far. Other solutions for the combination of walking and vision-controlled reaching of a static and mobile target during walking were proposed in [Stasse 2008] and [Brandao 2013]. Other approaches include adaptation of randomized motion planning algorithms to generate complex body motion in a constrained environment [Dalibard 2013], but with the disadvantage of high computational time. A further work based on imitation and learning has been proposed by [Miihlig 2010], which also combines walking and grasping as two separate tasks. [Gienger 2010] proposed an algorithm for the computation of optimal stance locations with respect to the position of a reaching target, where a dynamical systems approach was used to generate the reaching behavior. [Yoshida 2007] used a task priority approach, based on a generalized inverse kinematics, in order to organize several sub-tasks, including stepping, hand motion, and gaze control. Another work has exploited global path planning in combination with walking pattern generators (WPGs) [Kajita 2003], in order to generate collision-free dynamically stable gait paths. A first attempt to transfer human reaching movements to humanoid robots by using motion-primitives was proposed in [Taïx 2013]. In this work the primitives were extracted by using PCA and the behavior was successfully implemented on the HRP-2 robot by involving the trunk and arm joints. The use of motion primitives in robotics was also proposed in [Gams 2013], which even includes the integration of force-feedback. Systems which are able to modulate dynamical movement primitives to generate complex motion in real-time were proposed by [Ijspeert 2013] and [Ajallooeian 2013].

3.2 System architecture

In this section the whole process that we used to generate walking to grasp motion is illustrated, starting from the recorded human data. The acquisition of data through motion capture, the scaling and the adaptation to match the humanoid robot constraints, the relative decomposition in dynamic primitives and the learning part have been developed by our Koroibot partner from Tübingen [Mukovskiy 2015b]. Our principal contribution was to implement the unstable trajectories inside the walking pattern generator (developed at LAAS-CNRS by Naveau et al. [Naveau 2017]) and to combine the two sub-tasks (grasping and walking) into a single one which is feasible and dynamically stable.

A general overview of the system architecture is shown in Figure 3.1. The extraction of the training data from the human data and the relative segmentation and re-targeting have been done offline. However, the generation of movement by the learned re-targeted motion primitives and the robot control have been performed online.

3.2.1 Human data

3.2.1.1 Drawer opening task

The modeling of walking-to-grasp was based on a motion capture data set obtained by recording humans walking toward a drawer and grasping an object. In the experiment, the initial distance from the drawer and the position of the object inside it was varied, in order to analyze the adapting behavior [Mukovskiy 2015a] (see Figure 3.2 and a related **video**[1] available online). The whole motion can be sub-divided in three parts:

1. normal walking, starting and ending with the left heel strike,
2. adaptive stepping until reaching the drawer with the left hand,
3. grasping, end of walking and taking the object with the right hand.

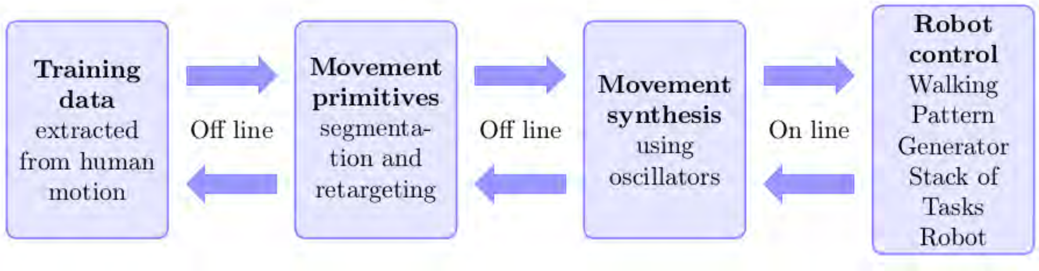
Training data
extracted from human motion
Off line
Movement primitives
segmenta-tion and retargeting
Off line
Movement synthesis
using oscillators
On line
Robot control
Walking Pattern Generator
Stack of Tasks
Robot

Figure 3.1: General overview of the system architecture.

The data set consists of the trajectories of ten trials of a single participant performing the task. The human data was recorded at Bielefeld University with a Vicon motion capture system, consisting of 12 MX-F20 CCD cameras (f=400Hz, accuracy of 1.5mm). The actor was equipped with 41 markers. The length of each action, in terms of space, is shown in Figure 3.3(a).

3.2.1.2 Preprocessing

The recorded motion capture was processed and animated with the 3D Character Animation Software MotionBuilder (Autodesk), using an avatar whose geometric parameters were adapted to the recorded subject. The trajectory were cut, starting at the first heel strike and ending once the object was reached. The kinematic model of HRP was created with the Computer Animation and Modeling Software Maya (Autodesk), neglecting kinematic constraints. All the ten trajectories were re-targeted to the HRP-2 model in MotionBuilder. In particular, the markers were fixed on the avatar body, scaled and synchronized, in order to "control" the virtual character motion by the recorded real trajectories. In other words, the avatar was "moved" by the real markers, reproducing the human motion. During re-targeting, the feet position was constrained to be parallel to the level ground. Also the step lengths were scaled in order to match the size difference between the actor and HRP-2. Once obtained the resulting scaled motion with the virtual character, the joint trajectories were extracted using the Denavit-Hartenberg (DH) convention. In turn, they were segmented and the step sizes were stored separately. The computed trajectories were further analyzed with Matlab (Mathworks ®) and re-sampled, resulting in a normalized duration of 1.6sec for each action. The data was divided into two subsets, separating pelvis trajecto-

---

[1] `https://tinyurl.com/he3dhb2`

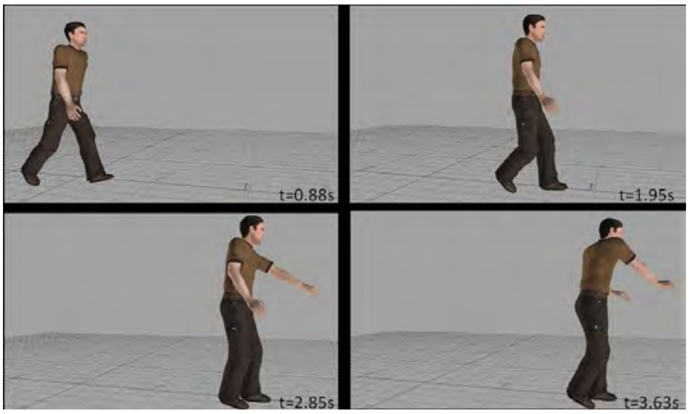

Figure 3.2: Illustration of important intermediate postures of the human behavior: step with initiation of reaching, standing while opening of drawer, and reaching for the object.

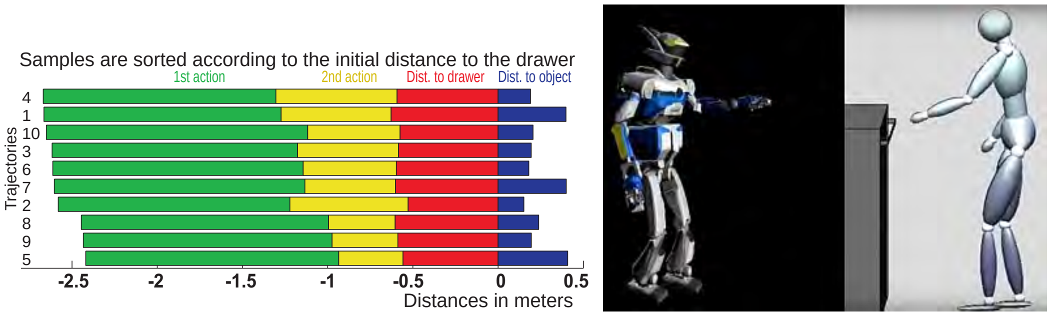

(a) (b)

Figure 3.3: Predictive planning of real human trajectories. Distances from the pelvis to the front panel of the drawer (green, yellow and red), and the distance between the front panel and the object (blue) for the ten trials (reproduced from [Mukovskiy 2015a]). (b) The result of the re-targeting process: human avatar and HRP-2 robot during drawer opening task.

ries (position and orientation in Transverse plane), and the upper body trajectories (HRP-2 joint angles extracted from DH representation). Pelvis position was rescaled in order to ensure the maximal admissible velocity propagation for HRP-2 (0.5 m/s). After such a rescaling, inverse kinematics method was applied to correct the upper body motion in order to satisfy the joint limits constraints during the reaching phase. We used the angular and linear velocity of the pelvis as input for the walking pattern generator. In Figure 3.3(b) the trajectories animated for a human avatar and the corresponding re-targeted trajectories for HRP-2 model are shown through Motion Builder. The related video is available here `http://tinyurl.com/j8qnbtp`.

3.2.1.3 Learning of the kinematic primitives

In order to learn low-dimensional representations of every individual segmented motions we applied the anechoic demixing algorithm [Omlor 2011, Chiovetto 2013], that represents the trajectories as linearly weighted superpositions of time-shifted source signals. The underlying *anechoic mixture model* approximates the joint trajectories in the form:

$$\underbrace{\xi_i(t)}_{angles} = m_i + \sum_j w_{ij} \underbrace{\sigma_j(t - \tau_{ij})}_{sources}$$

where, for each angle trajectory, $\xi_i(t)$ is represented as the linear mixture of j source signals $\sigma_j(t)$ with the linear weights w_{ij} plus the angle mean value m_i. The individual source signals can be shifted in time by delays τ_{ij}, which vary according to the angles and source components considered. It was shown that this method leads to compact approximations of human full-body trajectories, providing an accurate approximation of complex motions,

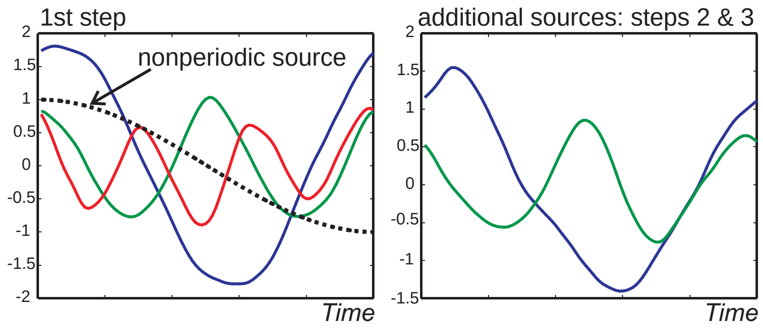

Figure 3.4: Extracted source signals.

often with less than 4-5 learned source functions. In our standard implementation, we first extracted the mean angle values from the data, then we estimated the weights of an additional non-periodic source component. Such a non-periodic function was pre-specified, given by the function $s_0(t) = cos(\pi t/T)$, where T was the time length of the slowest periodic source function. For the first action (walking forward) three periodic sources and a non periodic one were sufficient. To model the second, which requires adaptive steps, we added two periodic sources since only three were not sufficient. The weight of the last two source signals were learned from the residual (the difference between the original trajectories and the ones given by the learning with the three periodic sources and the non periodic one). The delay was constrained to be equal across the trial. In this way the blending between different motion styles is simplified, since the delays of the sources are identical over styles. The resulting shapes of learned source functions are presented in Figure 3.4.

3.2.1.4 Online kinematic motion synthesis of multi-action sequences

In order to synthesize whole body trajectories online we propose an architecture that generates the learned trajectories by expressing the source signals as stable solutions of an autonomous dynamical system, which can be regarded as a system of coupled central pattern generators (CPGs) [Omlor 2011, Chiovetto 2013]. Using this method, we generated online kinematic primitives from these dynamical systems, called dynamic primitives DMPs [Buchli 2006, Ijspeert 2008]. Then we mapped the solutions of the dynamic primitives onto source signals by Support Vector Regression (using a Radial Basis Function kernel and the LIBSVM Matlab® library [Chang 2001]). The resulting architecture is summarized at Figure 3.5. Since the attractors of this nonlinear system can be mapped to a circle in the phase plane, delays can be represented by a rotation angle of the vectors in state space. In this way, we are able to model coupled networks with delay between different CPGs by a set of coupled set of different equations without explicit time delays [Giese 2009a]. This

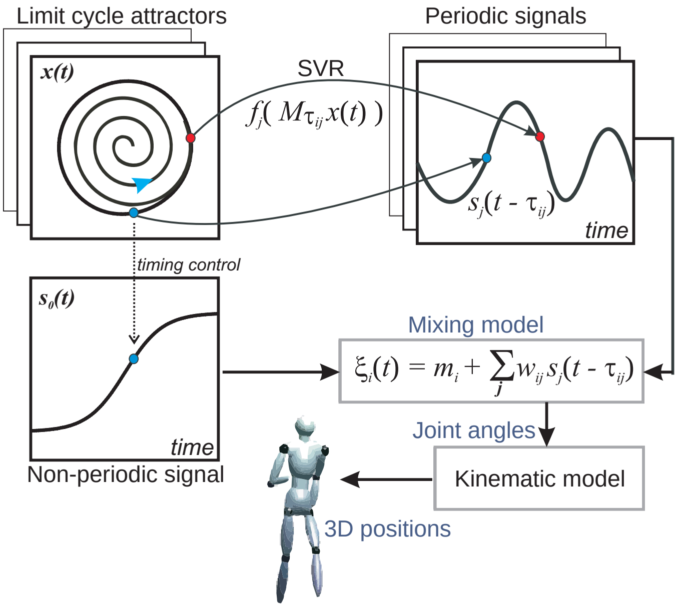
Limit cycle attractors
x(t)
SVR
$f_j(M_{\tau_{ij}} x(t))$
Periodic signals
$s_j(t - \tau_{ij})$
time
timing control
$s_0(t)$
time
Non-periodic signal
Mixing model
$\xi_i(t) = m_i + \sum_j w_{ij} s_j(t - \tau_{ij})$
Joint angles
Kinematic model
3D positions

Figure 3.5: Architecture for the online synthesis of body movements using dynamic primitives, [Giese 2009a]. This figure represents the module "Kinematic Pattern Synthesis" (see page 74)

results in a dynamic stable system, with methods of coupling based the on Contraction Theory [Park 2009]. The instantaneous phase of the leading DMP is even used to control the timing of the non-periodic source signal. In order to model the action with different styles, we learned nonlinear mappings between the task parameters and the weights of the source function in our mix model. These mappings were learned from training data using Locally Weighted Linear Regression (LWLR) [Atkeson 1997, Mukovskiy 2015a]. The relevant task parameters were step lengths and timings. To define the multi-steps sequence, we computed the step lengths as function of the estimated distance from the target. Based on training data, the achievable step ranges were computed: for the first phase, we automatically introduced additional steps if the target could not be reached within three steps, then for the second one we adjusted the step length in order to reach the target at a maximum comfort distance. The smooth interpolation of the weights of the kinematic primitives at the transition between the phases is described in [Mukovskiy 2015a].

As previously explained, the delay can be modeled as an additional rotation in the phase plane. Representing the attractors of this nonlinear system as circles, we can represent delays as a rotation of vectors, by an angle. In this way, for the periodic DMPs we chose a limit cycle oscillator (Andronov-Hopf oscillator) as canonical dynamics.

It can be characterized by two coupled nonlinear differential equations, where ω defines the eigenfrequency, for the pair of state variables $[x(t), y(t)]$:

$$\dot{x}(t) = [1 - (x^2(t) + y^2(t))]x(t) - \omega y(t)$$
$$\dot{y}(t) = [1 - (x^2(t) + y^2(t))]y(t) + \omega x(t))$$

The online phase-shifting is modeled as an additional rotation of the oscillator phase plane, such that, due to the circular shape of the attractor limit cycle of Andronov-Hopf oscillator, the trajectories on the attractor exhibit simple time-delays, c.f. [Giese 2009a].

3.2.2 Stack Of Tasks (SoT)

In this section we roughly present the framework Stack Of Tasks (SoT), implementing a Generalized Inverted Kinematics (GIK). The GIK introduced by Nakamura et al [Nakamura 1987] to control redundant robots is widely used in humanoid robotics [Gienger 2005, Neo 2005], as well as its counter part in the force domain. Based on the notion of task [Samson 1991], priority between tasks is introduced by projecting the tasks with lower priority in the kernel of tasks having a higher priority. The Stack of Tasks is mostly dedicated to implement the GIK formalism in an efficient manner.

Task definition

Let q be the vector of the robot articular positions. Let e_i be a tasks. Its Jacobian J_i is defined by:

$$\dot{e_i} = \frac{\partial e_i}{\partial q} = J_i \dot{q} \tag{3.1}$$

with J_i assumed to be of full rank. Assuming that the robot is controlled by $\dot{q}$, we can compute its value as:

$$\dot{q_i} = J_i^+ \dot{e_i}^* \tag{3.2}$$

where $\dot{e_i}^*$ is the desired motion in the task space and J_i^+ is the pseudo-inverse of J_i. The motion is generally constrained to follow a differential equation:

$$\dot{e_i}^* = -\lambda e_i \tag{3.3}$$

The following control law is:

$$\dot{q_i} = -\lambda J_i^+ \dot{e_i} \tag{3.4}$$

Finally, a task e_i is defined as a difference between a desired feature s_i^* and its current value s_i:

$$e_i = s_i - s_i^* \tag{3.5}$$

An example of desired feature could be a particular configuration (or a vector of configurations) of the right hand or the left hand that we want to reach, e.g. for grasping an object. Considering a secondary task e_2, it is defined as:

$$\dot{e}_2 = J_2 P \dot{q}_2 + J_2 \dot{q}_1^* \tag{3.6}$$

where $J_2 \dot{q}_1^*$ is the drift of the task. The control input $\dot{q}_2$ can be obtained by numerical inversion [Siciliano 1991]:

$$\dot{q}_2^* = (J_2 P)^+ (\dot{e}_2 - J_2 \dot{q}^*) + P_2 \dot{q}_3 \tag{3.7}$$

where P_2 is the projector into the null space of $J_2 P$. The same scheme can be reproduced iteratively to take into account any number of tasks until P_i is null.

Stack of Tasks

Let $(e_1, J_1)...(e_n, J_n)$ be *n* tasks with a priority order. The control law should ensure the realization of task e_{ith}, such that the e_i does not disturb the task e_j if $i > j$. A recursive computation of the joint velocity was proposed by Siciliano et al. [Siciliano 1991]:

$$\begin{cases} \dot{q}_0 & = 0 \\ \dot{q}_i & = \dot{q}_{i-1} + (J_i P_{i-1}^A)^+ (\dot{e} - J_i \dot{q}_{i-1}),\ i = 1..n \end{cases} \tag{3.8}$$

where P_i^A is the projector onto the null-space of the augmented Jacobian $J_i^A = (J_1, ..., J_i)$, realizing all the tasks in the stack $\dot{q} = \dot{q}_n$. The projector can be recursively computed by:

$$P_i^A = P_{i-1}^A - (J_i P_{i-1}^A)^+ J_i P_{i-1}^A \tag{3.9}$$

At each time *t*, one control iteration has to be performed. For each active task the systems computes the error related to a task. To this end, it is necessary to compute the feature $\mathrm{s}(q(t), t)$ related to the robot stat at time *t*. For some tasks the desired feature value s^* could be also dependent on *t*. Since an efficient mechanism should ensure that a value is not computed twice, the Stack of Task provides methods to share the information already processed. In other words, if an entity performs an operation, the resulting value is shared in order that if another entity had to do the same operation, the result is already available and accessible. An exhaustive and detailed description about the architecture of the Stack of Tasks have been provided by Mansard, Stasse et al in [Mansard 2009].

When facing simultaneous tasks, the corresponding equations can be grouped in a single system or, better, sorted in priority and solved each in the solutions set of higher priority tasks. Its limitation lies in the handling of inequality constraints, which are usually transformed into more restrictive equality constraints through potential fields. Kanoun et al. [Kanoun 2011] proposed a new prioritized task-regulation framework based on a sequence of quadratic programs (QP) that removes the limitation. They implemented and tested in simulation on the humanoid robot HRP-2. In other words, it is possible to rewrite a task as a QP because, though this formulation, both linear equalities and inequalities can be considered. A QP is composed of a quadratic cost function to be minimized, while satisfying the set of constraints [Fletcher 1971]. It can be seen as a two-level hierarchy, where the set of constraints has priority over the cost. Inequalities are set as the top priority. The introduction of slack variables is a classical solution to handle an equality at the second priority level [Boyd 2004]. In [Kanoun 2009], use of the slack variables was proposed to generalize the QP to more than two levels of hierarchy and, thus, to build a hierarchical quadratic problem (HQP) handling inequalities. If we consider a single task, the optimal solution to the problem can be expressed as:

$$\underset{\dot{q}}{min} \, \|J\dot{q} - \dot{e}^*\|^2 \tag{3.10}$$

By applying the QP resolution scheme, both equalities and inequalities can be considered. Considering two inequality bounds ($\underline{\dot{e}}^*$, $\overline{\dot{e}}^*$), where $\underline{\dot{e}}^*$ and $\overline{\dot{e}}^*$ are, respectively, the lower and upper bounds on the reference behavior, we have:

$$\underline{\dot{e}}^* \leq \dot{e}^* \leq \overline{\dot{e}}^* \tag{3.11}$$

For instance, in the case of two tasks with priority order $e_1 < e_2$, the QP expression is given by:

$$\begin{aligned} & \underset{\dot{q}, w_2}{min} \, \|w_2\|^2 \\ s.t. \quad & \underline{\dot{e}}_1^* \leq J_1\dot{q} + w_1^* \leq \overline{\dot{e}}_1^* \\ & \underline{\dot{e}}_2^* \leq J_2\dot{q} + w_2 \leq \overline{\dot{e}}_2^* \end{aligned}$$

where w_1 and w_2 are slack variables used to add some freedom to the solver if no solution can be found given the constraints. In robotics, when a constraint is expressed as an inequality, it is very likely to be put as the top priority: typically joint limits and obstacle avoidance. Using this framework, it is also possible to handle inequalities at the second priority level (i.e., in the cost function). A typical case is to prevent visual occlusion when possible, or to keep a low velocity if possible, without disturbing the robot behavior when it is not necessary. The same approach can be applied for solving Inverse Dynamics under constraints. These methods have been embedded in the SoT framework developed at LAAS-CNRS.

3.2.3 Walking Pattern Generator (WPG) with Dynamic Filter

In this section we provide an overview of the walking pattern generator and the dynamic filter that have been developed at LAAS-CNRS. The first WPG based on Model Predictive Control (MPC) was proposed by Kajita [Kajita 2003]. This method computed the reference nominal Zero Moment Point (ZMP) trajectory from the desired placements of feet during the gait cycle. A simplified linear inverted pendulum dynamics (also denoted as Cart-Table model) was used to link the Center of Mass (CoM) and the ZMP. In turn, Herdt et al. [Herdt 2010] proposed an "inverted" approach, with respect to the one of Kajita, that allows to exploit the position and the orientation velocities of the CoM as reference trajectories (for a time horizon of the next two steps), returning the foot placement and the optimal ZMP trajectories as results of the non linear model predictive control (NMPC). In the last years at LAAS-CNRS, Naveau et al. showed that real-time NMPC can be implemented on position controlled for humanoid robots. In [Naveau 2017], they proposed a WPG that takes into account simultaneously the position and the orientation of the feet. In addition, the algorithm exploits the Dynamic Filter that uses the whole-body dynamics to correct the center of mass trajectory of the underlying simplified mode. A more detailed description of the Dynamic Filter is provided below.

Re-paraphrasing these concepts in a more schematic way, in this work the WPG generates real-time dynamically stable reference trajectories for the CoM and ZMP, and the foot position. They are respectively noted as $\mathbf{CoM}^*$, $\mathbf{ZMP}^*$ and X^f. Once computed, they are given as inputs to the Dynamic Filter which operates as follows.

1. The joint trajectories are computed by an analytical inverse kinematics (*AIK*). This operation is very fast because it assumes that the CoM and the free flyer are rigidly connected. Moreover, such a inverse kinematics was developed specifically for the HRP2 model.

   $$(q,\, \dot{q},\, \ddot{q}) = AIK(single\_mass\_model,\, c,\, \dot{c},\, \ddot{c},\, X^f)$$

   where $q, \dot{q}, \ddot{q}$ are the joint position, velocity and acceleration and $c,\ \dot{c},\ \ddot{c}$ are the position, velocity and acceleration of the CoM.

2. Given $(q,\ \dot{q},\ \ddot{q})$, it is possible to compute the inverse kinematics (*ID*) in order to compute the ZMP of the real robot. We noted it as ZMP multi-body $\mathbf{ZMP}^{MB}$ and

it is an approximation of the multi-body dynamics of the real robot.

$$\begin{array}{ll} (\mathbf{f}, \tau) & = ID(\textit{complete\_model}, q, \dot{q}, \ddot{q}) \\ \mathbf{ZMP}_x^{MB} & = -\frac{\tau_y}{mg} \\ \mathbf{ZMP}_y^{MB} & = \frac{\tau_x}{mg} \\ \mathbf{ZMP}_z^{MB} & = 0 \end{array}$$

3. In turn, the error on the ZMP was computed on a preview window.

$$\mathbf{\Delta ZMP} = \mathbf{ZMP}^* - \mathbf{ZMP}^{MB}$$

4. The error $\mathbf{\Delta ZMP}$ can be used as input in the Preview Control proposed by Kajita et al. [Kajita 2003] to obtained the corresponding error for the CoM position, velocity and acceleration.

$$\mathbf{\Delta CoM} = KajitaPreviewControl(\mathbf{\Delta ZMP})$$

5. Finally, we sum this error to the reference CoM in order to obtain the corrected trajectory that will be used to compute the joint trajectory using a Generalize Inverse Kinematics (provided by the Stack of Task software).

$$\mathbf{CoM} = \mathbf{COM}^* + \mathbf{\Delta CoM}$$

We exploit this framework, developed at LAAS-CNRS for the humanoid robot HRP-2 [Naveau 2014, Naveau 2017], for the design of the WPG in our architecture.

3.2.4 Robotics Implementation

The implementation in the real robot was done in collaboration with Maximilien Naveau and Olivier Stasse at LAAS-CNRS, Gepetto Team. The lower part of the robot was controlled by the walking pattern generator with model predictive control, which computed the foot placements and the ZMP trajectory. The interesting part is that the walking pattern generator was able to generate a real-time stable walking given as input only the reference velocity and orientation of the pelvis. We can see this method as a top level approach to control the humanoid robotic platform in an easier way for the user. Moreover, the algorithm has been well tested and it can ensure stability and safety in terms of balance and self-collision. Since the upper body part can be considered as a perturbation that could destabilize the locomotion, the walking pattern generator included the dynamic filter [Naveau 2017] to compensate such perturbations. The upper body trajectories were further filtered before being sent to the system, in order to avoid discontinuities in velocity and acceleration. Moreover, an interpolation was necessary between the initial position and the first step motion, since the initial velocities were not equal to zero.

3.2.5 Overall architecture

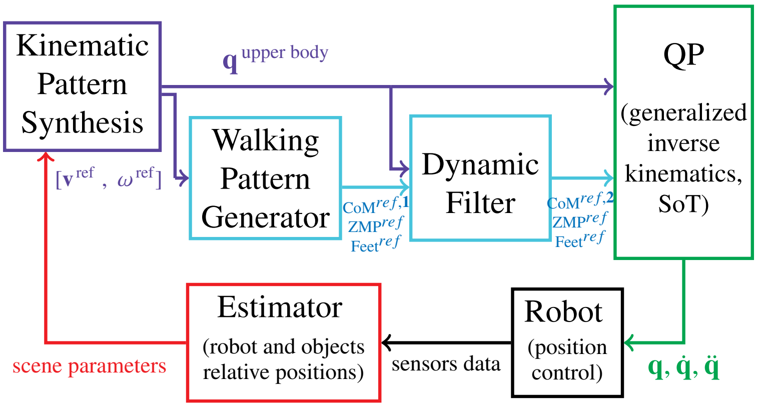
Kinematic Pattern Synthesis
$\mathbf{q}^{\text{upper body}}$
QP
(generalized inverse kinematics, SoT)
Walking Pattern Generator
Dynamic Filter
$[\mathbf{v}^{\text{ref}}, \omega^{\text{ref}}]$
$\text{CoM}^{ref,1}$
ZMP^{ref}
Feet^{ref}
$\text{CoM}^{ref,2}$
ZMP^{ref}
Feet^{ref}
Estimator
(robot and objects relative positions)
Robot
(position control)
scene parameters
sensors data
$\mathbf{q}, \dot{\mathbf{q}}, \ddot{\mathbf{q}}$

*Figure 3.6: Scheme of the feedback loop used to control the humanoid robot HRP-*2. $[v^{ref}, \omega^{ref}]$ *are respectively the linear and angular velocity and* $q^{upperbody}$ *the upper body joint trajectories computed from the kinematic pattern synthesis.* $q, \dot{q}, \ddot{q}$ *are respectively the generalized position and velocity vectors computed using the Stack of Tasks (SoT).*

In the following section we give a brief overview of the proposed robotics implementation (see Figure 3.6). The module labelled 'Kinematic Pattern Synthesis' is the system described in the previous Section 3.2.1. This module computes the upper body trajectories and the control inputs for the lower body (pelvis velocity and orientation). It is linked to the Walking Pattern Generator which computes the foot trajectories and the ZMP trajectories. Therefore they are sent to the dynamic filter which computes the appropriate compensation on the actual CoM position to make the whole body motion stable. The whole upper and lower body joint angles are then combined and the articular trajectories are computed by a generalized inverse kinematics using the Stack of Tasks, that allows to do inverse kinematics for an hierarchy of tasks. The operations performed in each task are in the null space of tasks with higher priority. Therefore, we compute the angular trajectories for the legs and the upper body. The executed behavior respects the dynamic stability constraints of the robot and, at the same time, the desired behavior of the upper body. During the motion execution, the real-world environment, the task parameters (step length and distance to the goal) and the current state of the robot are sent in the module *'Kinematic Pattern Synthesis'* which recomputes another set of upper body trajectories and low body inputs for adaptive interaction. This module has not been tested online yet.

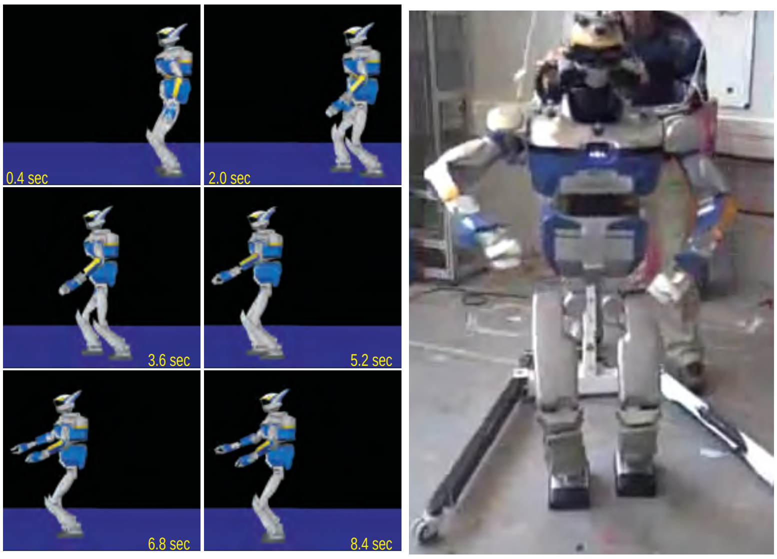

(a) (b)

Figure 3.7: (a) Off-line synthesized trajectories generated with the OpenHRP simulator. (b) The humanoid robot HRP-2 in LAAS-CNRS during the experiments.

3.3 Results

The experimental setup was divided in two steps. Firstly, the resulting motion was tested in simulation using the OpenHRP2 simulator (version 3.1) and the HRP-2 robot model. The robots started from half-sitting position (Figure 3.7(a), first image from top-left). The transition from this position to the first step is guided by a spline interpolation of each joint angle. The interpolation takes into account the linear and angular velocities during the first step. The transition time between the half-sitting position and the beginning of the first step is around one second. Three steps are then performed for reaching the drawer. At the end of the first phase, a further spline interpolation is required in order to make the stop phase as smooth as possible. An illustration of the executed motion is shown in Figure 3.7(a). At the end, it turned out that ten trajectories were not sufficient for the learning process to generate appropriate movements for reaching the drawer and grasping the object with good accuracy. For this reason, we did not consider the drawer in the real experiments.

3.3.1 Real Experiments

For the experiments the trajectories were re-sampled in order to be normalized with a duration of 1.6 second for each action. The data was divided in lower and upper body part: we sent the reference pelvis linear and angular velocity (v^{ref}, ω^{ref}) to control the legs and the steps, whereas the joint trajectories with relative velocity and acceleration $(q, \dot{q}, \ddot{q})$ were used as reference to control the torso and the arms. The pelvis velocity was rescaled to ensure the feasibility of the motion (max. speed 0.5 m/s). Since the perturbation provided by the chest motion (one of the heaviest part of the robot) was perturbation too much the equilibrium, we constrained the chest pitch joint to zero. Moreover, we scaled the yaw motion between the chest and the waist because it was creating an angular momentum around the vertical axis that the dynamic filter did not compensate. After these compensations, a customized inverse kinematics was applied to recompute the upper body trajectories in order to satisfy joint limit constraints and ensure a dynamical stable motion. In the final implementation on the real robot HRP-2, the upper body trajectories were further filtered using a Savitzky-Golay filter.

After training, for the learned parameters, the system generates human-like three-step sequences which cover a distance between 2.34 and 2.94 meters. This can be observed in **video**[2]. If the distance to goal exceeded such interval, the system automatically introduced additional gait steps in order to adapt the behavior for goal distance above 3 meters. In **video**[3] two examples of generated sequences for larger goal distances are presented.

The high degree of real-time online adaptivity is demonstrated in **video**[4]. The avatar has almost reached the target when suddenly the target jumps away towards a farther position, that can not be reached with the originally planned number of steps. Then the online planning algorithm automatically introduces an additional steps and adjusts the others, so that the behavior can successfully be accomplished.

A movie of the full 3-action sequence is presented in **video**[5], and a movie showing a 4-action sequence can be found in **video**[6]. As final step, the architecture was also tested using the real HRP-2 robot, see Figure 3.7(b).

3.3.1.1 Feasible motion

The trajectories were played successfully for 5 times consecutively with the real robot, as shown in **video**[7]. The forces measured on the vertical axis are depicted in Figure 3.8. Maximum force was less than $700\,N$, which is safe for the robot if we consider that during a static pose the forces applied on the feet are around $549.36\,N$ ($robot_{weight} * gravity = 56\,kg * 56 * 9.81 m/s^2$). The impact forces were less than half of the maximum threshold (over it, the sensors could break). We concluded that the motion performed was feasible and safe for the humanoid robot HRP-2.

---

[2] `http://tinyurl.com/jtkc6g7`

[3] `http://tinyurl.com/zu55rox`

[4] `http://tinyurl.com/hnxluuk`

[5] `http://tinyurl.com/jfda5ql`

[6] `http://tinyurl.com/j7dobcn`

[7] `http://tinyurl.com/jo42o55`

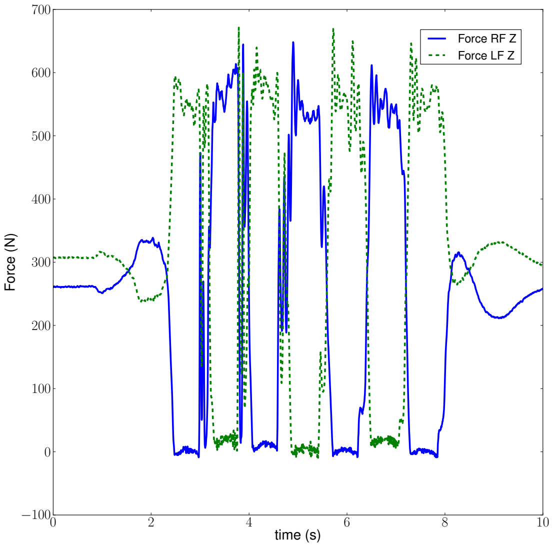

Figure 3.8: Forces on the vertical axis (z) measured during the experiment.

3.4 Conclusions

In this chapter, we have presented an architecture that combines the highly flexible online generation of coordinated full-body movements using dynamic primitives. The control architecture is based on a walking pattern generator that exploits nonlinear Model Predictive Control. The proposed architecture is suitable for the planning of complex coordinated full-body movements in real-time, and generates dynamically feasible behavior of the robot with appropriate balance control during walking. The high computation speed distinguishes the proposed framework from other approaches, which exploit optimum control for the synthesis of dynamically feasible complex full-body movements.

Ten trajectories of human walking and grasp task have been recorded. From this data, we animated a HRP-2 avatar after an appropriate re-targeting. The animations were processed by the software MotionBuilder (Autodesk) and the models created by Maya (Autodesk). Once satisfying unconstrained results were obtained in animation, the joint trajectories were extracted considering the kinematic robot constraints. In order to learn low-dimensional representations, we represent the trajectories as weighted linear combinations of time-shifted source signals in an anechoic mixture form. The trajectories generated by the learning were further analyzed with Matlab (Mathworks ®) and re-sampled and normalized in time. The data was divided into two subsets, separating pelvis and the upper-body trajectories. The former were considered as input to generate walking steps whereas the latter were used as reference motion for the grasping task. Results have shown the feasibility of the motion generated using this type of architecture.

CHAPTER 4

The geometry of confocal curves for passing through a door

The work presented in this chapter was done in an internal collaboration at LAAS-CNRS within the framework of ERC Actanthrope. The goal of this work was to implement some vision-based control laws to steer a robot through a door by using advanced geometric parametrization provided by confocal curves. In the following chapter we will present the strategies that we used to detect a door, identified by two landmarks attached to the vertical supports, and control the vehicle to pass through it. The originality of this work is that the proposed methods are able to directly provide the control inputs to steer the vehicle to accomplish the task, only using the landmarks coordinated directly measured in the camera plane. Therefore, our approach avoids the computational cost of a state observer that would require to localize the robot with respect to the goal. In the end of the chapter, we show the results in simulation and in a real scenario, where we employed the wheeled robot Robulab10, already presented in Chap. 1 and Chap. 2.

4.1 Introduction

Visual servoing techniques have been used both to drive a robot towards a target, with and without obstacles and for indoor navigation, as e.g. along a corridor. For instance, in [Dedieu 2000] two control strategies based on measurements coming from a pan camera and a 2D laser range sensor have been proposed for steering the vehicle towards a target amidst obstacles. In [Hayet 2012] a landmark-based navigation approach among obstacles has been developed for humanoid robots. It integrates high-level motion planning capabilities and a stack of feasible visual servoing tasks based on footprints following. The motion planning is based on the shortest path synthesis provided in [Salaris 2010, Bhattacharya 2007] where the limited Field–Of–View (FOV) problem is taken into account. In [Salaris 2011, López-Nicolás 2010] control laws to follow the shortest paths are also provided. In [Soueres 2005], a robust control strategy w.r.t. uncertainty on the depth of the target points and that takes into account the limits of actuator dynamics and the visibility constraint has been provided. On the other hand, in [Vassallo 1998] authors provided a visual-based control strategy to steer the vehicle along a corridor by using the vanishing point defined by the intersection of the corridor guidelines. For the same problem, in [Carelli 2002] the optic flow was also used in combination with the perspective lines of the corridor. In [Dev 1997] the temporal derivative of the optic flow has been exploited to determine the system state (orientation of the wall and distance to the wall), that is required to drive the robot through the center of the corridor.

Steering a vehicle through a door is one of the basic problem in visual servoing widely addressed in the literature. In [Pasteau 2016] a framework for vision-based autonomous indoor navigation in a wheelchair, capable of following a corridor and passing through doors using a single doorpost is provided. In particular, once a door is detected, the nearest doorpost, is considered and a control law able to steer the vehicle in front of the doorpost with a preassigned tolerance m is provided. Then, a circular path of radius m and centered at the doorpost is performed. In [Monasterio 2002] door crossing is solved combining vision and ultrasonic sensor information. The robot approaches the door until an adequate distance is reached. Door traversing is then performed using sonar sensors. A similar problem has been solved in [Dai 2013] for a large indoor surveillance robot equipped with a Kinect while crossing narrow doors. After having detected and located the door, the robot is steered through it by a nonlinear adaptive controller. A sensor based algorithm for guiding a wheelchair through a doorway has been proposed also in [Patel 2002]. The controller uses a camera and a laser range finder to perform the navigation. The problem of limited field-of-view constraints is also taken into account. In [Wang 2012] the same problem is solved by dynamically generating Bézier-curve based trajectories while in [Cheein 2010] the door crossing problem in unknown environment for a wheelchair has been solved by a dynamic path planning algorithm based on successive points determination. Finally, in [Cheein 2009] the authors propose a solution to a door crossing problem for an autonomous wheelchair equipped with a laser by solving a dynamic path planning algorithm based on successive points determination. An adaptive trajectory tracking control is then implemented to steer the wheelchair motion along the path in a smooth movement.

The approach that we propose in this chapter is different from the previous publications and the literature therein. Indeed, our method does not consist in a pre-planned path among via-points or a multi-stage strategy. On the contrary, we designed static feedback control laws (the vehicle velocities) that are functions of the current state of the system that is expressed in suitable coordinate systems that in turn can be directly measured in the image. As a consequence, the method avoids the computational cost of a state observer that would require to localize the robot. Moreover, no delay is added due to the time of convergence of a state observer to the true values. The use of static feedback control laws instead of dynamic ones simplifies the implementation of our method and the analysis of the overall controlled system in discrete time. Moreover, being a feedback and not a feed-forward control or a planning, it intrinsically possesses robustness against disturbances and uncertainties. Finally, as our method does not need the depth information, only a fixed monocular camera is needed as opposed to several other approaches where the camera data are often fused with other sensor data as e.g. sonar and laser.

In particular, the method we propose takes benefits from the geometry that naturally emerges from the problem statement. Seen from above, in the plane of the robot motion, the door is determined by two points: the footprints of its vertical supports. The originality of our approach is to introduce coordinate systems relative to these two points. The plane around the door is hence foliated by using confocal (the footprints of the door being the foci) hyperbolae and ellipses (a.k.a. elliptic coordinates system) and confocal circles that intersect at right angles (a.k.a. bipolar coordinates system). Using visual servoing we prove that these coordinates can be directly measured in the camera image plane. In other words, there exists a direct link between the geometry described by hyperbolae, ellipses and circles and the projection in the image plane of two landmarks located on the door supports and at the same height w.r.t. the the plane of the robot motion. We then provide feedback control laws based on these coordinate systems as well as proofs of asymptotic stability of the controlled system by using the Lasalle-Krasowskii principle. As both coordinates systems are immediately available in the image plane, we provide a so called Image–Based control scheme (see [Chaumette 2006], [Chaumette 2007] and [Hutchinson 1996]).

The chapter is structured as follows. The problem statement is given in section 4.2. In section 4.3 elliptic coordinates are introduced and the direct link between these coordinates and the image plane is established. In section 4.4 the control law able to steer the vehicle through the door by using these coordinates is proposed, and the stability of the closed–loop system is shown. A second coordinates system, aka bipolar coordinates, is then introduced in section 4.5 and the link with the image plane is established. A control law to accomplish the task by using these coordinates is then provided in section 4.6 and the stability of the controlled system is shown. In sections 4.7 and 4.8 simulations and experiments then illustrate the effectiveness of our control laws are shown. In particular, in 4.8 technical details about the implementation of the control on the real robot are provided. It is important to note that in own approach we did not implement a door detector algorithm, reasonably assuming that it will be always possible to determine two points in the image plane corresponding to the doorposts e.g. the top corners of the door. In section 4.9 a complete analysis of the FOV constraints and strategies to solve them are proposed. Some conclusions and a resume of perspectives and open problems close the chapter.

4.2 Problem Statement

Let us consider a vehicle moving on a plane where a right-handed reference frame $\langle W \rangle$ is defined with origin in O_W and axes X_W, Z_W. The configuration of the vehicle is described by $q(t) = (x(t), z(t), \theta(t))$, where $(x(t), z(t))$ is the position in $\langle W \rangle$ of a reference point of the vehicle, and $\theta(t)$ is the vehicle heading with respect to the X_W axis. Moreover, we assume that the dynamics of the vehicle is negligible. Using this notation, and denoting by $\nu(t)$ and $\omega(t)$ the robot linear and angular velocity, respectively, the kinematics exposes:

$$\begin{bmatrix} \dot{x} \\ \dot{z} \\ \dot{\theta} \end{bmatrix} = \begin{bmatrix} \cos\theta & 0 \\ \sin\theta & 0 \\ 0 & 1 \end{bmatrix} \begin{bmatrix} \nu \\ \omega \end{bmatrix}. \tag{4.1}$$

This is the so-called unicycle in the literature [Minguez 2008]. The vehicle is equipped with a rigidly fixed pinhole camera with reference frame $\langle C \rangle = \{O_c, X_c, Y_c, Z_c\}$ such that the optical center O_c corresponds to the robot center $[x(t), z(t)]^T$ and the optical axis Z_c is aligned with the robot forward direction (see Fig 4.1).

The main objective of this work is to steer this nonholonomic vehicle through a door by using measurements coming from the on–board camera. The door is represented by two visual landmarks located on each of its two vertical supports, at the same height h_w w.r.t. the plane of the robot motion. We denoted them by F^L and F^R (where R and L indicate the “Right” and “Left” support of the door). Without loss of generality, we assume that the Cartesian coordinates of these two points w.r.t. $\langle W \rangle$ are $F^R = (0, h_w, a)$ and $F^L = (0, h_w, -a)$, respectively.

Based on the pinhole camera model [Hartley 2003], the position of the projection of the landmark in the image plane is given by:

$$^I x_i = \alpha_x \frac{^c x_i}{^c z_i}, \tag{4.2}$$

$$^I y_i = \alpha_y \frac{h}{^c z_i}, \tag{4.3}$$

with $i = \{R, L\}$ and where $^c x_i$ and $^c z_i$ are the coordinates of the *i–th* landmark in the camera frame $\langle C \rangle$, h is the height of the landmarks w.r.t the plane (X_c, Z_c), while α_x and α_y are the camera intrinsic parameters, achievable by a calibration procedure and representing the focal length of the camera in terms of pixel dimensions in the x and y direction respectively. Notice that, plane (X_c, Z_c) usually does not coincide with the plane (X_W, Z_W). Finally, the velocity of the landmark w.r.t. the camera reference frame due to vehicle movement is given by:

$$\begin{aligned} {}^c\dot{x}_i &= \omega\, {}^c z_i \\ {}^c\dot{y}_i &= 0 \\ {}^c\dot{z}_i &= -\nu - \omega\, {}^c x_i\,, \end{aligned} \tag{4.4}$$

with $i = \{R, L\}$.

Remark 1 *In next sections, we assume a camera with a large FOV (as humans beings) so that the problem of keeping the landmarks in view is alleviated. This assumption does not impact the use of the control laws provided in next sections on a real system where the camera has a limited FOV. However, in Section 4.9, the FOV limits in case of a fixed on–board camera will be taken into account and analyzed.*

Remark 2 *Even though the methodology used in this work to design the control laws can be used also for different nonholonomic systems, e.g. unicycle, car-like and trailers, the feedback control laws developed in the next sections work only with the unicycle. However, the obtained trajectories can be directly used as reference trajectories for those nonholonomic vehicles as long as a tracking controller is provided.*

4.3 Some Basic Geometry Around The Door

In this section we describe the intrinsic geometry that naturally emerges around the door and we show how this geometry is useful to design a feedback control law that steers the vehicle through it.

Referring to Figure 4.1, assume that the forward velocity of the vehicle is constant, e.g. $\nu = 1$, and that the vehicle moves while satisfying the following equality:

$${}^I x_R(t) \equiv -{}^I x_L(t)\,, \tag{4.5}$$

for all $t \in [0, T]$. In this case the vehicle is aligned with the bisector of angle $\widehat{F^L O_c F^R}$. In other words, the bearing angles[1] $\alpha_R(t)$ and $\alpha_L(t)$ w.r.t. each landmark have equal amplitude but opposite signs. Indeed, from (4.2) and (4.5) we have:

$$\frac{{}^c x_R}{{}^c z_R} \equiv -\frac{{}^c x_L}{{}^c z_L} \qquad \Rightarrow \qquad \tan\alpha_R(t) \equiv -\tan\alpha_L(t) \tag{4.6}$$

and hence $\alpha_R(t) = -\alpha_L(t) = \frac{\alpha(t)}{2}$.

---

[1] The bearing angle w.r.t. a goal is the angle between the heading of the robot and the direction to the goal.

Moreover, by deriving the first equality in (4.6) and substituting (4.4) with $\nu = 1$, we obtain the control ω that steers the vehicle along a path where (4.6) is satisfied, i.e.

$$\omega = -\frac{{}^{c}x_L {}^{c}z_R^2 + {}^{c}x_R {}^{c}z_L^2}{{}^{c}x_R {}^{c}x_L {}^{c}z_R^2 + {}^{c}x_R^2 {}^{c}z_L^2 + {}^{c}z_R^2 {}^{c}z_L ({}^{c}z_R + {}^{c}z_L)} . \tag{4.7}$$

By using this strategy, the vehicle moves along a *hyperbola*, i.e. the locus of points where the absolute value of the difference between distances to the two foci (i.e. the projections on the motion plane of the two landmarks), is constant. Indeed, let us consider the distances $\rho_R = \sqrt{{}^{c}x_R^2 + {}^{c}z_R^2}$ and $\rho_L = \sqrt{{}^{c}x_L^2 + {}^{c}z_L^2}$ between the robot and each landmark respectively. By using (4.4) with $i = R, L$, respectively, and by setting $\nu = 1$, the dynamics of ρ_R and ρ_L reduces to

$$\dot{\rho}_R = -\frac{z_R}{\rho_R}, \quad \dot{\rho}_L = -\frac{z_L}{\rho_L} .$$

As $z_R = \rho_R \cos\alpha_R$ and $z_L = \rho_L \cos\alpha_L$, if the control ω given by: (4.7) is applied, $\alpha_R = \alpha_L = \alpha/2$ and hence

$$\dot{\rho}_R - \dot{\rho}_L = -\cos\alpha_R + \cos\alpha_L = 0.$$

We conclude that $\rho_R - \rho_L = K = const.$ along the path.

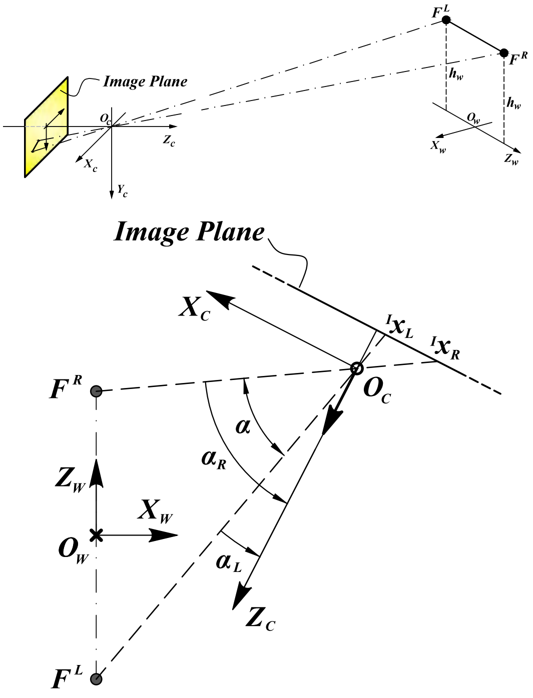

Figure 4.1: Objective: to steer a vehicle through a door using only visual measures. The door is represented by two landmarks, F^L and F^R and the vehicle, represented as a directed point, has an on-board camera and is subject to nonholonomic constraints.

The parametric equations of a generic hyperbola with foci F^R and F^L are given by:

$$\begin{aligned} x &= a\cos\eta\sinh\xi \\ z &= a\sin\eta\cosh\xi \end{aligned} \tag{4.8}$$

with $\xi \in [0,\infty]$ and η constant with values in $[-\pi,\pi)$. Constant K is equal to $2a\sin\eta$, i.e. the distance between the two vertices. In the canonical form we have: $\frac{z^2}{a^2\sin^2\eta} - \frac{x^2}{a^2\cos^2\eta} = \cosh^2\xi - \sinh^2\xi = 1$. Hence, curves with constant η form hyperbolae. In the special case of $\eta \in \{0,\pm\pi\}$, the hyperbola degenerates into a straight line passing perpendicularly through the middle of the segment [F^R, F^L] (see Figure 4.2).

Notice that, by using the strategy described above, the vehicle definitely goes through the door. Indeed, any such hyperbola crosses the segment between the landmarks. However, among all hyperbolae, the one followed by the vehicle depends on initial conditions. As a consequence, the vehicle might pass too near to the left or to the right jamb of the door. The ideal a good behavior would be to go as close as possible to the middle of the door. We will address this issue in section 4.4.

Coming back to the parametric equations of the hyperbola (4.8), let us consider the case in which ξ is constant and η varies. Such curves, which are known as *ellipses*, can be expressed in the canonical form as: $\frac{x^2}{a^2\sinh^2\xi} + \frac{z^2}{a^2\cosh^2\xi} = \cos^2\eta + \sin^2\eta = 1$. The bundle of hyperbolae, obtained for different values of η and the bundle of ellipses, obtained for different values of ξ, form an orthogonal coordinate system, a.k.a. *elliptic coordinates*, in which the coordinate lines are confocal ellipses and hyperbolae.

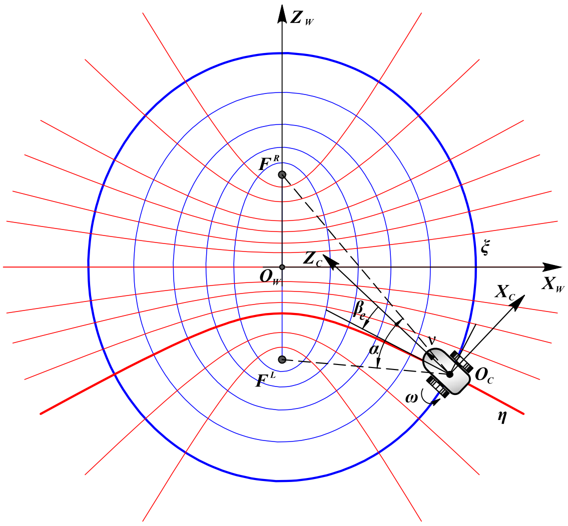

Figure 4.2: Elliptic coordinate system. Ellipses and hyperbolae intersect perpendicularly.

4.3.1 Elliptic Coordinates

Denoting by $\rho_R = \sqrt{(z-a)^2+x^2}$ and $\rho_L = \sqrt{(z+a)^2+x^2}$ the distance from the foci, i.e. the projections in the plane of the robot motion of the landmarks F^R and F^L, respectively, the elliptic coordinates (ξ, η) can be expressed as:

$$\xi = \operatorname{arccosh}\left(\frac{\rho_R+\rho_L}{2a}\right), \quad \eta = \frac{\pi}{2} - \arccos\left(\frac{\rho_L-\rho_R}{2a}\right) \tag{4.9}$$

Notice that, at the limit $a \to 0$, elliptic coordinates reduce to polar coordinates (ρ, ψ). In particular, $\eta \to \psi$ and $a\cosh\xi \to \rho$. This also happens when the vehicle is sufficiently far from the door. To complete this set of coordinates and to univocally describe the vehicle configurations, let us introduce a generalization of the bearing angle that is the angle between the heading of the vehicle and the tangent to the hyperbola passing through the vehicle position:

$$\beta_e = \arctan(\tanh\xi \,\tan\eta) - \theta + \pi\,. \tag{4.10}$$

Remark 3 *Assuming a calibrated camera, elliptic coordinates can be directly computed from the measurements of features in the image plane, hence basically without a state observer, even if h is unknown. Indeed, from* (4.2) *and* (4.3) *we have:*

$$\rho_i = \frac{\alpha_y}{\alpha_x}\frac{h}{{}^I y_i}\sqrt{{}^I x_i^2+\alpha_x^2}\,, \qquad i = R, L\,.$$

while the distance between the two landmarks is given by:

$$2a = \frac{\alpha_y h}{\alpha_x {}^I y_R {}^I y_L}\sqrt{\left({}^I x_R {}^I y_L - {}^I x_L {}^I y_R\right)^2 + \alpha_x^2\left({}^I y_L - {}^I y_R\right)^2}\,.$$

Hence,

$$\xi = \operatorname{arccosh}\left(\frac{{}^I y_L\sqrt{{}^I x_R^2+\alpha_x^2}+{}^I y_R\sqrt{{}^I x_L^2+\alpha_x^2}}{\sqrt{\left({}^I x_R {}^I y_L - {}^I x_L {}^I y_R\right)^2 + \alpha_x^2\left({}^I y_L - {}^I y_R\right)^2}}\right) \tag{4.11}$$

$$\eta = \frac{\pi}{2} - \arccos\left(\frac{{}^I y_L\sqrt{{}^I x_R^2+\alpha_x^2}-{}^I y_R\sqrt{{}^I x_L^2+\alpha_x^2}}{\sqrt{\left({}^I x_R {}^I y_L - {}^I x_L {}^I y_R\right)^2 + \alpha_x^2\left({}^I y_L - {}^I y_R\right)^2}}\right) \tag{4.12}$$

that does not depend on h. Notice that, (4.11) *and* (4.12) *come from the definition of the elliptic coordinates* (4.9)*. For geometric properties, $\rho_R+\rho_L \geq 2a$ and $\rho_R-\rho_L \leq 2a$ and hence, the arguments in* (4.11) *and* (4.12) *are always well defined. Moreover, for the* *particular 3D positions of landmarks, the denominators cannot be equal to zero.*

Finally, it is easy to prove that the bearing angle β_e is given, in the image plane, by:

$$\beta_e = -\frac{1}{2}\left(\arctan\left(\frac{{}^I x_R}{\alpha_x}\right) + \arctan\left(\frac{{}^I x_L}{\alpha_x}\right)\right) \tag{4.13}$$

Notice that, in case of landmarks at different height, results in Remark 3 do not hold anymore, as coordinates (ξ, η) depend also on those values. However, the heights are constant and can be considered known or estimated by an observer.

4.3.2 Kinematic Model of the vehicle in Elliptic Coordinates

The vehicle kinematic model in elliptic coordinates $\zeta = (\xi, \eta, \beta_e)$, with $\xi \in [0, \infty)$ and $\eta \in (-\pi/2, \pi/2)$ is:

$$\begin{aligned}
\dot{\xi} &= -\frac{\nu \cos\beta_e \sec\eta \operatorname{sech}\xi}{a\sqrt{1+\tan^2\eta \tanh^2\xi}} \\
\dot{\eta} &= \frac{2\nu \cos\eta \cosh\xi (\sin\gamma + \cos\gamma \tan\eta \tanh\xi)}{a(\cos(2\eta) + \cosh(2\xi))} \\
\dot{\beta}_e &= -\omega - \frac{2\nu(\cos\beta_e \operatorname{sech}\xi \sin\eta - \sin\beta_e \sec\eta \sinh\xi)}{a(\cos(2\eta)+\cosh(2\xi))\sqrt{1+\tan^2\eta \tanh^2\xi}}
\end{aligned} \tag{4.14}$$

and $\gamma = \beta_e - \arctan(\tan\eta \tanh\xi)$. Notice that the denominators of previous equations is equal to zero if $\cos(2\eta) + \cosh(2\xi) = 0$. However, as $\cosh(2\xi) \geq 1$, being exactly 1 when the vehicle is on the segment [F^R, F^L], the expression can be zero only on [F^R, F^L] if and only if $\eta = \pm\pi/2$. Being $\eta = \pm\pi/2$ only on the half-lines from F^R and F^L to infinity, i.e. along the Z_W axis, outside the segment [F^R, F^L], the denominators of the kinematic model in elliptic coordinates can never be zero.

Next section is dedicated to the design of a feedback control law that steers the vehicle through the middle of the door by exploiting the planar geometry that has been previously described.

Remark 4 *The problem to be solved can be viewed as determining a smooth and time-invariant feedback control law for stabilizing the system at $\zeta = 0$ by a smooth. However, the existence of such control law for this kind of nonholonomic systems is subject to Brockett's result [Brockett 1983]. In the special case of* (4.14)*, i.e. a driftless affine-in-control system, the input vector fields are linearly independent at the origin. Moreover, the number*

$\sec\eta = \frac{1}{\cos\eta}$; $\operatorname{sech}\eta = \frac{1}{\cosh\eta}$

of controls is less than the number of state variables. Hence, we can conclude that there exists no solution to the stabilization problem by a smooth and time invariant feedback control law. Notice that, in polar coordinates, i.e. the degenerate case of elliptic coordinates in case of $a \to 0$*, a solution to the stabilization problem at the origin exists, as proved in [Aicardi 1995].*

4.4 Feedback Control Law in Elliptic Coordinates

Let us consider the problem of designing a feedback control law that steers the vehicle through the door as close as possible to the middle. To design a such control law, let us first consider the following change of inputs:

$$\nu = w\,a\,\cos\eta\cosh\xi\sqrt{1+\tan^2\eta\tanh^2\xi} \tag{4.15}$$

$$\omega = -\omega_o + \frac{2u(\cos\beta\,\mathrm{sech}\,\xi\sin\eta - \sin\beta\sec\eta\sinh\xi)}{a(\cos(2\eta)+\cosh(2\xi))\sqrt{1+\tan^2\eta\tanh^2\xi}} \tag{4.16}$$

where w and ω_o are new control variables. By substituting (4.15) and (4.16) in (4.14) the kinematic model reduces to

$$\begin{aligned} \dot{\xi} &= -w\cos\beta_e \\ \dot{\eta} &= w\sin\beta_e \\ \dot{\beta}_e &= \omega_o\,. \end{aligned} \tag{4.17}$$

The objective is now to design w and ω_o such that η and β_e converge to zero. Let us hence assume $w = \bar{w}$ and consider the following candidate of Lyapunov:

$$V(\eta,\beta_e) = \frac{1}{2}\left(\lambda\eta^2 + \beta_e^2\right),$$

where λ is a positive constant parameter. Its time derivative, after substituting (4.17), expresses:

$$\dot{V}(\eta,\beta_e) = \bar{w}\lambda\eta\sin\beta_e + \beta_e\omega_o\,, \tag{4.18}$$

and by choosing

$$\omega_o = -K\beta_e - \bar{w}\lambda\eta\frac{\sin\beta_e}{\beta_e} \leqslant 0 \tag{4.19}$$

with $K > 0$ a constant parameter, we obtain

$$\dot{V}(\eta,\beta_e) = -K\beta_e^2\,,$$

This derivative is negative semi-definite. However, the control ω_o is well definite and smooth everywhere. Let us define $R = \{(\eta, \beta_e) | \dot{V} = 0\}$: in this case, we have that $R = \{(\eta, \beta_e) | \beta_e = 0\}$, i.e. β_e is constantly zero. As a consequence, in R, also $\dot{\beta}_e = 0$. Hence, it is straightforward to observe that the only trajectory of (4.17) in R with control input given by (4.19) is such that $\dot{\beta}_e = 0 = \omega_o = -\bar{w}\lambda\eta$. By assuming that $\bar{w}$ and λ are not zero, the previous equality is verified only if η is equal to zero as well. In conclusion, R does not contain any trajectory of the system, except the trivial trajectory $(\eta, \beta_e) = (0, 0)$. All conditions of the local Krasowskii-Lasalle principle are satisfied. We hence conclude that every trajectory starting from inside a given level curve of V that contains the origin, converges to the origin as $t \to \infty$. Moreover, as V is radially unbounded, we can conclude on the global asymptotic stability of the origin. Of course, other nonlinear control approaches could be used with system (4.17) to steer the vehicle through the door. For example, an input-output feedback linearization with η as measurement.

The control law (4.19), basically solves a path following problem in elliptic coordinates. A similar solution can be obtained in Cartesian coordinates to stabilize the vehicle along the Z_W axis (models (4.1) and (4.17) are very similar). However, elliptic coordinates have some advantages: they can be obtained directly from measurements in the image plane (hence basically a state observer is not required). Moreover, all hyperbolae pass through the door, hence guaranteeing that the vehicle goes through it.

Remark 5 *Each hyperbola intersects each ellipse in two points, symmetric w.r.t. the Z_W axis. The control laws developed in this work are immune to this fact as long as in remarks 3 the order of the landmarks is respected: the landmark on the left side, labelled by "L", and the landmark on the right side, labelled by "R". On the other hand, by using this strategy, the vehicle cannot go through the door from the half-plane characterized by $x > 0$ starting from the half-plane with $x < 0$ and vice-versa. However, in a real scenario this is not a standard situation.*

4.5 The Bundle of circles

The feedback control laws provided in the previous section is not able to steer the vehicle through the middle of the door but only near to it. The distance between the middle of the door and the point where the vehicle crosses the door depends on initial conditions and hence, the values of the constant parameters K and λ in (4.19) should be suitably chosen to reduce as much as possible this error.

In this section, we will provide a feedback control law able to drive the vehicle exactly to the middle of the door, independently from the initial configuration. We will start by analyzing the angle between the directions towards the two landmarks (angle α in Figure 4.3) and its first time derivative. Then, we will show how this study brings to a particular geometry, i.e. two mutually orthogonal bundles of circles, that can be exploited to solve the problem at hand, overcoming all drawbacks of the control law furnished in the previous section.

For any point $O_c = (x, z)$ there always exists a circle C_α passing through O_c and through the projections of landmarks F^L and F^R in the motion plane (see Figure 4.3). The angle $\alpha = \widehat{F^L O_c F^R}$ is constant along C_α (a.k.a. angle at the circumference).

Of course, on the contrary, for each value $\alpha \in [0, \pi]$ there are two circles passing through F^R and F^L and symmetric w.r.t. the Z_W axis whose angle at the circumference is α: by varying $\alpha \in [0, \pi]$ we obtain a bundle of circles $\mathcal{C}_\alpha$ that, with the previous defined bundle of hyperbolae, form a skew coordinates system.

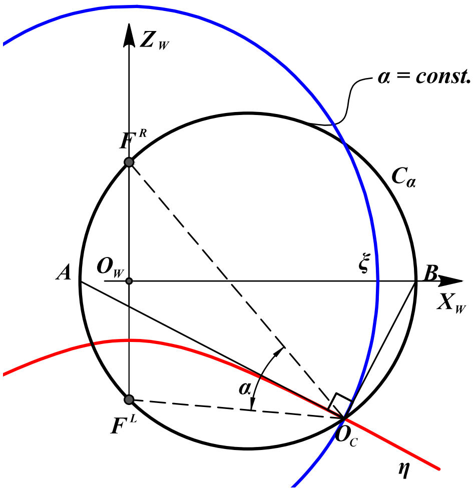

Figure 4.3: For any point $O_c = (x, z)$ there always exists a circle C_α passing through O_c and the projections in the motion plane of landmarks F^L and F^R. The angle at the circumference α is constant along C_α. Notice that, the tangent and perpendicular line in O_c to the hyperbola through O_c, intersect the X_W axis in points A and B, respectively. The segment $\overline{AB}$ is the diameter of circle C_α.

Indeed, circles and hyperbolae do not intersect orthogonally. The expression of α in terms of ξ and η is

$$\alpha = \arccos\left(1 - \frac{4\cos^2\eta}{\cos(2\eta) + \cosh(2\xi)}\right), \tag{4.20}$$

while its time derivative $\dot{\alpha}$, which is not reported here for the sake of space, assumes the maximum value when

$$\beta_e = \beta_{max} = -\operatorname{sgn}(\eta)\arccos\left(\frac{\sqrt{2}\cos\eta\cosh\xi}{\sqrt{\cos(2\eta) + \cosh(2\xi)}}\right), \tag{4.21}$$

hence necessarily $\beta_e \neq 0$. Indeed, if $\beta_e \equiv \beta_{max}$ the vehicle is aligned to the perpendicular to the circle C_α passing through the current position of the vehicle. Of course, this happens for all values of α and for all points in C_α. The set of all possible curves orthogonal to all members of $\mathcal{C}_\alpha$ constitutes a second bundle of circles $\mathcal{C}_\alpha^\perp$, as shown in Figure 4.4. In other words, for any point $Q \in C_\alpha$ there always exists a circle $C_\alpha^\perp$ of $\mathcal{C}_\alpha^\perp$, perpendicular to C_α in Q. Moreover, $C_\alpha^\perp$ crosses perpendicularly all circles of $\mathcal{C}_\alpha$.

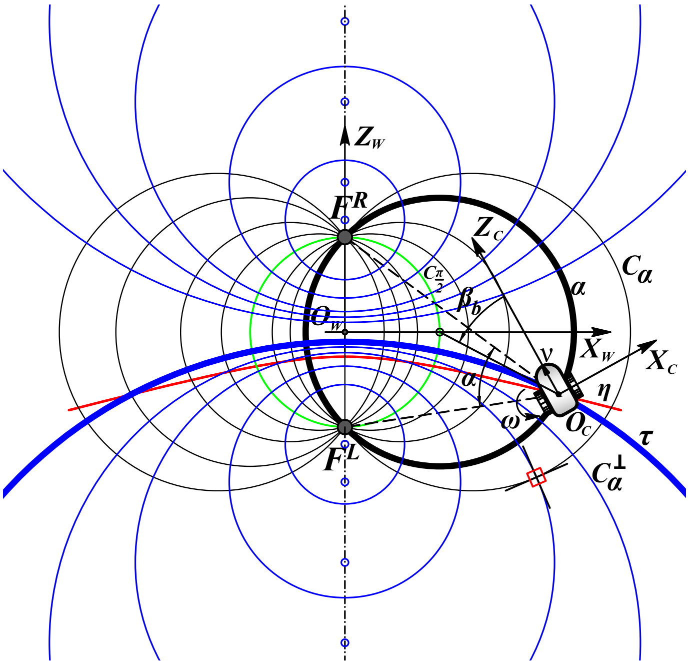

Figure 4.4: The bipolar coordinate system consists of two orthogonal bundles of circles. Starting from the same point O_c, circle $C_\alpha^\perp$ crosses segment $\overline{F^L F^R}$ in a point which is closer to the middle of the door than the one reachable by following the hyperbola through O_c.

4.5.1 Bipolar Coordinates

The orthogonal bundles of circles previously introduced can be regarded as an orthogonal coordinates system also known as bipolar coordinates. The relationships between bipolar coordinates τ and α and the Cartesian coordinates x and z are:

$$x = \frac{a \sin\alpha}{\cosh\tau - \cos\alpha}, \quad z = \frac{a \sinh\tau}{\cosh\tau - \cos\alpha},$$

assuming poles F^R and F^L on the Z_W axis. Moreover, τ and α assume values in the following ranges $-\infty < \tau < \infty$ and $0 \leq \alpha \leq \pi$. The bipolar coordinates expressed in terms of Cartesian ones are:

$$\begin{aligned} \tau &= \log\left(\frac{\rho_L}{\rho_R}\right) \\ \alpha &= \arccos\left(\frac{\rho_R^2 + \rho_L^2 - 4a^2}{2\rho_R\rho_L}\right). \end{aligned} \tag{4.22}$$

From previous equations, after some algebra, it is possible to show that curves with constant τ are given by: $x^2 + \left(z - \frac{a}{\tanh\tau}\right)^2 = \frac{a^2}{\sinh^2\tau}$, which is the equation of a circle whose center is on the Z_W axis with coordinates $(0, \frac{a}{\sinh\tau})$ and radius $R = \frac{a}{|\sinh\tau|}$. These circles have been previously denoted by $C_\alpha^\perp \in \mathcal{C}_\alpha^\perp$. On the other hand, if α is constant, we obtain curves given by: $\left(x - \frac{a}{\tan\alpha}\right)^2 + z^2 = \frac{a^2}{\sin^2\alpha}$ which is the equation of a circle passing through the projection in the motion plane of landmarks F^R and F^L, centered on the X_W axis at $(\frac{a}{\tan\alpha}, 0)$ and radius $R = \frac{a}{|\sin\alpha|}$. These circles have been previously denoted by $C_\alpha \in \mathcal{C}_\alpha$.

To describe the position of the vehicle in the motion plane w.r.t. the door, let us consider a slightly different pair of coordinates, i.e. τ and $\hat{\alpha} = \pi - \alpha$. Notice that, $\hat{\alpha}$ is the supplementary angle of the angle at the circumference. Moreover, the middle of the door is the origin of those coordinates. Finally, as for elliptic coordinates, to univocally describe the vehicle configuration, let us introduce the angle β_b between the heading of the vehicle and the tangent to the circle $C_\alpha^\perp$ passing through the vehicle position. The expression of this angle w.r.t. α and τ and θ is:

$$\beta_b = \arctan\left(\frac{\sin\alpha \sinh\tau}{1 - \cos\alpha\cosh\tau}\right) - \theta + \pi. \tag{4.23}$$

Remark 6 *Assuming a calibrated camera, bipolar coordinates can be computed directly from the image plane measurements. Indeed, τ can be expressed in terms of image coordinates of the couple of features as $\tau = \log\left(\frac{{}^I y_L \sqrt{{}^I x_R^2 + \alpha_x^2}}{{}^I y_R \sqrt{{}^I x_L^2 + \alpha_x^2}}\right)$. Moreover, $\hat{\alpha}$ can be easily obtained as $\hat{\alpha} = \pi - \left(\arctan\left(\frac{{}^I x_L}{\alpha_x}\right) - \arctan\left(\frac{{}^I x_R}{\alpha_x}\right)\right)$, while β_b can be determined from* (4.23)*, where θ can be obtained combining* (4.10) *with* (4.13)*. Hence, also β_b can be found* *directly from image plane measurements.*

4.5.2 Kinematic model of the vehicle in bipolar coordinates

The kinematic model of the vehicle in bipolar coordinates $\lambda = (\tau,\, \hat{\alpha},\, \beta_b)$ is

$$\begin{aligned}
\dot{\tau} &= \frac{\nu}{a}\left((1+\cos\hat{\alpha}\cosh\tau)\sin\left(\beta_b - \operatorname{arccot}\left(\cot\hat{\alpha}\coth\tau + \csc\hat{\alpha}\operatorname{csch}\tau\right)\right)+\right.\\
&\quad \left.+\cos\left(\beta_b - \operatorname{arccot}\left(\cot\hat{\alpha}\coth\tau + \csc\hat{\alpha}\operatorname{csch}\tau\right)\right)\sin\hat{\alpha}\sinh\tau\right)\\
\dot{\hat{\alpha}} &= \frac{\nu}{a}\left(-\cos\left(\beta_b - \operatorname{arccot}\left(\cot\hat{\alpha}\coth\tau + \csc\hat{\alpha}\operatorname{csch}\tau\right)\right)(\cos\hat{\alpha}\cosh\tau+1)+\right.\\
&\quad \left.+\sin\hat{\alpha}\sin\left(\beta_b - \operatorname{arccot}\left(\cot\hat{\alpha}\coth\tau + \csc\hat{\alpha}\operatorname{csch}\tau\right)\right)\sinh\tau\right)\\
\dot{\beta}_b &= -\omega - \frac{\nu}{a}\frac{(\cos\hat{\alpha}+\cosh\tau)^2(\cos\beta_b\csc\hat{\alpha}+\operatorname{csch}\tau\sin\beta_b)}{(\cos\hat{\alpha}-\cosh\tau)\sqrt{1+(\cot\hat{\alpha}\coth\tau+\csc\hat{\alpha}\operatorname{csch}\tau)^2}}\,.
\end{aligned} \tag{4.24}$$

Based on (4.20) and (4.21) the maximum value $\dot{\hat{\alpha}}_{max}$ of $\dot{\hat{\alpha}}$ is obtained along circles of $\mathcal{C}_\alpha^\perp$, i.e. with $\beta_b = 0$. By the second of (4.24) we have:

$$\dot{\hat{\alpha}}_{max} = \dot{\hat{\alpha}}\Big|_{\beta_b=0} = -\frac{\nu(\cos\hat{\alpha}+\cosh\tau)}{a}\,. \tag{4.25}$$

For positive values of ν, the function (4.25), is negative and equal to zero if $\tau = 0$ and $\hat{\alpha} = \pi$ (or $\alpha = 0$), i.e. very far from the door.

4.5.3 A simple strategy to steer the vehicle through the door exploiting the geometric properties of the bundle of circles

A strategy to steer the vehicle through the middle of the door follows from these geometric facts: for any point $Q \in C_\alpha^\perp$ the tangent line to $C_\alpha^\perp$ passes through the center of the circle C_α through Q. Moreover, the center of C_α is in turn at the intersection between axis X_W and the circle $C_{2\alpha}$ (i.e. a circle of $\mathcal{C}_\alpha$ whose angle at the circumference is 2α). In particular, the center of circle $C_{\pi/2}$ coincides with the middle of the door (see Figure 4.4). Hence, starting from points Q such that $\alpha < \pi/2$, a possible strategy is to follow a circle $C_\alpha^\perp$ of bundle $\mathcal{C}_\alpha^\perp$ until the circumference characterized by $\alpha = \pi/2$ is reached. Then, it is sufficient to move along a straight line to pass through the middle of the door.

Even though the strategy previously described is able to steer the vehicle through the middle of the door, it has some drawbacks w.r.t. the feedback control law given by (4.29) and (4.28). Indeed, while during the first phase a feedback control law guarantees that the vehicle follows a circle of $\mathcal{C}_\alpha^\perp$ until $C_{\pi/2}$, during the second phase, a feedforward control with $\omega = 0$ and $u = const.$ is applied. Moreover, the crossing angle, which is not $\pi/2$, depends on the point reached on the circle $C_{\pi/2}$. Finally, if at the beginning $\alpha > \pi/2$, the vehicle has to reach $C_{\pi/2}$ backward. Next section is dedicated to the design of a feedback control law in bipolar coordinates overcoming all drawbacks of the simple strategy described in this subsection.

4.6 Feedback Control Law in Bipolar Coordinates

The main idea of designing the feedback control law in bipolar coordinates is to define a smooth vector field $E(\cdot)$ obtained by derivation of an appropriate potential function $F(\cdot)$. Let us hence consider the following function:

$$F(\tau,\hat{\alpha}) = \frac{(-\cos\hat{\alpha} + K\cosh\tau)}{a}, \tag{4.26}$$

where K is a positive constant. This function is always positive and has a global minimum at the middle of the door, i.e. when $\tau = 0$ and $\hat{\alpha} = 0$ (see also Figure 4.5). Notice that, function $F(\cdot)$ is very similar to (4.25). Considering $F(\tau,\hat{\alpha})$ as a potential function, the associated vector field is:

$$E(\tau,\hat{\alpha}) = \nabla F(\tau,\hat{\alpha}) = \frac{\cosh\tau - \cos\hat{\alpha}}{a^2}\begin{bmatrix} K\sinh\tau \\ -\sin\hat{\alpha}\end{bmatrix}. \tag{4.27}$$

Figure 4.6(a) shows level curves of $F(\tau,\hat{\alpha})$ as well as the vector field. Notice that, all flow lines converge toward the point $(\tau,\hat{\alpha}) = (0,0)$, that, in Cartesian coordinates, corresponds to the middle of the door. In Figure 4.6(b), the same potential field and associated vector field in Cartesian coordinates is also reported.

The objective is now to determine a feedback control law that steers the vehicle along the vector field represented in Figure 4.6(a) in bipolar coordinates, or represented in Figure

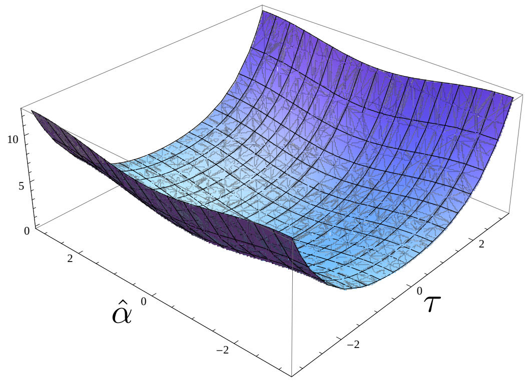

Figure 4.5: Function $F(\tau,\hat{\alpha})$ for different values of $\hat{\alpha}$ and τ and $K = 1$. The minimum is at the origin, i.e. at the middle of the door.

4.6(b) in Cartesian ones. Let ϕ be the bearing angle β_b when the vehicle is aligned with the vector field at any point $(\tau, \hat{\alpha})$. The angle ϕ can be easily obtained from (4.27),

$$\phi = -\arctan 2\left(K \sinh \tau, \sin \hat{\alpha}\right).$$

Let us define the error $\sigma = \beta_b - \phi$ and force the dynamics of σ to be $\dot{\sigma} = -K_\beta \sigma$, $K_\beta > 0$, by:

$$\begin{aligned} \omega = {} & K_\beta(\beta_b - \phi) + \dot{\phi} + \\ & -\frac{\nu}{a}\frac{(\cos\hat{\alpha} + \cosh\tau)^2(\cos\beta_b \csc\hat{\alpha} + \operatorname{csch}\tau \sin\beta_b)}{(\cos\hat{\alpha} - \cosh\tau)\sqrt{1 + (\cot\hat{\alpha}\coth\tau + \csc\hat{\alpha}\operatorname{csch}\tau)^2}}, \end{aligned} \tag{4.28}$$

Once the vehicle is aligned with the vector field, it should reach the middle of the door. To do that, let us consider the following continuously differentiable function V in terms of τ, $\hat{\alpha}$ and σ,

$$V = \frac{1}{2}(\tau^2 + \hat{\alpha}^2 + \sigma^2),$$

and consider its time derivative along the trajectories of the system. By using (4.28) we obtain

$$\dot{V} = -K_\beta\left(\beta_b - \phi\right)^2 - \nu\frac{(\cos\hat{\alpha} + \cosh\tau)(\hat{\alpha}\cos\beta_b - \tau\sin\beta_b)}{a}.$$

and, by choosing the forward velocity as:

$$\nu = K_\nu(\hat{\alpha}\cos\beta_b - \tau\sin\beta_b), \tag{4.29}$$

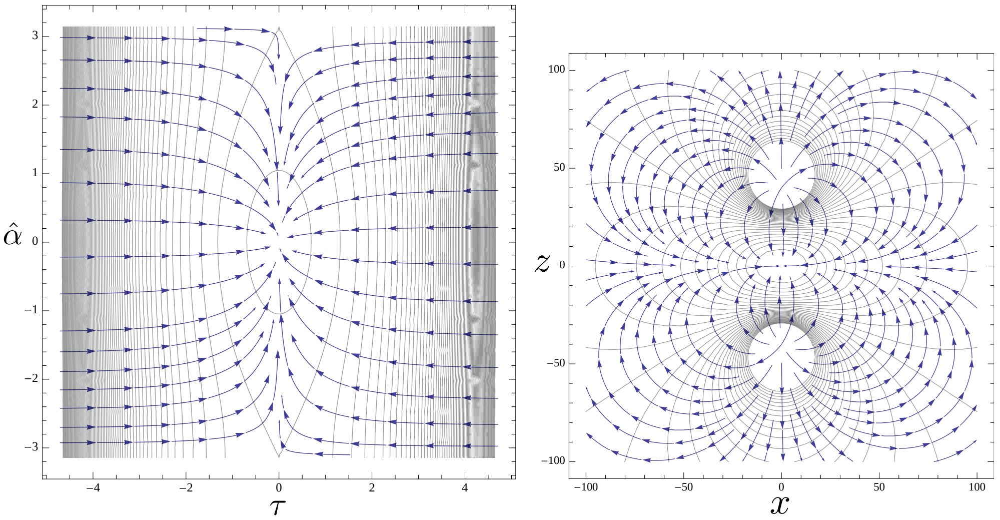

(a) Vector field $E(\tau, \hat{\alpha})$.

(b) Vector field $E(\tau, \hat{\alpha})$ expressed in Cartesian coordinates.

Figure 4.6: Vector field obtained as the gradient of $F(\tau, \hat{\alpha})$ with $K = 1$.

we finally have:

$$\dot{V} = -K_1\,(\beta_b - \phi)^2 - \frac{(\cos\hat{\alpha} + \cosh\tau)(\hat{\alpha}\cos\beta_b - \tau\sin\beta_b)^2}{a} \leq 0\,,$$

which is negative semi-definite. As the function V is positive definite, according to the Lasalle's invariance principle, the system trajectories converge to the largest invariant set $R = \{\lambda | \dot{V}(\lambda) = 0\}$. By simple computation, $R = R_1 \cup R_2$ where $R_1 = \{\lambda | \{\hat{\alpha}\cos\beta_b - \tau\sin\beta_b = 0\} \cap \{\beta_b = \phi\}\}$ and $R_2 = \{\lambda | \{\hat{\alpha} = 0, \tau = 0\} \cap \{\beta_e = \phi\}\}$. After simple algebra, we obtain that $R_1 = \{\lambda | \{\hat{\alpha} = \pi\} \cap \{\tau = 0\}\}$ while $R_2 = \{\lambda | \lambda = 0\}$. It is possible to show that, if $K \neq 0$, R_1 is not an invariant set. Indeed, for $\lambda = [0,\ \pi, 0]^T$ we have $\nu \neq 0$ and thus the system can escape from R_1. As a consequence, the point $\lambda = (0, 0, 0)$ is the only invariant set and we can conclude on the local asymptotic stability of the origin. Moreover, as the Lyapunov function is radially unbounded, we can conclude on the global asymptotic stability of the origin. Differently from the control law developed in Section 4.4, the control law developed in this section is able to steer the vehicle exactly through the middle of the door.

As for hyperbolae and ellipses, each circle of bundle C_α intersects each circle of bundle $C_\alpha^\perp$ in two points, symmetric w.r.t. the Z_W axis. Also the control laws in bipolar coordinates are immune to this fact by following the same reasoning as in Remark 5.

4.7 Simulations

In this section, simulations showing the effectiveness of control laws proposed in Sections 4.4 and 4.6 are presented. For both cases, two virtual scenario are considered. In the first one, the robot is inside a room and the objective is to leave the room passing through the door. In the second one, the robot is in a corridor and the objective is to enter a room passing through the door. The door is represented by two 3D points located at $(0, 70, 40)$ cm and at $(0, 70, -40)$ cm w.r.t. a global reference frame. These points are at the same height above the plane of the robot motion. The 3D points of the scene are projected in the image plane through a simulated pinhole camera. The size of the image is 640×480 and the characteristic angle of the camera is almost π. Moreover, the image frames are captured with a frequency of 15 frames per second. If possible, both elliptic and bipolar coordinates are computed through image measurements and different levels of white Gaussian noise with standard deviation $\sigma = 5, 15$ pixel to points in the image plane is also added. Indeed, as in this work the camera is fixed on the robot, it is not possible in the second scenario (see Figs. 4.8(c) and 4.9(c)) to perform the task without loosing at least one landmark, even if a very large FOV has been considered. For this reason, in the second scenario we directly assume that elliptic or bipolar coordinates are available and some white Gaussian noise, equivalent to have a 5 pixel Gaussian noise in the image plane, is directly added to the state variables.

In Figs. 4.8 and 4.9 trajectories of the vehicle are shown with and without noise for the two cases, chosen among the several trajectories analyzed for each case. The absolute average error w.r.t. the middle of the door is also reported in the caption of each picture with and without noise, i.e. ε_w and ε_{wo}, respectively. The simulations confirm that both feedback control laws work properly in spite of image noise. Moreover, while the control law in elliptic coordinates is only able to steer the vehicle near the middle of the door (the error depends on the constant parameters in the control law), the one in bipolar coordinates can drive the vehicle exactly to the middle of the door. However, this is not the only difference. In particular, in bipolar coordinates the behavior of the vehicle is more suitable to accomplish the task of entering in a room from a corridor. On the other hand, both methods are able to accomplish the task of going out of a room even if the trajectories followed by the vehicle are quite different, being more suitable the one in elliptic coordinates. Indeed, in elliptic coordinates, small variations in the control parameters traduce in very different shape of the trajectories. However, to reduce as much as possible the crossing error at the entrance of the door, this parameters should be selected as a function of the initial conditions. It is important to note that both the control laws in elliptic and bipolar coordinates guarantee good performance with levels of image noise up to 15 pixels, which constitutes a very high amount of noise. The use of a feedback control expressed in elliptic and bipolar coordinates seems to play a very important role in reducing the effects of noise. Future works will be dedicated to deeply analyze this aspect. However, the control law in bipolar coordinates seems to be more sensitive to image noise than the control law in elliptic coordinates when the vehicle is far away from the door, making difficult the tuning of the control parameters. On the other hand, the control laws in bipolar coordinates work very well near the door, especially while entering a room from the corridor. This may suggest a possible strategy: *use elliptic control laws when the robot is far away from the door and bipolar ones when it is sufficiently near the door or when the vehicle is very near the wall.* As a final observation, it is important to point out that, even if the method relies on the assumption that the two landmarks are at the same height, we have simulated our method also in case of differences in height up to 10 cm, observing that the method works quite well also in this case. Both control laws depend on the parameter a which is half of the width of the door. This parameter is constant and can be assumed to be known or estimated via a suitable observer. However, Figure 4.7 shows how errors in the estimation of a influence the trajectories of the vehicle. In particular, starting from the same configuration, we have considered three cases: $a = 40$ cm (the actual value),

$a = 80$ cm (twice the actual value) and $a = 20$ cm (half of the actual value). Simulations show that errors in the estimation of the parameter a do not compromise the effectiveness of the control laws. The feedback control law in elliptic coordinates seems to be more sensitive to variations of the parameter a than the one in bipolar coordinates.

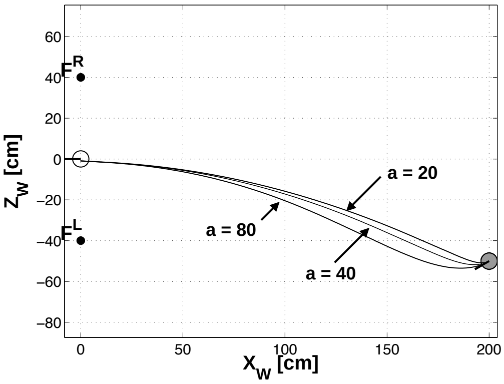

(a) Control laws in elliptic coordinates developed in section 4.4.

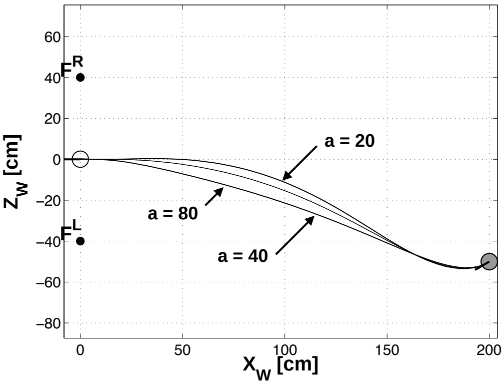

(b) Control laws in bipolar coordinates developed in section 4.6.

Figure 4.7: Trajectories of the vehicle starting from the same initial configuration $q = (200, -50, 7\pi/6)$*, for different values of* a *in the control law:* $a = 40$ *cm (the actual value),* $a = 80$ *cm (twice the actual value) and* $a = 20$ *cm (half of the actual value).*

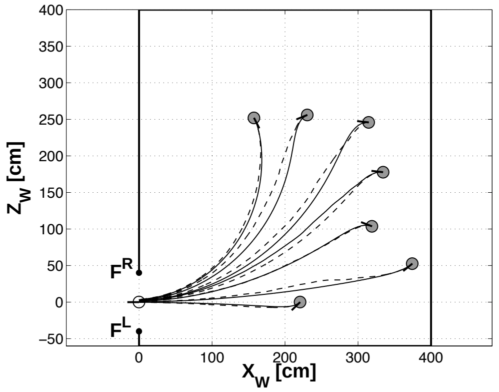

(a) $\sigma = 5$ pixel: $\varepsilon_w = 2.00 \pm 1.15$ cm and $\varepsilon_{wo} = 1.79 \pm 1.02$ cm.

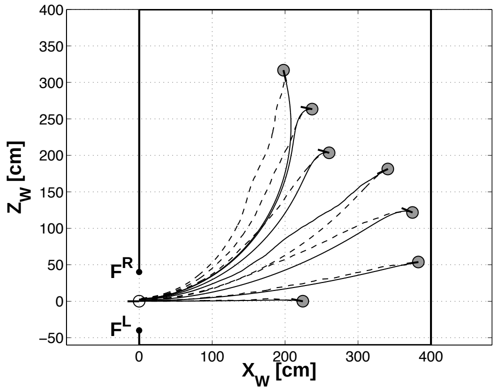

(b) $\sigma = 15$ pixel: $\varepsilon_w = 2.61 \pm 1.43$ cm and $\varepsilon_{wo} = 1.88 \pm 1.03$ cm.

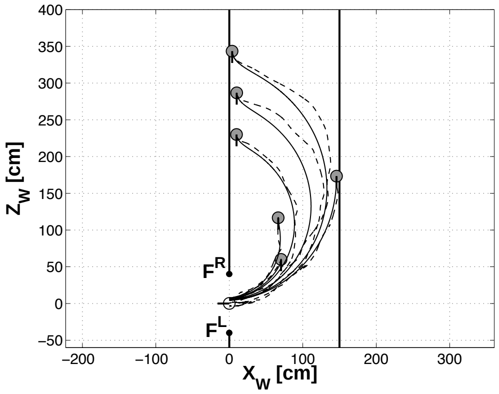

(c) $\sigma = 5$ pixel: $\varepsilon_w = 4.43 \pm 4.68$ cm and $\varepsilon_{wo} \approx 6.85 \pm 2.92$ cm.

Figure 4.8: Simulations with the feedback control law in elliptic coordinates: trajectories of the vehicle without and with white Gaussian noise, representing continuous and dashed lines, respectively. The vehicle leaves a room in (a), (b) and enters a room from a corridor (c), by passing through a door.

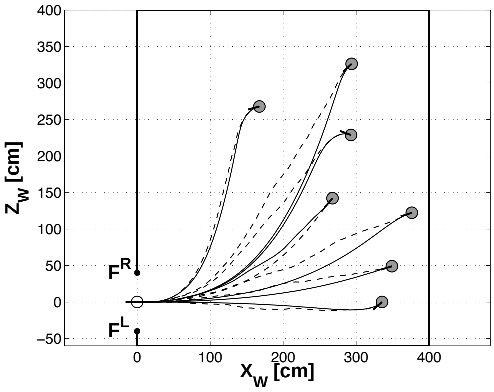

(a) $\sigma = 5$ pixel: $\varepsilon_w = 0.0028 \pm 0.096$ cm and $\varepsilon_{wo} = 0.0017 \pm 0.0011$ cm.

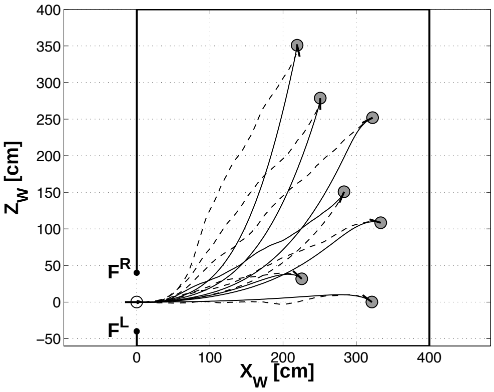

(b) $\sigma = 15$ pixel: $\varepsilon_w = 0.14 \pm 0.70$ cm and $\varepsilon_{wo} = 0.0017 \pm 0.001$ cm.

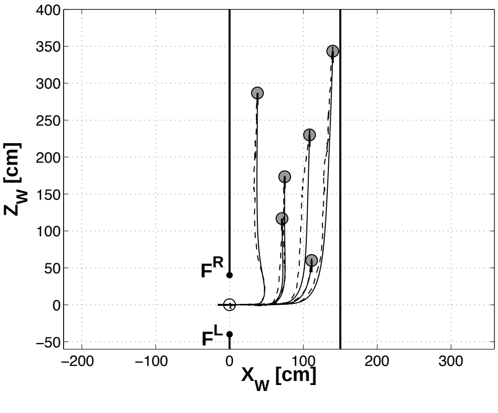

(c) $\sigma = 5$ pixel: $\varepsilon_w = 0.1 \pm 0.33$ cm and $\varepsilon_{wo} \approx 0$ cm.

Figure 4.9: Simulations with the feedback control law in bipolar coordinates: trajectories of the vehicle with and without white Gaussian noise, representing continuous and dashed lines, respectively. The vehicle leaves a room in (a), (b) and enters a room from a corridor (c), by passing through a door.

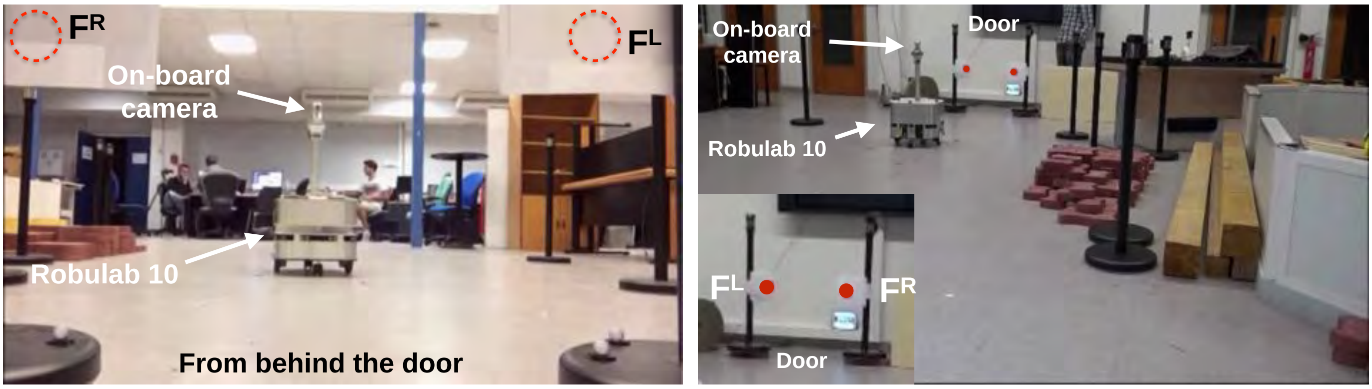

Figure 4.11: Experimental setup.

4.8 Experiments

Referring to Figure 4.11, the experimental setup was comprised of a Vivotek Wireless Network Camera with Pan–Tilt (PT7137) (see Figure 4.10) fixed at the middle of the wheel axis of the RobuLAB–10 (by Robosoft) mobile platform. The image resolution was 640×480 and the camera horizontal and vertical FOV amplitude were around 50 deg and 40 deg, respectively. Moreover, in our experiments, the pan–tilt mechanism was not used. The camera was calibrated by the Matlab© calibration toolbox. The result of this procedure, has furnished the focal length: $\alpha_x = 712.28 \pm 3.32$ pixel and $\alpha_y = 711.93 \pm 3.27$ pixel; the principal point: $P_{cc} = [330.98,\ 273.42] \pm [6.69,\ 6.06]$ pixel; the skew: $\alpha_c = 0$, angle of pixel axes is $\pi/2$; the distortion: $K_c = [-0.40,\ 0.24,\ 0.0018,\ -0.00011,\ 0] \pm [0.02,\ 0.09,\ 0.0015,\ 0.0012,\ 0]$; the pixel error: $p_{err} = [0.35,\ 0.29]$ pixel.

Figure 4.10: PT7137 camera

Notice that, the camera presents a radial distortion. The noise level was estimated to have a standard deviation $\sigma = 0.05$ pixel and the controller rate was around 20 Hz. The distance between the two landmarks was 68 cm.

4.8.1 Technical Details

Without loss of generality and to simplify the experimental setup, we have decided to avoid the use of door detection algorithms from which the two landmarks characterizing the door can be obtained. The door is indeed represented by two red circular landmarks at the same height from the plane of the robot motion. It is important to note that in own approach we did not implement a door detector algorithm, reasonably assuming that it will be always possible to determine two points in the image plane corresponding to the doorposts, e.g. the top corners of the door. In the method proposed we assumed that the two landmarks are at the same height. In case they are not, it is necessary to estimate it. Moreover, in such case, both bipolar and elliptic coordinates would depend not only on the positions of the landmarks in the image plane but also on their respective heights. The algorithms have been developed in C++. Two scripts were run in parallel, communicating with each other by ROS Hydro. The first one was dedicated to grab an image from the wireless camera and provide information about the position of the landmarks in the image plan. The second program was dedicated to receive the information about landmarks and compute the control inputs ν and ω and to send them to the vehicle. An exhaustive description of the two programs is provided in the following sections. They are called "Image Processing" and "Robot Control" algorithm.

Image Processing

The aim of the first program was to read the data from the wireless camera, detect and track the landmarks. The connection was establish through UDP protocol that allowed real-time video streams. However, some packets might be lost due to network burst traffic and images might be obscured. To solve this problem, invalid information were considered as an exception. If too many of theme occurred (around half second) and the system was not able to receive correct and valid images, the robot was safety stopped. Since the quality of the image was really poor (the camera was a web-cam, concerned to remain at a fixed position, resolution 640x480, 60Hz, frame rate 30 fps), it was necessary to apply several filtering in order to obtain a robust detection and tracking of the landmarks. We mainly used OpenCV (version 2.4.9) [Bradski 2000] and ViSP (Visual Servoing Platform, version 2.9.0) [Marchand 2005] libraries. The first step was to convert the image colors from RGB to HSV space, since the latter has the desirable property to identify a particular color using a single value (Hue) instead of three. Afterward a Gaussian smoothing was applied to blur the image and reduce the noise. Since the quality of the data was low and the application of filters further reduced image details, it was necessary to find an efficient compromise between noise-reduction and quality. Moreover, a direct detection of the red landmarks was not the most robust solution since several parameters were required (dimension of the landmarks, threshold for the edge detector, dimension of the mask for features detection, parameters of the Gaussian filter) and their values were too dependent on the light conditions of the environment. In order to obtain a robust detection and tracking system of the landmarks, different approach have been tested. Mainly, we used OpenCV for the detection of the features and ViSP to track them. Since the landmarks had circular shapes, the program was made to detect two ellipses.

Once they were detected, we used ViSP library for the tracking. If one of landmarks was lost, the software stopped the tracking and the research of the ellipses started again. Tests showed that the research was sufficiently fast to maintain the smoothness robot trajectory. Different approaches were tested and compared to detect and track the landmarks.

Detection : Two approaches were tested based on circles or ellipses detection. Both of them require to isolated the red color by setting the HSV values ($H = [95, 145]$, $S = [75, 142]$, $V = [90, 150]$) and turning them to white, while the rest of the pixels were set to black. Following this elementary method, we obtained a white and black image in which the two landmarks were clearly visible. The circle detection approach was based on the OpenCV function *HoughCircles* and it provided good performances. However, when the robot was not moving perpendicularly to the door, the landmarks (that were circles) became more elliptical and the algorithm was not able to detect them anymore. To solve this problem, we tested a 2-step approach based on ellipse detection: firstly we used *findContours* to highlight the landmarks and then *fitEllipse* to localize them (the functions are based respectively on [Suzuki 1985] and [Fitzgibbon 1996] algorithms).

Tracking : OpenCV provides functions to find circles or ellipse and the ViSP library provides several tools to track objects like moving-edge tracking, template tracking, ellipse tracking and blobs tracking. After many tests, we found out that blobs tracking provided the best performance for our task. We used *vpDot2* class which requires the initial position of the blobs that we need to track. To this end, the position of the two landmarks detected by OpenCV were provided. This approach, even if it is not direct, allowed us to have a robust tracking system. Although the ViSP library provides functions to automatically detect circles or ellipses in a image, the basic OpenCV tools finally guaranteed more robust results for the initial landmarks detection. However, the tracking task by OpenCV was not smooth, probably due to the low quality of the image and the noise. We finally concluded that OpenCV ellipse detector and ViSP blob tracker was the optimal combination for our purpose, given the limited performance of the camera. In the last step, the position of the landmarks in the camera plane (*u* and *v* coordinates) were sent to the Robot Control algorithm using ROS Hydro.

Robot Control

The aim of this program was to compute the robot control inputs v and ω based on the landmarks position in the camera plane provided by Image Processing algorithm. The communication between robot and computer station was established through UDP protocol.

The way we controlled the robot is explained in Appendix A. In Image Processing control we focused only on the landmarks detection and we did not set any kind of control. We limited the previous algorithm because of computational time limits: image data is quite heavy and it was necessary to minimize the number of operations. However, several problems could occur due to such a lack of security control. To this end, the Robot Control algorithm had to perform several security checks before sending the control signal to the real robot.

- *Image Data validation*: if the landmarks were correctly detected, a 6D-vector $m = [u_1, v_1, r_1, u_2, v_2, r_2]$ was sent from Image Processing to Robot Control (u_1, v_1, r_1, u_2, v_2, r_2 were respectively the two coordinates in the camera plane and the ray of the landmarks). However, if the landmarks were not correctly detected, the vector m was not 6-dimension and the security system had to safety stop the robot motion. Since the software must provide smooth motion and it is important that the robot does not hiccup, the angular velocity ω was set to zero and the linear velocity v remained constant. The idea was that if the landmarks were still in front of the camera and it could be still possible re-detect them, without needing to turn the robot and then the camera. Regardless, if after half second the landmarks were not re-detected correctly, the robot was forced to stop.

- *Landmark role-assign*: The 6-vector m contained information about the two landmarks. However, there was not a specific order and it was necessary to clarify, before computing the control law, which information was relative to the left landmark rather than the right one. A simple check on u coordinates was sufficient to solve this problem.

- *Control inputs*: once the control inputs ω and v were computed, a last check was done to understand if their value were reasonable (if their values were respectively higher than 1.6 m/s and 2 π). If they were not, the robot was safely stopped.

Because of the limited FOV aperture, the robot lost the landmarks while passing through the door. Indeed, as shown in the next paragraph, there is a region around the door where the robot cannot maintain in view the landmarks. To circumvent this problem, in our experiments, the parameters in the control laws were chosen in order to align the vehicle with the line passing through the middle of the door, perpendicularly to the segment $[F^L, F^R]$, just before losing the landmarks. Starting from this configuration, which is quite near to the door, depending on the FOV amplitude, an open loop control law with $\omega = 0$ and $\nu = const.$ was applied. Of course, other solutions might be used. For example, if the heights of the landmarks were available, by using the last measurements of the landmarks in the image plane (just before going outside) and the pinhole camera model, a prediction of the future positions of the landmarks in the image plane could be obtained. These predictions can be used in the feedback control laws provided in this work to steer the vehicle through the door even if the landmarks are outside of the image plane. The heights of the landmarks can be assumed to be known or estimated by a suitable procedure or observer.

4.8.2 Experimental Results

Figure 4.12 and 4.13 report the trajectories of the robot starting from different initial configurations and obtained by applying the feedback control laws based on elliptic and bipolar coordinates, respectively. The state variables of the robot and hence the trajectories towards the door have been measured by using the Motion Analysis Capture system. Of course, no information coming from this sensor system are used in the control laws which provide a purely Image-Based visual servo control. A **video**[2] of the experiments is available.

---

[2] $http://projects.laas.fr/gepetto/uploads/Members/ICRA2015\_video.mp4$

4.9 Analysis of FOV limits

The control laws developed in this work did not take into account the Field–Of–View (FOV) limits of the on–board camera. In this section we will study and analyze this aspect.

Let us first consider the region of points that violate the FOV limits for any orientation of the robot. In other words, in this region, both landmarks cannot be maintained inside the FOV, whatever the orientation of the vehicle.

Let γ and $\hat{\gamma}$ be the horizontal and vertical FOV aperture, respectively. Because of horizontal FOV limits, there exists a region Z_1 around the door such that the two landmarks cannot be simultaneously maintained between the left and right bounds of the image plane. It is straightforward to show (see [Salaris 2010]) that Z_1 is bounded by two arcs of circle (C_γ^a and C_γ^b) whose angle at the circumference is exactly equal to γ (see Figure 4.14(a)).

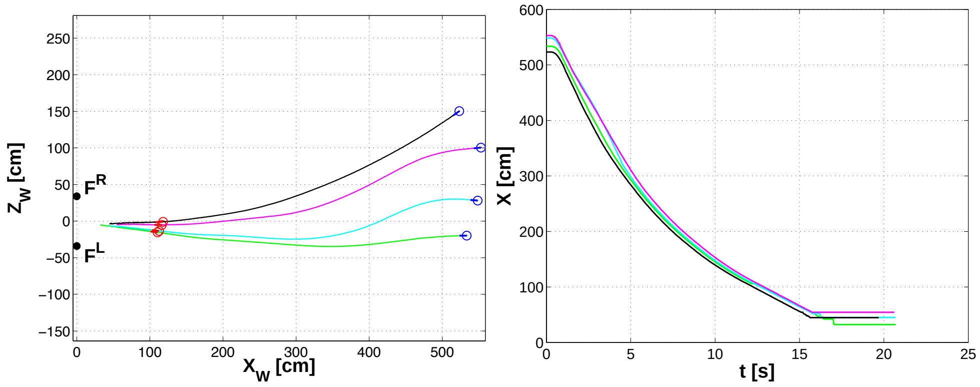

(a) Trajectories followed by the vehicle.

(b) x.

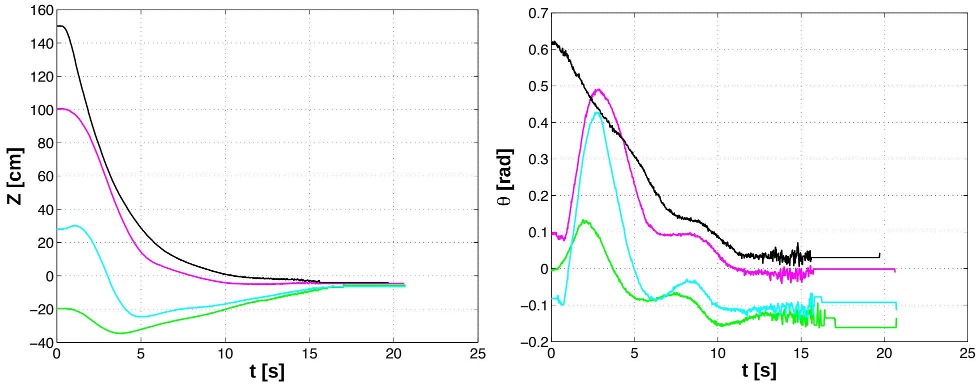

(c) z

(d) θ.

Figure 4.12: Experimental results obtained applying the control law in elliptic coordinates. The control parameters are $w = 0.0012$*,* $K = 0.7$ *and* $\lambda = 310$*, an the average linear velocity* $v = 0.3$ *m/s.*

Because of vertical FOV limits, considering each landmark separately, there is a region around it that the vehicle cannot reach while maintaining the landmark between the upper and lower bounds of the image plane. Also in this case, it is easy to show (see [Salaris 2015a]) that this regions is bounded by two circumferences ($C_{\hat{\gamma}}^R$ and $C_{\hat{\gamma}}^L$ for the right and left landmark) centered at the projection of the landmark on the motion plane and with radius equal to $R_b = \frac{h}{\tan(\hat{\gamma}/2)}$ (see Figure 4.14(b)). However, if we consider the problem of maintaining both landmarks between the upper and lower bounds of the image plane, the region Z_2 that the vehicle cannot reach is a planar capsule delimited by two straight lines s_I and two semicircle ends (see Figure 4.14(b)). This is a direct consequence of the fact that when the landmark is on the upper (or lower) bound of the image plane, the vehicle is aligned with the tangent to the involute of circle passing through the current position of the vehicle (see [Salaris 2015a]). These involute of circles, named by I^R and I^L (see Figure 4.14(b)), have $C_{\hat{\gamma}}^R$ and $C_{\hat{\gamma}}^L$, respectively, as base circles. When both features

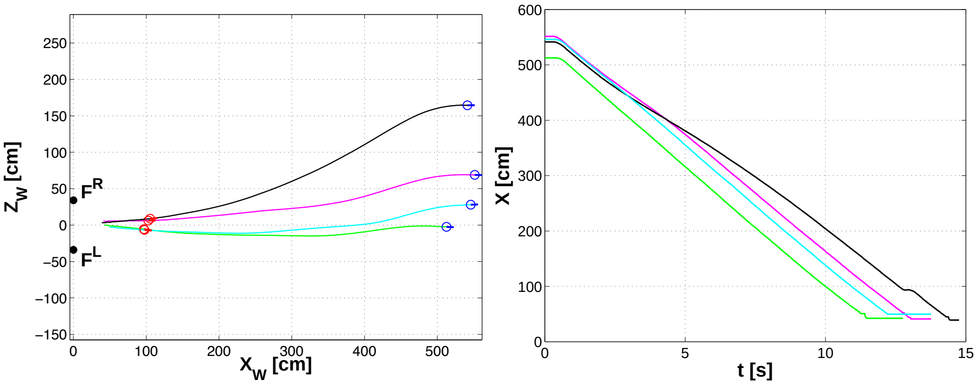

(a) Trajectories followed by the vehicle.

(b) x.

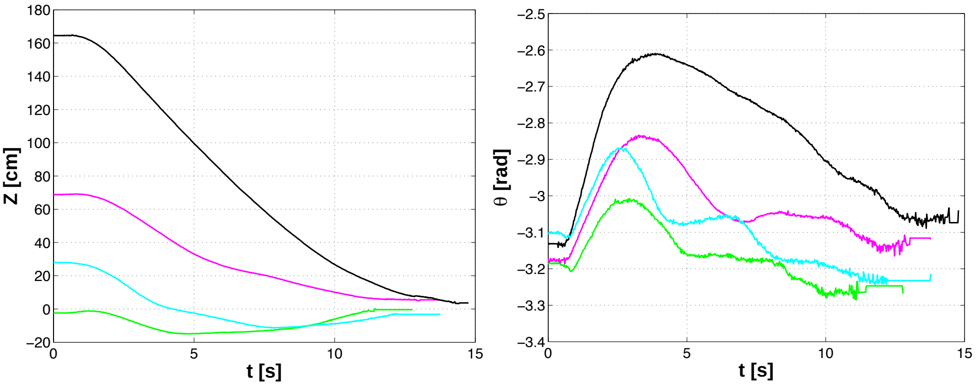

(c) z

(d) θ.

Figure 4.13: Experimental results obtained applying the control law in bipolar coordinates. The control parameters are $K = 2$, $K_1 = 4$ *and* $K_\nu = 0.15$. *Average linear velocity of* 0.4 *m/s.*

are on the upper (or lower) vertical border of the image plane, the vehicle is aligned with the tangent line to both involutes I^R and I^L. Moreover, by geometrical construction, the perpendicular line to each involute in any point of it, is tangent to the base circle.

Considering now horizontal and vertical FOV limits together: the region that the vehicle cannot reach while maintaining both landmarks inside the image plane is $Z_1 \cup Z_2$. In Figure 4.14(c) the subdivision of the motion plane based on previous analysis is shown in case of $\gamma < 2\arcsin\left(R_b/a\right)$, i.e. along the X_W axis, the horizontal FOV limits are activated before the vertical ones while approaching the door.

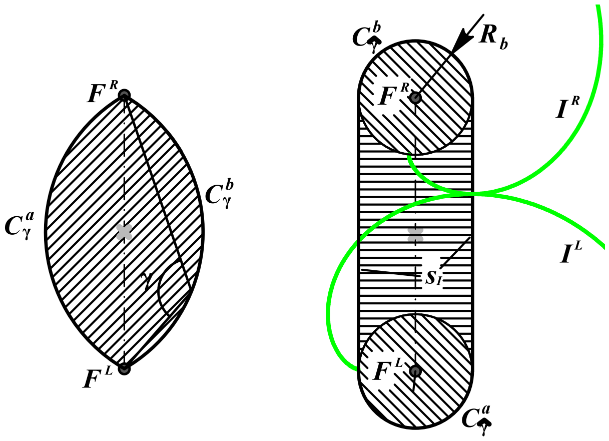
F^R
C_γ^a
C_γ^b
γ
F^L
C_γ^b
R_b
F^R
I^R
I^L
s_l
F^L
C_γ^a

(a) Horizontal FOV limits.

(b) Vertical FOV limits.

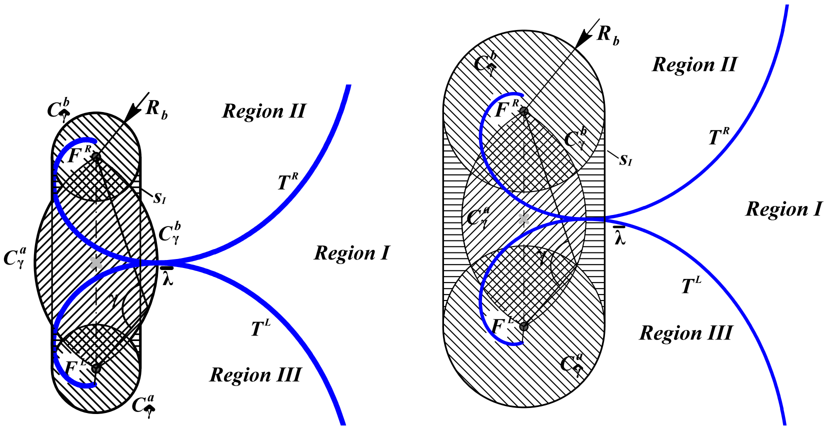
C_γ^b
R_b
Region II
F^R
s_l
T^R
C_γ^a
C_γ^b
λ
Region I
γ
T^L
F^L
Region III
C_γ^a
R_b
C_γ^b
Region II
F^R
C_γ^b
s_l
T^R
Region I
C_γ^a
λ
γ
T^L
Region III
F^L
C_γ^a

(c) Subdivision of the motion plane in regions according to the FOV limits in case of $\gamma < 2\arcsin\left(R_b/a\right)$.

(d) Subdivision of the motion plane in case of $\gamma \geq 2\arcsin\left(R_b/a\right)$.

Figure 4.14: Analysis of the FOV limits.

4.9.1 Control strategy in case of FOV limits

From the previous section, it is clear that the vehicle cannot reach the middle of the door while maintaining both landmarks in sight. To avoid this problem, the control law developed in Section 4.6 can be modified in order to reach the configuration $\bar{\lambda} = [0, \pi - \gamma, 0]^T$, i.e. point $\bar{\lambda}$ in Figure 4.14(c), instead of the configuration $\bar{\lambda} = [0, \pi, 0]^T$. This can be done by considering the modified potential function

$$F_\gamma(\hat{\alpha}, \tau) = \frac{(-\cos(\hat{\alpha} - (\pi - \delta)) + K \cosh\tau)}{a}$$

and vector field

$$E_\gamma(\tau, \hat{\alpha}) = \frac{\cosh\tau - \cos(\hat{\alpha} - (\pi - \delta))}{a} \begin{bmatrix} K \sinh\tau \\ -\sin(\hat{\alpha} - (\pi - \delta)) \end{bmatrix} .$$

and finally the following candidate Lyapunov function

$$V = \frac{1}{2}\left(\tau^2 + (\hat{\alpha} - (\pi - \delta))^2 + \sigma^2\right) , \tag{4.30}$$

where $\delta = \gamma$. Once the vehicle reaches $\bar{\lambda}$, an open loop control can be applied, e.g. with controls $\nu = const.$ and $\omega = 0$. However, especially from a practical point of view, depending on both the value of γ (and hence the distance between the reached point and the door) and the final error which depends also on the image noise, this strategy might steer the vehicle very far from the middle of the door. In this case, an estimation of the landmark positions based on the camera model can be used until a new pair of landmarks is available. To do that, the height of the landmarks must be known, e.g. from an observer that estimates h during the first phase, in which the vehicle is approaching $\bar{\lambda}$. Once h is obtained, it can be used to estimate landmark positions on the image plane (even though their are outside it) that can be in turn used in the feedback control laws.

Finally, when the vehicle is sufficiently far from the door, the horizontal limits of the FOV become more restrictive than the vertical ones. From results reported in [Salaris 2010], when the landmark moves on the right or on the left border of the image plane, the vehicle moves along a logarithmic spiral rotating counterclockwise or clockwise, respectively, around the projection on the motion plane of the landmark position. Depending on the value of γ, there exist two logarithmic spirals, T^R and T^L in Figure 4.14(c), passing through $\bar{\lambda}$, whose characteristic angle[3] is constant and equal to $\gamma/2$. The spirals are tangent in $(\tau, \pi - \gamma)$ and subdivide the motion plane in three regions. Referring to

---

[3] Given a point $Q = (\rho_Q, \psi_Q)$ on a logarithmic spiral rotating around point O_W, the characteristic angle is the angle between the tangent to the spiral in Q and the radial line at the point Q.

Figure 4.14(c), starting from Region II and III with an orientation such that both landmarks are in view, the vehicle cannot reach point $\bar{\lambda}$ while maintaining both landmarks inside the FOV along the whole trajectory. From these regions, a preliminary maneuver that steers the vehicle in Region I is needed to achieve the task. Indeed, from Region I the control law obtained from (4.30) might be able to steer the vehicle in $\bar{\lambda}$ by appropriately choosing the control parameters. If one feature reaches the right or left border of the image plane, the vehicle can move along the logarithmic spiral until point $\bar{\lambda}$ is reached. In this case, the value of δ to be used in the Lyapunov function (4.30) is $2 \arcsin(R_b/a)$. Previous analysis is valid even if $R_b \geq a \sin(\gamma/2)$, or $\gamma \geq 2 \arcsin(R_b/a)$. In this case, the point $\bar{\lambda}$ is in the middle of the line s_I where logarithmic spiral are not tangent (see Figure 4.14(d)). In particular, if $\gamma = \pi$, C_γ^a and C_γ^b reduce to the segment $\overline{F^R F^L}$ while the logarithmic spirals become two circles centered at the projection on the motion plane of each landmark and passing through the middle of the door.

4.10 Conclusions

In this chapter, a geometric approach to steer a robot subject to nonholonomic constraints through a door by using visual measures coming from a fixed on-board monocular camera, has been provided. The planar geometry that, in a natural way, has been built around the door consists of bundle of hyperbolae, ellipses and orthogonal circles. The method proposed is able to accomplish such an task through static feedback control laws that are functions of the current state of the system expressed in suitable coordinate, directly measured in the camera plane. Indeed, our approach does not consist in a pre-planned path among via-points or a multi-stage strategy. Therefore, we avoid the computational cost of a state observed that would require to localize the robot. Realistic simulations and experiments have been also reported to show that the method proposed is robust against disturbances and uncertainties.

Conclusion and Perspectives

The first part of this thesis work has been done within the framework of the European project KoroiBot which aimed to improve humanoid robots capabilities inspired by humans. In this context, we investigated some principles that underlie the organization of human walking, with the aim to transfer them to humanoid robots. Our work in this direction gave rise to two main contributions. First, in collaboration with specialists in crowd simulation and motion planning at INRIA-Rennes, we investigated the human principles which guide collision avoidance strategies during goal-directed locomotion. Then, in collaboration with our KoroiBot partner from Tübingen, we proposed a novel approach to synthesize realistic complex humanoid robot movements based on motion primitives. Aside the KoroiBot project, we had an internal collaboration at LAAS-CNRS with Paolo Salaris and Jean-Paul Laumond which led a the third contribution. It concerns the synthesis of vision-based controllers based on original parametrization for passing through a door. This work has been supported by European Research Council within the ERC Actanthrope. The outcomes related to these three contributions are detailed below. Some perspectives are developed in each case.

Identification of human walking strategies for avoiding a moving obstacle

One of the first steps of our study has been to record humans walking motions in order to investigate and identify the natural and biological strategies to avoid a moving obstacle. The main idea was to create situations for which the behavior of the walker was considerably perturbed by an external agent. To this aim, we programmed a wheeled robot that had to cross the pedestrian path. Considering the related works on this topic, we started a collaboration with specialists on human locomotion at INRIA-Rennes. They previously investigated the strategies used by two pedestrians crossing each other and they found out that both participants were able to predict the future crossing order. Moreover, it turned out that the collision avoidance is collaboratively performed by both participants and that the walker giving way contributes more than the one passing first. They concluded that it exists a natural tacit understanding of roles which guides humans avoidance strategies. In order to determine if those observed principles could be extended to the case of a human crossing a moving robot, we reproduced the same experimental setup by replacing one of the walkers by a wheeled robot. Initially, we considered the robotic platform *TurtleBot*[4] that has open-source software and it is well known in the scientific community. However, due to its limited speed and dimensions, we observed that the behavior of the participants was not sufficiently perturbed. For this reason, we considered the wheeled robot *Robulab10* that is heavier and faster.

---

[4] http://www.turtlebot.com/

In the first part of this study we decided to control the robot in a passive way. The word "passive" means that the robot is moving straight at constant speed and it is not reacting to the participant adaptations. All the analyzes were based on the concept of signed minimal predicted distance (smpd), which provides information about the future crossing order given the position, the velocity and the orientation of both agents. Since the speed and the direction of the moving obstacle were set constant, only the walker contributed to solve the collision avoidance. In this case we observed that humans preferentially give way to the robot, even though this choice is not optimal to avoid collision. Moreover, humans never decided, in the cases in which they were second in the crossing order, to accelerate and pass as first. We correlated this behavior to the notion of danger and safety, hypothesizing that during walking the humans set some prioritized sub-tasks as reaching the goal, scanning the environment, avoiding obstacles, etc. The conservative strategy observed led to conclude that avoiding the collision and, in particular, the preservation of the personal space, are the sub-tasks with higher priority during walking. From these observations, we concluded that, since the robot is not reacting but keeps moving straight, the participants did not feel comfortable to interact with it and, sometimes, they could have been even surprised. In addition, since the pedestrian is the only one to solve the collision avoidance then the task requires more effort from his side. Finally, it results that the passive behavior of the robot is somehow counterintuitive for the human.

In the second part of this study, having in mind the results observed in the passive case, we reproduced the same experimental setup but by controlling the robot in a reactive way. Our goal was to observe the human behavior in this case and compare with the ones previously examined. In order to be cooperative, the robot was programmed to follow the avoidance strategies observed in humans when crossing each other: accelerating at the beginning of the interaction and then turning to pass ahead the participant or decelerating and turning to pass behind . The results showed that the comfort of the walkers was improved: they solved all the tasks (reaching the goal and the collision avoidance) with smoother adaptation and their behavior was more natural. We interpreted this phenomenon by the fact that it is easier for the pedestrian to understand the ongoing situation when the robot is taking decision too in a human-like way. This outcome is reasonable if we correlate the concept of implicit strategies for collision avoidance: people interact with each other daily and they do it almost the same way. These adaptations are optimized, learned and improved by our life experience. For these reason, it is easier for a walker to predict how to solve collision avoidance if the robot is acting like a human.

Future Works

The conclusion of these two studies opens path for future research. We addressed questions as: Do humans understand when a robot is cooperating rather than passive? Do they adapt their strategies accordingly? Is it useful to transfer human locomotion strategies to an autonomous robot? We observed that the humans behave more naturally if the robot moves in a human-like way and the collision avoidance is bilaterally solved, mainly at the beginning of the reaction phase. No extreme changes of direction or drastic speed variation are needed to make humans understand the robot intentions. Given these results, we raise new questions: would it be possible to further improve the comfort of the humans if the robot would have humans aspects? This concept could be even related to the challenge of integrating humanoid robots in the human society. Assuming that humanoid robots of the future will have communication skills similar to the human ones, it is normal to hypothesize that we could maximize the use of such abilities to better succeed the collision avoidance task. In fact, pedestrians interact each other mainly in two ways: verbal and non-verbal communication. Normally, some basic postures (or body messages) are sufficient to clearly show own intentions. However, in wavering situation, it is often necessary to perform more showy movements, e.g. stepping laterally ("I am going left/right"), stopping and waiting ("I am giving way to you"), performing longer steps and accelerating ("I am passing as first"). Hand signals, face expressions, eyes contact are also common methods to communicate with others. Although people may talk, that would be the faster and easier way, the lack of confidentiality led to have more nonverbal messages. Given these observations, which level of communication would be optimal to have an exhaustive understanding in terms of locomotion strategies? Which actions could make easier the collision avoidance for humans? Would it be faster to adapt and behave naturally with humanoid robots, if they use gestures and/or they talk during an interact? or people would be frightened because it is unnatural? We believe that the work we have done in Chap. 1 and Chap. 2 could serve as an interesting basis for addressing these questions with humanoid robots.

Use of motion primitives to implement complex movements on humanoid robots

In Chap. 3 we proposed a whole body controller based on movement primitives extracted from human behavior. This work has been done in collaboration with our neuroscientists partners from Tübingen in the framework of the KoroiBot project. The considered notion of motion primitive was defined in space and in time and based on kinematic data acquired by a motion capture system [Giese 2009b, Mukovskiy 2013]. In this context, ten trajectories of a human during walking-to-grasp tasks have been recorded. Since humans and humanoid robots are different in terms of size, step lengths, joint limits, torque limits, etc., the recorded whole body movements have been rescaled and retargeted in order to match the kinematics of the humanoid robot HRP-2. Once the scaled motions were obtained, we extracted the joint trajectories and then we segmented and normalized them in terms of time. The step lengths were analyzed too but they were stored separately. At this point, two subsets of trajectories were collected: one concerning the pelvis linear and angular velocity and the other one related to the upper-body configurations. In order to learn low-dimensional representations of each segmented motion, we applied the anechoic demixing algorithm. By this method, all the trajectories could have been represented as a linear weighted superpositions of source signals shifted in time. To represent the entire walking-to-grasp movement, we used a total of five periodic source signals and two nonperiodic ones. Since the trajectories generated for the legs did not provide stable walking for our robotic platform, we decided to use the walking pattern generator and the related dynamic filter developed at LAAS-CNRS roughly described in Section 3.2.3. In conclusion, the control of the lower body was driven by the pelvis trajectory whereas the upper-body was controlled by the motion primitives extracted from human data. The global task was divided in three phases. In the first one, three steps were generated to reach the object to grasp. If they were not sufficient to arrive at the target, additional steps were automatically introduced. For this first action, three source signals have been considered. The second phase consists in approaching the target: the robot has to decelerate and stop at the optimal distance for grasping the object. To model this action and the third phase, which required adaptive steps and upper body motion for grasping, we added two periodic sources. The proposed algorithm has been tested in realistic simulation (OpenHRP2) and in the real humanoid robot HRP-2. It resulted that all the motions generated were feasible.

Future Works

As a future work, it could be interesting to extend the training set which should include some additional motion data that maximize the variation of parameters for each individual action. The training set will have to contain only feasible behaviors, that are extracted directly from the robot simulator. In other words, instead of building the training set with the human data, we propose to use the joint trajectories computed by the generalized inverse kinematics in the Stack of Tasks. In this way, the learning process would be based on feasible data and it would provide motions that are more appropriated. Moreover, the learning process should take into account that the pitch joint of the chest is fixed to zero and that the ground could be not flat. Since the joint trajectories in the training set are extracted from feasible motion, the generated movements from the learning process should be more dynamically stable for the robot and increase the flexibility and computational efficiency of the proposed architecture. It would be also interesting to record other kinds of actions and test them based on the same algorithm.

Vision-based control to pass though a door

In Chap. 4 we described a novel vision-based control to steer a robot to pass through a door. We considered a nonholonomic wheeled robot that was equipped with a fixed on-board monocular camera. In the proposed approach, we built around the door a planar geometry of bundle of hyperbolas, ellipses and orthogonal circles. The method is able to steer the vehicle through the door by static feedback control laws that are function of the current state of the system expressed in suitable coordinates that can be directly measured in the camera image plane. In other word, given the position of the two landmarks in the image plane, our method is able to directly provide the control inputs to steer the vehicle to accomplish the task. Therefore, our approach avoids the computational cost of a state observer that would require to localize the robot with respect to the goal. In this work, the theoretical contribution consists in elaborating two feedback control laws, in elliptic and bipolar coordinates respectively. Both controllers have been tested in simulation and on the real robot. The experimental results confirmed that both feedback control laws work properly in spite of image noise. Moreover, while the control law in elliptic coordinates is only able to steer the vehicle near the middle of the door, the one in bipolar coordinate can drive the vehicle exactly to the middle of the door. This is not the only major difference. In fact, in bipolar coordinates the behavior of the vehicle is more suitable to accomplish the task of entering inside the door from a corridor, whereas the elliptic coordinates provide more suitable trajectory to move close to the door. Although both methods guarantee good performance despite image noise, the control law in bipolar coordinates turns out to be more sensitive to noise than the elliptic one if the vehicle is distant from the door, making difficult the tuning of the control parameters. We conclude that an optimal strategy might be to use the elliptic control law when the robot is far from the door and then switch to bipolar strategy when it is sufficiently close to it or when it is really near the adjacent walls.

Future Works

This work can be easily extended to other navigation and control problems, as e.g. controlling the vehicle amidst obstacles, under the condition that pairs of features correspond to the 3D position of the obstacles and that they can be extracted from the image plane. The vision-based strategy presented in this work can also be related to human locomotion. In [Mombaur 2010], by modeling the human locomotion as a unicycle [Arechavaleta 2008], an inverse optimal control approach was used for understanding the cost functional that humans minimize during a rest–to–rest task, as e.g. to approach a door. The results enlighten the role of the bearing angle, and by consequence the role of vision, in the formation of locomotor trajectories. In Figure 4.15(c) some examples of trajectories followed by humans are reported. Subjects, starting from the same initial configuration, have to reach different final positions with the same orientation, i.e. 120 deg in Figure 4.15(c). We reproduced the similar experiment by simulating the unicycle vehicle controlled by the feedback control laws in elliptic and bipolar coordinates developed in Chap. 4. Results of this simulation are reported in Figs. 4.15(a) and 4.15(b). Strikingly the trajectories followed by the vehicle resemble the human ones. As a future work it should be interesting to continue the study in this direction and evaluate the effect of varying the different control parameters. It would be also interesting to introduce a pan–tilt mechanism to take into account that humans can turn the head and gaze [Hicheur 2005]. However, when a human subject goes toward a target at a constant velocity it is shown that he behaves as a nonholonomic system: its velocity remains roughly tangent to its sagittal plane [Arechavaleta 2008].

For all these reasons, it would be interesting to integrate this methodology in walking pattern generators to steer humanoid robots, e.g. the HRP-2, towards a target. In particular, it would be interesting to study how the proposed planar geometry allows to combine both the bearing angle and the focus of expansion to generate a visual feedback control of locomotion as humans do [Warren 2001].

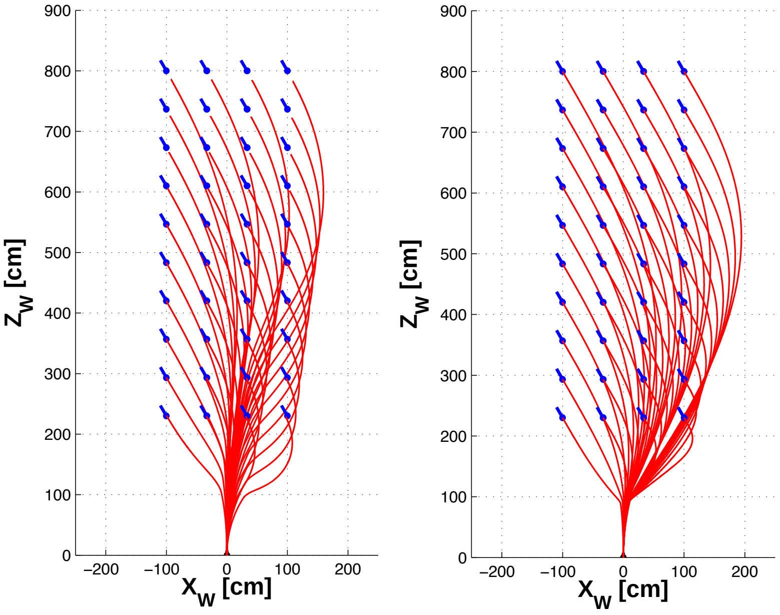

(a) By elliptic coordinates.

(b) By bipolar coordinates.

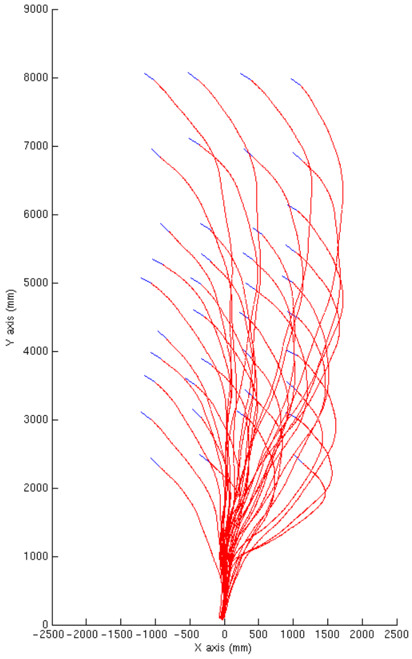

(c) By humans (From [Arechavaleta 2008], courtesy of the authors).

Figure 4.15: Some examples of trajectories with the same final orientation, generated by the control laws in elliptic and bipolar coordinates and by Humans. In (a), (b) and (c) the final orientation is 120 *deg. (a) By elliptic coordinates. (b) By bipolar coordinates. (c) By humans (from, [Arechavaleta 2008] courtesy of the authors).*

APPENDIX A

Mobile Robot *Robulab10*

A.1 Robulab10 Motion Control

In this appendix we present the technical details about the wheeled robot Robulab from RobuSoft and the methods used to control it. The software that is going to be presented was developed as basis to implement the tracking control exploited in Chap. 1 and Chap. 2 and the vision-based control laws described in Chap. 4.

A.1.1 The robotic platform

Robulab10 is a multi-purpose mobile robot designed to embed various "applications modules". It is a generic base plate (platform) industrialized to be used for various applications thanks to the additional modules that can be integrated, e.g. a Pant–Tilt camera on the top. The robot is equipped with an internal computer called RobuBOX that provides different features i.e. manual remote control by joypad, obstacle detection, wire or wireless control. Although the control of the robot is mainly developed for Microsoft Robotics Studio, also some basic functions, needed by most of automatic guided vehicles, are provided. In particular, it is possible to control the robot by a remote station by a wireless communication through an UDP connection.

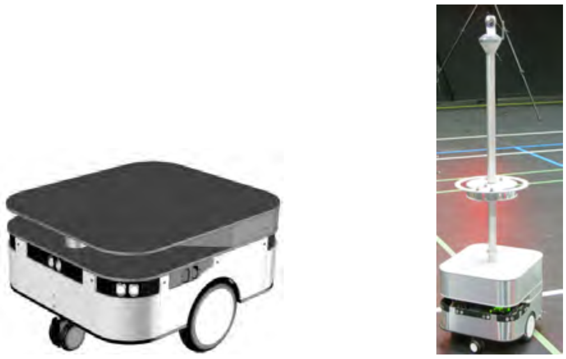

(a) (b)

Figure A.1: (a) The basic version of Robulab10 and (b) the one with the Pan–Tilt camera PT7137 mounted on the top used for the experiments.

Dimension	450 x 400 x 243 mm. (L x W x H)
Payload	30 Kg
Weight	20 Kg, including batteries
Max speed	4 m/s
Communication	Wi-Fi and LAN

Table A.1: Main technical features of Robulab10.

A.1.2 Robot Remote Control

In order to control the robot we connected our remote station through wi-fi connection and we send low-level messages by an UDP connection. These messages have to be sent with a particular order. To define the priority of the messages, we have to specify their priority by some square brackets. An example is reported below. The principal commands are:

- *Alive* : needed to avoid that WatchDog[1] stops the robot;
- *Start* : it allows to set the robot in remote-control mode;
- *Drive* : it is the move command. The linear and and angular velocity must be expressed in cm/s and rad/sec.

Example: to move the robot straight at 1.4 m/s, instructions that have to be sent ($f = 50$Hz):

[1] Alive
[2] Start
[3] Drive 140 0

The programming language considered was C++. I created the class *Robulab10* that had to be defined at the beginning of the program. The class provided three main methods:

- *establish_connection()* : it checks and creates the sockets to establish the UDP connection. The IP address of the robot must be defined inside this function in order to send the message. This method must be called just after the definition of the class;
- *move_robot(double lin_vel, double ang_vel)* : to send the control inputs;
- *stop_robot()* : it stops immediately the robot;

The code aims to be user-friendly and open source [2]. Unfortunately, the official documentation is not anymore available and it has not been possible to improve further the software with new functions. The code developed can be used by any user and can be integrated with other communications e.g. ROS and YARP. In our experiments, we used ROS to communicate with the MoCap (Vicon or Motion Analysis) for obtaining the robot position and orientation. Therefore, we computed the robot inputs by using path following control (predefined path) or tracking control (reference behavior). The developed software is compatible and tested with ROS Groovy, Hydro and Indigo version.

---

[1] The WatchDog, sometimes called as *computer operating properly timer*, is an electronic timer that is used to detect and recover from computer malfunctions. The WatchDog in Robulab10 checks every 800ms if the robot is in "Alive" mode or not. If it is not, the robot is stopped.

[2] `https://github.com/Christian-Vassallo/robot_follow_mocap/blob/master/src/Robulab10Class.hpp`

Bibliography

[Aicardi 1995] M. Aicardi, G. Casalino, A. Bicchi et A. Balestrino. *Closed loop steering of unicycle like vehicles via Lyapunov techniques*. IEEE Robotics & Automation Magazine, vol. 2, no. 1, pages 27–35, 1995. (Cited in page 90.)

[Ajallooeian 2013] M. Ajallooeian, J. van den Kieboom, A. Mukovskiy, MA. Giese et AJ. Ijspeert. *A general family of morphed nonlinear phase oscillators with arbitrary limit cycle shape*. Physica D: Nonlinear Phenomena, vol. 263, pages 41–56, 2013. (Cited in page 63.)

[Ajoudani 2014] A. Ajoudani, J. Lee, A. Rocchi, M. Ferrati, EM. Hoffman, A. Settimi, DG Caldwell, A. Bicchi et NG. Tsagarakis. *A manipulation framework for compliant humanoid COMAN: Application to a valve turning task*. In Humanoid Robots (Humanoids), 2014 14th IEEE-RAS International Conference on, pages 664–670, 2014. (Cited in page 62.)

[Albrecht 2012] S. Albrecht, P. Basili, S. Glasauer, M. Leibold et M. Ulbrich. *Modeling and analysis of human navigation with crossing interferer using inverse optimal control*. IFAC Proceedings Volumes, vol. 45, no. 2, pages 475–480, 2012. (Cited in page 42.)

[Arechavaleta 2008] G. Arechavaleta, JP. Laumond, H. Hicheur et A. Berthoz. *On the nonholonomic nature of human locomotion*. Autonomous Robots, vol. 25, no. 1-2, pages 25–35, 2008. (Cited in pages xi, 120 et 121.)

[Atkeson 1997] CG. Atkeson, AW. Moore et S. Schaal. *Locally Weighted Learning*. A.I. Review, vol. 11, pages 11–73, 1997. (Cited in page 68.)

[Basili 2013] P. Basili, M. Saglam, T. Kruse, M. Huber, A. Kirsch et S. Glasauer. *Strategies of locomotor collision avoidance*. Gait and posture, vol. 37, no. 3, pages 385–390, 2013. (Cited in pages 19 et 42.)

[Bhattacharya 2007] S. Bhattacharya, R. Murrieta-Cid et S. Hutchinson. *Optimal paths for landmark-based navigation by differential-drive vehicles with field-of-view constraints*. IEEE Transactions on Robotics, vol. 23, no. 1, pages 47–59, 2007. (Cited in page 81.)

[Boyd 2004] Stephen Boyd et Lieven Vandenberghe. Convex optimization. Cambridge university press, 2004. (Cited in page 71.)

[Bradski 2000] G. Bradski. Dr. Dobb's Journal of Software Tools, 2000. (Cited in page 104.)

[Brandao 2013] M. Brandao, L. Jamone, P. Kryczka, N. Endo, K. Hashimoto et A. Takanishi. *Reaching for the unreachable: integration of locomotion and whole-body movements for extended visually guided reaching*. In Proc. of 13th IEEE-RAS Int. Conf. on Humanoid Robots (Humanoids), pages 28–33, 2013. (Cited in page 63.)

[Breazeal 2005] C. Breazeal, CD. Kidd, AL. Thomaz, G. Hoffman et M. Berlin. *Effects of nonverbal communication on efficiency and robustness in human-robot teamwork*. In 2005 IEEE/RSJ International Conference on Intelligent Robots and Systems, pages 708–713. IEEE, 2005. (Cited in page 41.)

[Brockett 1983] RW. Brockett*et al.* *Asymptotic stability and feedback stabilization*. Differential geometric control theory, vol. 27, no. 1, pages 181–191, 1983. (Cited in page 89.)

[Buchli 2006] J. Buchli, L. Righetti et AJ. Ijspeert. *Engineering Entrainment and Adaptation in Limit Cycle Systems - from biological inspiration to applications in robotics*. Biol. Cyb., vol. 95, no. 6, pages 645–664, 2006. (Cited in pages 62 et 67.)

[Buss 2011] M. Buss, D. Carton, B. Gonsior, K. Kuehnlenz, C. Landsiedel, N. Mitsou, R. de Nijs, J. Zlotowski, S. Sosnowski, E. Strasser*et al.* *Towards proactive human-robot interaction in human environments*. In Cognitive Infocommunications (CogInfoCom), 2011 2nd International Conference on, pages 1–6. IEEE, 2011. (Cited in page 41.)

[Carelli 2002] R. Carelli, C. Soria, O. Nasisi et E. Freire. *Stable AGV corridor navigation with fused vision-based control signals*. In IECON 02 [Industrial Electronics Society, IEEE 2002 28th Annual Conference of the], volume 3, pages 2433–2438. IEEE, 2002. (Cited in page 81.)

[Carton 2013] D. Carton, A. Turnwald, D. Wollherr et M. Buss. *Proactively approaching pedestrians with an autonomous mobile robot in urban environments*. In Experimental Robotics, pages 199–214. Springer, 2013. (Cited in pages 20, 41 et 58.)

[Carton 2016] D. Carton, W. Olszowy et D. Wollherr. *Measuring the Effectiveness of Readability for Mobile Robot Locomotion*. International Journal of Social Robotics, pages 1–21, 2016. (Cited in page 42.)

[Chang 2001] CC. Chang et CJ. Lin. *LIBSVM: a library for support vector machines*, 2001. Software available at `http://www.csie.ntu.edu.tw/~cjlin/libsvm`. (Cited in page 67.)

[Chaumette 2006] F. Chaumette et S. Hutchinson. *Visual servo control. I. Basic approaches*. IEEE Robotics & Automation Magazine, vol. 13, no. 4, pages 82–90, 2006. (Cited in page 83.)

[Chaumette 2007] F. Chaumette et S. Hutchinson. *Visual servo control, Part II: Advanced approaches*. IEEE Robotics and Automation Magazine, vol. 14, no. 1, pages 109–118, 2007. (Cited in page 83.)

[Cheein 2009] FA. Cheein, C. De La Cruz, R. Carelli et TF. Bastos-Filho. *Solution to a door crossing problem for an autonomous wheelchair*. In 2009 IEEE/RSJ International Conference on Intelligent Robots and Systems, pages 4931–4936. IEEE, 2009. (Cited in page 82.)

[Cheein 2010] F. Cheein, C. De La Cruz, T. Bastos et R. Carelli. *Slam-based cross-a-door solution approach for a robotic wheelchair*. Int J Adv Robot Syst, vol. 7, no. 2, pages 155–164, 2010. (Cited in page 82.)

[Chiovetto 2013] E. Chiovetto, A. d'Avella, D. Endres et MA. Giese. *A unifying algorithm for the identification of kinematic and electromyographic motor primitives*. Bernstein Conference, vol. 0, page 0, April 2013. not reviewed. (Cited in pages 66 et 67.)

[Cinelli 2007] ME. Cinelli et AE. Patla. *Travel path conditions dictate the manner in which individuals avoid collisions*. Gait and Posture, vol. 26, no. 2, pages 186–193, 2007. (Cited in page 20.)

[Cinelli 2008] ME. Cinelli et AE. Patla. *Locomotor avoidance behaviours during a visually guided task involving an approaching object*. Gait and posture, vol. 28, no. 4, pages 596–601, 2008. (Cited in page 20.)

[Dai 2013] DW. Dai, GL. Jiang, J. Xin, X. Gao, LL. Cui, YS Ou et GQ. Fu. *Detecting, locating and crossing a door for a wide indoor surveillance robot*. In Robotics and Biomimetics (ROBIO), 2013 IEEE International Conference on, pages 1740–1746. IEEE, 2013. (Cited in page 82.)

[Dalibard 2013] S. Dalibard, A. El Khoury, F. Lamiraux, A. Nakhaei, M. Taïx et JP. Laumond. *Dynamic Walking and Whole-Body Motion Planning for Humanoid Robots:*

an Integrated Approach. Int. Journal of Robotics Research, vol. 32, no. 9-10, pages 1089–1103, 2013. (Cited in page 63.)

[Dedieu 2000] D. Dedieu, V. Cadenat et P. Souères. *Mixed camera-laser based control for mobile robot navigation.* In Intelligent Robots and Systems, 2000.(IROS 2000). Proceedings. 2000 IEEE/RSJ International Conference on, volume 2, pages 1081–1086. IEEE, 2000. (Cited in page 81.)

[Dev 1997] A. Dev, B. Krose et F. Groen. *Navigation of a mobile robot on the temporal development of the optic flow.* In Intelligent Robots and Systems, 1997. IROS'97., Proceedings of the 1997 IEEE/RSJ International Conference on, volume 2, pages 558–563. IEEE, 1997. (Cited in page 81.)

[Dragan 2013] A. Dragan et S. Srinivasa. *Generating legible motion.* 2013. (Cited in pages 41 et 58.)

[Dragan 2015] AD. Dragan, S. Bauman, J. Forlizzi et SS. Srinivasa. *Effects of robot motion on human-robot collaboration.* In Proceedings of the Tenth Annual ACM/IEEE International Conference on Human-Robot Interaction, pages 51–58. ACM, 2015. (Cited in pages 20 et 58.)

[Englsberger 2014] J. Englsberger, T. Koolen, S. Bertrand, J. Pratt, C. Ott et A. Albu-Schäffer. *Trajectory generation for continuous leg forces during double support and heel-to-toe shift based on divergent component of motion.* pages 4022–4029, Sept 2014. (Cited in page 63.)

[Fajen 2003] BR. Fajen et WH. Warren. *Behavioral dynamics of steering, obstable avoidance, and route selection.* Journal of Experimental Psychology: Human Perception and Performance, vol. 29, no. 2, page 343, 2003. (Cited in page 42.)

[Feng 2012] AW. Feng, Y. Xu et A. Shapiro. *An example-based motion synthesis technique for locomotion and object manipulation.* pages 95–102. ACM, 2012. (Cited in page 62.)

[Fitzgibbon 1996] A. W. Fitzgibbon, R. B. Fisher*et al.* *A buyer's guide to conic fitting.* DAI Research paper, 1996. (Cited in page 105.)

[Flash 2005] Tamar Flash et Binyamin Hochner. *Motor primitives in vertebrates and invertebrates.* Current opinion in neurobiology, vol. 15, no. 6, pages 660–666, 2005. (Cited in pages 11 et 12.)

[Fletcher 1971] R Fletcher. *A general quadratic programming algorithm*. IMA Journal of Applied Mathematics, vol. 7, no. 1, pages 76–91, 1971. (Cited in page 71.)

[Gams 2008] A. Gams, L. Righetti, AJ. Ijspeert et J. Lenarčič. *A dynamical system for online learning of periodic movements of unknown waveform and frequency*. In Biomedical Robotics and Biomechatronics, 2008. BioRob 2008. 2nd IEEE RAS & EMBS International Conference on, pages 85–90. IEEE, 2008. (Cited in page 62.)

[Gams 2013] A. Gams, B. Nemec, L. Zlajpah, M. Wächter, AJ. Ijspeert, T. Asfour et A. Ude. *Modulation of Motor Primitives using Force Feedback: Interaction with the Environment and Bimanual Tasks*. In Proc. IEEE/RSJ Int. Conf. on Intelligent Robots and Systems (IROS 2013), pages 5629–5635, 2013. (Cited in page 63.)

[Gérin-Lajoie 2005] M. Gérin-Lajoie, CL. Richards et BJ. McFadyen. *The negotiation of stationary and moving obstructions during walking: anticipatory locomotor adaptations and preservation of personal space*. Motor control, vol. 9, no. 3, pages 242–69, 2005. (Cited in page 20.)

[Gienger 2005] Michael Gienger, Herbert Janssen et Christian Goerick. *Task-oriented whole body motion for humanoid robots*. In 5th IEEE-RAS International Conference on Humanoid Robots, 2005., pages 238–244. IEEE, 2005. (Cited in page 69.)

[Gienger 2010] M. Gienger, M. Toussaint et C. Goerick. *Whole-body motion planning–building blocks for intelligent systems*. In Motion Planning for Humanoid Robots. 2010. (Cited in page 63.)

[Giese 2009a] MA. Giese, A. Mukovskiy, A. Park, L. Omlor et JJE. Slotine. *Real-Time Synthesis of Body Movements Based on Learned Primitives*. In D. Cremers et al., editeur, Stat. and Geom. Appr. to Vis. Mot. Anal., LNCS5604, pages 107–127. Springer, 2009. (Cited in pages ix, 62, 67, 68 et 69.)

[Giese 2009b] MA. Giese, A. Mukovskiy, A. Park, L. Omlor et JJE. Slotine. *Real-Time Synthesis of Body Movements Based on Learned Primitives*. In D. Cremers et al., editeur, Stat. and Geom. Appr. to Vis. Mot. Anal., LNCS5604, pages 107–127. Springer, 2009. (Cited in pages 12 et 117.)

[Goffman 1971] Erving Goffman. Relations in public. microstudies of the public order. london (allen lane) 1971. 1971. (Cited in page 42.)

[Goodrich 2007] MA. Goodrich et AC. Schultz. *Human-robot interaction: a survey*. Foundations and trends in human-computer interaction, vol. 1, no. 3, pages 203–275, 2007. (Cited in page 19.)

[Hartley 2003] R. Hartley et A. Zisserman. Multiple view geometry in computer vision. Cambridge university press, 2003. (Cited in page 84.)

[Hayet 2012] JB. Hayet, C. Esteves, G. Arechavaleta, O. Stasse et E. Yoshida. *Humanoid locomotion planning for visually guided tasks*. International Journal of Humanoid Robotics, vol. 9, no. 02, page 1250009, 2012. (Cited in page 81.)

[Herdt 2010] Andrei Herdt, Holger Diedam, Pierre-Brice Wieber, Dimitar Dimitrov, Katja Mombaur et Moritz Diehl. *Online walking motion generation with automatic footstep placement*. Advanced Robotics, vol. 24, no. 5-6, pages 719–737, 2010. (Cited in page 72.)

[Hicheur 2005] H. Hicheur, S. Vieilledent et A. Berthoz. *Head motion in humans alternating between straight and curved walking path: combination of stabilizing and anticipatory orienting mechanisms*. Neuroscience letters, vol. 383, no. 1, pages 87–92, 2005. (Cited in page 120.)

[Hsu 2005] E. Hsu, K. Pulli et J. Popovic. *Style translation for human motion*. ACM Trans. on Graphics, vol. 24, pages 1082–1089, 2005. (Cited in page 62.)

[Huang 2014] Y. Huang et M. Kallmann. *Planning Motions for Virtual Demonstrators*. In Intelligent Virtual Agents, pages 190–203. Springer, 2014. (Cited in page 62.)

[Huber 2014] M. Huber, YH. Su, M. Krüger, K. Faschian, S. Glasauer et J. Hermsdörfer. *Adjustments of speed and path when avoiding collisions with another pedestrian*. PloS one, vol. 9, no. 2, page e89589, 2014. (Cited in pages 19 et 42.)

[Hutchinson 1996] S. Hutchinson, GD. Hager et PI. Corke. *A tutorial on visual servo control*. IEEE transactions on robotics and automation, vol. 12, no. 5, pages 651–670, 1996. (Cited in page 83.)

[Ijspeert 2008] AJ. Ijspeert. *Central pattern generators for locomotion control in animals and robots: A review*. Neural Networks, vol. 21, no. 4, pages 642–653, 2008. (Cited in page 67.)

[Ijspeert 2013] AJ. Ijspeert, J. Nakanishi, H. Hoffmann, P. Pastor et S. Schaal. *Dynamical movement primitives: Learning attractor models for motor behaviors*. Neural Computation, vol. 25, no. 2, pages 328–373, 2013. (Cited in page 63.)

[Jansen 2011] SEM. Jansen, A. Toet et PJ. Werkhoven. *Human locomotion through a multiple obstacle environment: Strategy changes as a result of visual field limitation*.

Experimental Brain Research, vol. 212, no. 3, pages 449–456, 2011. (Cited in page 19.)

[Johnson 2015] M. Johnson, B. Shrewsbury, S. Bertrand, T. Wu, D. Duran, M. Floyd, P. Abeles, D. Stephen, N. Mertins, A. Lesman*et al. Team IHMC's lessons learned from the DARPA robotics challenge trials*. Journal of Field Robotics, vol. 32, no. 2, pages 192–208, 2015. (Cited in page 63.)

[Kajita 2003] S. Kajita, F. Kanehiro, K. Kaneko, K. Fujiwara, K. Harada, K. Yokoi et H. Hirukawa. *Biped walking pattern generation by using preview control of zero-moment point*. Taipe, Taiwan, September 2003. (Cited in pages 63, 72 et 73.)

[Kanoun 2009] Oussama Kanoun, Florent Lamiraux, Pierre-Brice Wieber, Fumio Kanehiro, Eiichi Yoshida et Jean-Paul Laumond. *Prioritizing linear equality and inequality systems: application to local motion planning for redundant robots*. In Robotics and Automation, 2009. ICRA'09. IEEE International Conference on, pages 2939–2944. IEEE, 2009. (Cited in page 71.)

[Kanoun 2011] Oussama Kanoun, Florent Lamiraux et Pierre-Brice Wieber. *Kinematic control of redundant manipulators: Generalizing the task-priority framework to inequality task*. IEEE Transactions on Robotics, vol. 27, no. 4, pages 785–792, 2011. (Cited in page 71.)

[Karamouzas 2010] I. Karamouzas et M. Overmars. *Simulating human collision avoidance using a velocity-based approach*. 2010. (Cited in page 42.)

[Kato 2015] Y. Kato, T. Kanda et H. Ishiguro. *May i help you?: Design of human-like polite approaching behavior*. In Proceedings of the Tenth Annual ACM/IEEE International Conference on Human-Robot Interaction, pages 35–42. ACM, 2015. (Cited in pages 20 et 58.)

[Knorr 2016] AG. Knorr, L. Willacker, J. Hermsdörfer, S. Glasauer et M. Krüger. *Influence of Person-and Situation-Specific Characteristics on Collision Avoidance Behavior in Human Locomotion*. 2016. (Cited in pages 19 et 20.)

[Koenemann 2015] J. Koenemann, A. Del Prete, Y. Tassa, E. Todorov, O. Stasse, M. Bennewitz et N. Mansard. *Whole-body Model-Predictive Control Applied to the HRP-2 Humanoid*. In IEEE/RSJ International Conference on Intelligent Robots and Systems (IROS), pages 3346–3351, 2015. (Cited in page 61.)

[Koschorreck 2012] J. Koschorreck et K. Mombaur. *Modeling and Optimal Control of Human Platform Diving With Somersaults and Twists.* Optimization and Engineering, vol. 13, no. 1, pages 29–56, 2012. (Cited in page 61.)

[Kruse 2013] T. Kruse, AK. Pandey, R. Alami et A. Kirsch. *Human-aware robot navigation: A survey.* Robotics and Autonomous Systems, vol. 61, no. 12, pages 1726–1743, 2013. (Cited in pages 19 et 35.)

[Kuindersma 2015] S. Kuindersma, R. Deits, M. Fallon, A. Valenzuela, H. Dai, F. Permenter, T. Koolen, P. Marion et R. Tedrake. *Optimization–based locomotion planning, estimation, and control design for the Atlas humanoid robot.* Autonomous Robots, pages 1–27, 2015. (Cited in page 62.)

[Land 2013] WM. Land, DA. Rosenbaum, S. Seegelke et T. Schack. *Whole-body posture planning in anticipation of a manual prehension task: Prospective and retrospective effects.* Acta Psychologica, vol. 114, pages 298–307, 2013. (Cited in page 62.)

[Levine 2012] S. Levine, J. M. Wang, A. Haraux, Z. Popović et V. Koltun. *Continuous Character Control with Low-Dimensional Embeddings.* ACM SIGGRAPH 2012. ACM Transactions on Graphics, Article N.28, vol. 31, no. 4, page 28, 2012. (Cited in page 61.)

[Lichtenthäler 2012] C. Lichtenthäler, T. Lorenzy et A. Kirsch. *Influence of legibility on perceived safety in a virtual human-robot path crossing task.* In 2012 IEEE RO-MAN: The 21st IEEE International Symposium on Robot and Human Interactive Communication, pages 676–681. IEEE, 2012. (Cited in page 41.)

[Lichtenthäler 2013] C. Lichtenthäler et A. Kirsch. *Towards legible robot navigation-how to increase the intend expressiveness of robot navigation behavior.* In International conference on social robotics-workshop embodied communication of goals and intentions, 2013. (Cited in pages 20, 41 et 58.)

[López-Nicolás 2010] G. López-Nicolás, N. R Gans, S. Bhattacharya, C. Sagues, JJ. Guerrero et S. Hutchinson. *Homography-based control scheme for mobile robots with nonholonomic and field-of-view constraints.* IEEE Transactions on Systems, Man, and Cybernetics, Part B (Cybernetics), vol. 40, no. 4, pages 1115–1127, 2010. (Cited in page 81.)

[Mansard 2009] Nicolas Mansard, Olivier Stasse, Paul Evrard et Abderrahmane Kheddar. *A versatile generalized inverted kinematics implementation for collaborative work-*

ing humanoid robots: The stack of tasks. In Advanced Robotics, 2009. ICAR 2009. International Conference on, pages 1–6. IEEE, 2009. (Cited in page 70.)

[Marchand 2005] E. Marchand, F. Spindler et F. Chaumette. *ViSP for visual servoing: a generic software platform with a wide class of robot control skills*. IEEE Robotics and Automation Magazine, vol. 12, no. 4, pages 40–52, December 2005. (Cited in page 104.)

[Miihlig 2010] M. Miihlig, M. Gienger et JJ. Steil. *Human-Robot Interaction for Learning and Adaptation of Object Movements*. In Proc. of IEEE/RSJ Int. Conf. on Intelligent Robots and Systems (IROS 2010), pages 4901–4907, 2010. (Cited in page 63.)

[Minguez 2008] J. Minguez, F. Lamiraux et JP. Laumond. *Motion planning and obstacle avoidance*. In Springer handbook of robotics, pages 827–852. Springer, 2008. (Cited in page 84.)

[Mombaur 2010] K. Mombaur, A. Truong et JP. Laumond. *From human to humanoid locomotion an inverse optimal control approach*. Autonomous robots, vol. 28, no. 3, pages 369–383, 2010. (Cited in page 120.)

[Monasterio 2002] I. Monasterio, E. Lazkano, I. Rañó et B. Sierra. *Learning to traverse doors using visual information*. Mathematics and computers in simulation, vol. 60, no. 3, pages 347–356, 2002. (Cited in page 82.)

[Mukovskiy 2013] A. Mukovskiy, JJE. Slotine et MA. Giese. *Dynamically stable control of articulated crowds*. Journal of Computational Science, vol. 4, no. 4, pages 304–310, 2013. (Cited in pages 12 et 117.)

[Mukovskiy 2015a] A. Mukovskiy, W. Land, T. Schack et MA. Giese. *Modeling of predictive human movement coordination patterns for applications in computer graphics*. Journal of WSCG, vol. 23, no. 2, pages 139–146, 2015. (Cited in pages ix, 62, 64, 66 et 68.)

[Mukovskiy 2015b] A Mukovskiy, C. Vassallo, M. Naveau, O. Stasse, P. Souères et Giese MA. *Learning Movement Primitives for the Humanoid Robot HRP-2*. In IEEE IROS 2015 Workshop on "Towards truly human-like bipedal locomotion: the role of optimization, learning and motor primitives". Hamburg, Germany, 2015. (Cited in page 64.)

[Mukovskiy 2016] A. Mukovskiy, C. Vassallo, M. Naveau, O. Stasse, P. Souères et MA. Giese. *Adaptive synthesis of dynamically feasible full-body movements for the*

Humanoid Robot HRP-2 by flexible combination of learned dynamic movement primitives. Robotics and Autonomous Systems, 2016. Corrected version under review. (Not cited.)

[Nakamura 1987] Yoshihiko Nakamura et Hideo Hanafusa. *Optimal redundancy control of robot manipulators*. The International Journal of Robotics Research, vol. 6, no. 1, pages 32–42, 1987. (Cited in page 69.)

[Naveau 2014] M. Naveau, J. Carpentier, S. Barthelemy, O. Stasse et P. Soueres. *META-POD - Template META-PrOgramming applied to Dynamics: CoP-CoM trajectories filtering*. 2014. (Cited in page 73.)

[Naveau 2017] M. Naveau, M. Kudruss, O. Stasse, C. Kirches, K. Mombaur et P. Soueres. *A Reactive Walking Pattern Generator Based on Nonlinear Model Predictive Control.* vol. 2, no. 1, pages 10–17, 2017. (Cited in pages 61, 64, 72 et 73.)

[Neo 2005] Ee Sian Neo, Kazuhito Yokoi, Shuuji Kajita, Fumio Kanehiro et Kazuo Tanie. *A switching command-based whole-body operation method for humanoid robots*. IEEE/ASME Transactions on Mechatronics, vol. 10, no. 5, pages 546–559, 2005. (Cited in page 69.)

[Olivier 2012] AH. Olivier, A. Marin, A. Crétual et J. Pettré. *Minimal predicted distance: A common metric for collision avoidance during pairwise interactions between walkers*. Gait and Posture, vol. 36, no. 3, pages 399–404, jul 2012. (Cited in pages viii, 19, 20, 21, 22, 28, 32, 35 et 42.)

[Olivier 2013] AH. Olivier, A. Marin, A. Crétual, A. Berthoz et J. Pettré. *Collision avoidance between two walkers: role-dependent strategies.* Gait and posture, vol. 38, no. 4, pages 751–6, 2013. (Cited in pages 10, 20, 21, 28, 36, 42, 53, 57 et 58.)

[Omlor 2011] L. Omlor et MA. Giese. *Anechoic Blind Source Separation using Wigner Marginals*. J. of Machine Learning Res., vol. 12, pages 1111–1148, 2011. (Cited in pages 66 et 67.)

[Ondrej 2010] J. Ondrej, J. Pettré, AH. Olivier et S. Donikian. *A synthetic-vision based steering approach for crowd simulation*. In ACM Transactions on Graphics (TOG), volume 29, page 123. ACM, 2010. (Cited in page 20.)

[Park 2009] A. Park, A. Mukovskiy, J. E. Slotine et MA. Giese. *Design of Dynamical Stability Properties in Character Animation.* In VRIPHYS, pages 85–94, 2009. (Cited in page 68.)

[Pasteau 2016] F. Pasteau, VK. Narayanan, M. Babel et F. Chaumette. *A visual servoing approach for autonomous corridor following and doorway passing in a wheelchair*. Robotics and Autonomous Systems, vol. 75, pages 28–40, 2016. (Cited in page 81.)

[Patel 2002] S. Patel, SH. Jung, JP. Ostrowski, R. Rao et CJ. Taylor. *Sensor based door navigation for a nonholonomic vehicle*. In Robotics and Automation, 2002. Proceedings. ICRA'02. IEEE International Conference on, volume 3, pages 3081–3086. IEEE, 2002. (Cited in page 82.)

[Patla 2006] AE. Patla et M. Greig. *Any way you look at it, successful obstacle negotiation needs visually guided on-line foot placement regulation during the approach phase*. Neuroscience letters, vol. 397, no. 1, pages 110–114, 2006. (Cited in page 19.)

[Rosenbaum 2008] DA. Rosenbaum. *Reaching while walking: reaching distance costs more than walking distance*. Psych. Bull. Rev., vol. 15, pages 1100–1104, 2008. (Cited in page 62.)

[Salaris 2010] P. Salaris, D. Fontanelli, L. Pallottino et A. Bicchi. *Shortest paths for a robot with nonholonomic and field-of-view constraints*. IEEE Transactions on Robotics, vol. 26, no. 2, pages 269–281, 2010. (Cited in pages 81, 108 et 111.)

[Salaris 2011] P. Salaris, L. Pallottino, S. Hutchinson et A. Bicchi. *From optimal planning to visual servoing with limited fov*. In 2011 IEEE/RSJ International Conference on Intelligent Robots and Systems, pages 2817–2824. IEEE, 2011. (Cited in page 81.)

[Salaris 2015a] P. Salaris, A. Cristofaro, L. Pallottino et A. Bicchi. *Epsilon-Optimal Synthesis for Vehicles With Vertically Bounded Field-Of-View*. IEEE Transactions on Automatic Control, vol. 60, no. 5, pages 1204–1218, 2015. (Cited in page 109.)

[Salaris 2015b] P. Salaris, C. Vassallo, P. Souères et J-P. Laumond. *Image-based control relying on conic curves foliation for passing through a gate*. In 2015 IEEE International Conference on Robotics and Automation (ICRA), pages 684–690. IEEE, 2015. (Not cited.)

[Salaris 2015c] P. Salaris, C. Vassallo, P. Souères et JP. Laumond. *The geometry of confocal curves for passing through a door*. IEEE Transactions on Robotics, vol. 31, no. 5, pages 1180–1193, 2015. (Not cited.)

[Samson 1991] Claude Samson, Bernard Espiau et Michel Le Borgne. Robot control: the task function approach. Oxford University Press, 1991. (Cited in page 69.)

[Shoulson 2014] A. Shoulson, N. Marshak, M. Kapadia et NI. Badler. *ADAPT: The Agent Development and Prototyping Testbed*. IEEE Trans. on Visualiz. and Comp. Graphics (TVCG), vol. 99, pages 1–14, 2014. (Cited in page 62.)

[Siciliano 1991] Bruno Siciliano et J-JE Slotine. *A general framework for managing multiple tasks in highly redundant robotic systems*. In Advanced Robotics, 1991.'Robots in Unstructured Environments', 91 ICAR., Fifth International Conference on, pages 1211–1216. IEEE, 1991. (Cited in page 70.)

[Soueres 2005] P. Soueres, S. Tarbouriech et B. Gao. *A robust vision-based controller for mobile robots navigation: application to the task sequencing problem*. In 2005 IEEE/RSJ International Conference on Intelligent Robots and Systems, pages 2191–2196. IEEE, 2005. (Cited in page 81.)

[Stasse 2008] O. Stasse, F. Saïdi, K. Yokoi, B. Verrelst, B. Vanderborght, A. Davison, N. Mansard et C. Esteves. *Integrating walking and vision to increase humanoid autonomy*. International Journal of Humanoid Robotics, vol. 5, no. 02, pages 287–310, 2008. (Cited in page 63.)

[Stasse 2014] O. Stasse, F. Morsillo, M. Geisert, N. Mansard, M. Naveau et C. Vassallo. *Airbus/future of aircraft factory HRP-2 as universal worker proof of concept*. In 2014 IEEE-RAS International Conference on Humanoid Robots, pages 1014–1015. IEEE, 2014. (Not cited.)

[Suzuki 1985] S. Suzuki*et al.* *Topological structural analysis of digitized binary images by border following*. Computer Vision, Graphics, and Image Processing, vol. 30, no. 1, pages 32–46, 1985. (Cited in page 105.)

[Taïx 2013] M. Taïx, MT. Tran et E. Souères P. Guigon. *Generating human-like reaching movements with a humanoid robot: A computational approach*. J. of Computational Science, vol. 4, pages 269–284, 2013. (Cited in page 63.)

[Tassa 2012] Y. Tassa, T. Erez et E. Todorov. *Synthesis and stabilization of complex behaviors through online trajectory optimization*. pages 4906–4913. IEEE, 2012. (Cited in page 61.)

[Vallis 2003] LA. Vallis et BJ. McFadyen. *Locomotor adjustments for circumvention of an obstacle in the travel path*. Experimental brain research, vol. 152, no. 3, pages 409–414, 2003. (Cited in page 19.)

[van Basten 2009] BJH. van Basten, SEM. Jansen et I. Karamouzas. *Exploiting motion capture to enhance avoidance behaviour in games*. In International Workshop on Motion in Games, pages 29–40. Springer, 2009. (Cited in page 42.)

[Vassallo 1998] RF. Vassallo, HJ. Schneebeli et J. Santos-Victor. *Visual navigation: combining visual servoing and appearance based methods*. In International Symposium on Intelligent Robotic Systems, SIRS, volume 98. Citeseer, 1998. (Cited in page 81.)

[Vassallo 2017] C. Vassallo, AH. Olivier, P. Souères, A. Crétual, O. Stasse et Pettré J. *How do walkers avoid a mobile robot crossing their way?* Gate and Posture, vol. 51, pages 97 – 103, 2017. (Cited in pages 19, 42 et 58.)

[Wang 2008] J. M. Wang, D. J. Fleet et A. Hertzmann. *Gaussian Process Dynamical Models for Human Motion*. IEEE Trans. on Pattern Analysis and Machine Intelligence, vol. 30, no. 2, pages 283–298, 2008. (Cited in page 62.)

[Wang 2012] S. Wang, L. Chen, H. Hu et K. McDonald-Maier. *Doorway passing of an intelligent wheelchair by dynamically generating bezier curve trajectory*. In Robotics and Biomimetics (ROBIO), 2012 IEEE International Conference on, pages 1206–1211. IEEE, 2012. (Cited in page 82.)

[Warren 2001] WH. Warren, BA. Kay, WD. Zosh, AP. Duchon et S. Sahuc. *Optic flow is used to control human walking*. Nature neuroscience, vol. 4, no. 2, pages 213–216, 2001. (Cited in page 120.)

[Warren 2008] WH. Warren et BR. Fajen. *Behavioral dynamics of visually guided locomotion*. In Coordination: neural, behavioral and social dynamics, pages 45–75. Springer, 2008. (Cited in page 20.)

[Weigelt 2010] M. Weigelt et T. Schack. *The Development of End-State Comfort Planning in Preschool Children*. Exper. Psych., vol. 57, no. 6, pages 476–782, 2010. (Cited in page 62.)

[Yoshida 2007] E. Yoshida, A. Mallet, F. Lamiraux, Kanoun. O., O. Stasse, M. Poirier, PF. Dominey, JP Laumond et K. Yokoi. *Give me the Purple Ball – he said to HRP-2 N.14*. In IEEE RAS/RSJ Conference on Humanoids Robots, pages 89–95, 2007. (Cited in page 63.)

[Zheng 1994] YF. Zheng. Recent trends in mobile robots, volume 11. World scientific, 1994. (Cited in page 27.)

Résumé en français:

Cette thèse a été effectuée dans le cadre du projet européen Koroibot dont l'objectif est le développement d'algorithmes de marche avancés pour les robots humanoïdes. Dans le but de contrôler les robots d'une manière sûre et efficace chez les humains, il est nécessaire de comprendre les règles, les principes et les stratégies de l' homme lors de la locomotion et de les transférer à des robots. L'objectif de cette thèse est d'étudier et d'identifier les stratégies de locomotion humaine et créer des algorithmes qui pourraient être utilisés pour améliorer les capacités du robot. La contribution principale est l'analyse sur les principes de piétons qui guident les stratégies d'évitement des collisions. En particulier, nous observons comment les humains adapter une tâche de locomotion objectif direct quand ils ont à interférer avec un obstacle en mouvement traversant leur chemin. Nous montrons les différences entre la stratégie définie par les humains pour éviter un obstacle non-collaboratif et le stratégie pour éviter un autre être humain, et la façon dont les humains interagissent avec un objet si se déplaçant en manier simil à l'humaine. Deuxièmement, nous présentons un travail effectué en collaboration avec les neuroscientifiques de calcul. Nous proposons une nouvelle approche pour synthétiser réalistes complexes mouvements du robot humanoïde avec des primitives de mouvement. Trajectoires humaines walking-to-grasp ont été enregistrés. L'ensemble des mouvements du corps sont reciblées et proportionnée afin de correspondre à la cinématique de robots humanoïdes. Sur la base de cette base de données des mouvements, nous extrayons les primitives de mouvement. Nous montrons que ces signaux sources peuvent être exprimées sous forme de solutions stables d'un système dynamique autonome, qui peut être considéré comme un système de central pattern generators (CPGs). Sur la base de cette approche, les stratégies réactives walking-to-grasp ont été développés et expérimenté avec succès sur le robot humanoïde HRP-2 au LAAS-CNRS. Dans la troisième partie de la thèse, nous présentons une nouvelle approche du problème de pilotage d'un robot soumis à des contraintes non holonomes par une porte en utilisant l'asservissement visuel. La porte est représentée par deux points de repère situés sur ses supports verticaux. La plan géométric qui a été construit autour de la porte est constituée de faisceaux de hyperboles, des ellipses et des cercles orthogonaux. Nous montrons que cette géométrie peut être mesurée directement dans le plan d'image de la caméra et que la stratégie basée sur la vision présentée peut également être lié à l'homme. Simulation et expériences réalistes sont présentés pour montrer l'efficacité de nos solutions.

Mots clés: Modèles inspirés de l'humain, locomotion des robots, interaction homme-robot, robots humanoid, systéme de capture de mouvement

Abstract:

This thesis has been done within the framework of the European Project Koroibot which aims at developing advanced algorithms to improve the humanoid robots locomotion. It is organized in three parts. With the aim of steering robots in a safe and efficient manner among humans it is required to understand the rules, principles and strategies of human during locomotion and transfer them to robots. The goal of this thesis is to investigate and identify the human locomotion strategies and create algorithms that could be used to improve robot capabilities. A first contribution is the analysis on pedestrian principles which guide collision avoidance strategies. In particular, we observe how humans adapt a goal-direct locomotion task when they have to interfere with a moving obstacle crossing their way. We show differences both in the strategy set by humans to avoid a non-collaborative obstacle with respect to avoid another human, and the way humans interact with an object moving in human-like way. Secondly, we present a work done in collaboration with computational neuroscientists. We propose a new approach to synthetize realistic complex humanoid robot movements with motion primitives. Human walking-to-grasp trajectories have been recorded. The whole body movements are retargeted and scaled in order to match the humanoid robot kinematics. Based on this database of movements, we extract the motion primitives. We prove that these sources signals can be expressed as stable solutions of an autonomous dynamical system, which can be regarded as a system of coupled central pattern generators (CPGs). Based on this approach, reactive walking-to-grasp strategies have been developed and successfully experimented on the humanoid robot HRP at LAAS-CNRS. In the third part of the thesis, we present a new approach to the problem of vision-based steering of robot subject to non-holonomic constrained to pass through a door. The door is represented by two landmarks located on its vertical supports. The planar geometry that has been built around the door consists of bundles of hyperbolae, ellipses, and orthogonal circles. We prove that this geometry can be directly measured in the camera image plane and that the proposed vision-based control strategy can also be related to human. Realistic simulation and experiments are reported to show the effectiveness of our solutions.

Key words: Human-inspired models, robot locomotion, human-robot interaction, motion capture system